Atmospheric Ammonium Deposition to the North Pacific Ocean: Source Origins and Implications

by

Alexandra B. MacFarland

B.S., Suffolk University: Boston, MA, 2020

M.Sc., Brown University: Providence, RI, 2022

A dissertation submitted in partial fulfillment of the requirements for the degree of Doctor of Philosophy in the Department of Earth, Environmental, and Planetary Sciences at Brown University

Providence, Rhode Island, USA

May 2025

Signature page

This dissertation by Alexandra B. MacFarland is accepted in its present form by the Department of Earth, Environmental and Planetary Sciences as satisfying the dissertation requirement for the degree of Doctor of Philosophy.

Date 4/8/25

Meredith G. Hastings, Ph.D., Advisor

Recommended to the Graduate Council

Date 4/8/25

Timothy Herbert, Ph.D., Reader

Date 4/8/25

Colleen Dalton, Ph.D., Reader

Date 4/8/25

Christopher Horvat, Ph.D., Reader

Date 4/8/25

Autumn Oczkowski, Ph.D., Reader

Approved by the Graduate Council

Date _____

Thomas A. Lewis, Dean of the Graduate School

Curriculum Vitae

Alexandra Brook MacFarland

Education:

- **Doctorate:**

  Department of Earth, Environmental, and Planetary Sciences (DEEPS)
  Brown University, Providence, RI 02912 Degree: Doctor of Philosophy
  Expected Graduation: May 2025

- **Masters:**

  Department of Earth, Environmental, and Planetary Sciences (DEEPS)
  Brown University, Providence, RI 02912 Degree: Master of Science
  Graduation Date: May, 2022
  Title: Investigation of Coastal Ammonium Aerosol Sources in the Northwest Pacific Ocean

- **Undergraduate:**

  Center for Urban Ecology and Sustainability (CUES)
  Suffolk University, Boston, MA 02108 Degree: Bachelor of Science
  Major: environmental science, minor: biology GPA: 3.98/4.00
  Graduation Date: May 2020

Career-Related Courses/ Skills:

- **Recent Coursework**: Ocean Biogeochemical Cycles, Environmental Geochemistry, Environmental Stable Isotopes, Paleoceanography, Global Water Cycle, Measuring Climate and Environmental Change with Geophysical Data, Foundational Readings in the Earth Sciences, Weather and Climate, Community and Professional Development

- **Teaching Assistant**
  - Water in Our World (Fall 2021, Fall 2024; undergraduate class)

        - Content: fundamental concepts in physical hydrological science; human modifications and environmental problems associated with a perturbed water cycle
    - Ocean Biogeochemical Cycles (Fall 2023; undergraduate and graduate student class)
        - Content: developed simple box models of ocean chemistry to emphasize the major sources and removal processes of biologically important compounds in the ocean, and the rates at which the controlling processes occur; carbon chemistry in the ocean, the equilibration of oceanic carbon with the atmosphere and carbonate sediments, and current alteration of ocean biogeochemistry by uptake of anthropogenic CO_2, ocean acidification, and coastal eutrophication

- **Lab and Software Skills**: Experience in Gas Chromatography - Isotope Ratio Mass Spectrometry, denitrification method to determine $\delta^{15}N\text{-}NO_3^-$, azide method to determine $\delta^{15}N\text{-}NH_4^+$ (quantitative oxidation using hypobromite (BrO^-)), nutrient analyses using a UV-Vis analyzer (Westco SmartChem 2.0), HYSPLIT Airmass Back Trajectories, R language, Matlab language, Stable Isotope Mixing Model (SIMMR), and collecting/processing/preparing aerosol and precipitation samples for ion concentrations and stable isotopic analyses.

- **Graduate Fieldwork**: I collected cruise-based aerosol samples aboard the Hawaii Ocean Time Series ship in Oahu, Hawaii during the summer of 2022. Glass fiber filters (total bulk particles) on a high-volume aerosol sampler were collected in order to study the aerosol composition and ammonium isotope values over the open ocean. Open ocean studies are limited but vital for a better understanding of the relationship between atmospheric deposition and changes in ocean biogeochemistry.

Honors and Awards:

- NASA-Rhode Island Space Grant Consortium Graduate Student Fellowship (Spring 2023, Spring 2024)
- Institute at Brown for Environment and Society Graduate Research, Training & Travel Award (Spring 2021, Spring 2022)
- UESS Conference, Honorable mention, Graduate student technical competition (2021)
- Brown University, Graduate Fellowship (2020-2021).

Research Projects:

- **Doctor of Philosophy**; Summer 2022 – Spring 2025; Department of Earth, Environmental, and Planetary Sciences; Brown University**.**
    - **Advisor**: Dr. Meredith Hastings, studying the reactive nitrogen cycle.
    - **Project:** Quantifying Coastal and Open Ocean Nitrogen Deposition to the North Pacific Ocean
        - Calculated annual dry deposition values of inorganic nitrogen to the North Pacific Ocean based on observational data from Changdao Island, China (coastal site) and Oahu, Hawaii (open ocean site)
        - Tested Monte Carlo model simulations of atmospheric deposition to the coastal and open ocean to show that atmospheric nitrogen is being deposited to the open ocean
        - Determined the seasonal area of coastal vs open ocean in the North Pacific Ocean via air mass back trajectory calculations using HYSPLIT software

    - **Project:** Investigation of Open Ocean Ammonium Aerosol Sources in the North Pacific Ocean (Oahu, Hawaii)
        - Quantified the amount of inorganic nitrogen entering the North Pacific Ocean off Oahu, Hawaii through atmospheric deposition.
        - Constrained an open ocean $\delta^{15}N\text{-}NH_4^+$ marine source signature as well as a natural external signature of seabird guano emissions

    - **Project:** Solid phase extraction methodology for robust isotope analysis of atmospheric ammonium.
        - Expanded upon a solid phase extraction methodology with a focus on concentrating laboratory standards and an in-house quality control solution as well as evaluated the method's ability to extract ammonium from marine aerosol samples that exhibited matrixes that impeded the chemical conversion of ammonium to nitrous oxide gas when using the well-established chemical method for $\delta^{15}N\text{-}NH_4^+$ analysis created by Zhang *et al*. (2007).

- **Master of Science;** Fall 2020-Spring 2022*;* Department of Earth, Environmental, and Planetary Sciences; Brown University
    - **Advisor**: Dr. Meredith Hastings, studying the reactive nitrogen cycle.
    - **Title:** Investigation of coastal ammonium aerosol sources in the Northwest Pacific Ocean.
    - **Goals:** (1) to understand and quantify the influence of anthropogenic emissions of reactive N on atmospheric ammonium and (2) to determine the atmospheric composition and sources of ammonium to the North Pacific Ocean with a focus on seasonal trends.
        - Quantified the amount of inorganic nitrogen entering the North Pacific Ocean off the coast of Eastern China through atmospheric deposition.
        - Analyzed ammonium isotope values and used an isotope mixing model, along with a suite of other tools, to determine that the largest ammonium source contributor annually is agricultural emissions.

Publications:

MacFarland, A.B., Walters, W.W., Altieri, K.E., Hastings, M.G. Under Review. Investigation of Open Ocean Ammonium Aerosol Sources in the North Pacific Ocean (Oahu, Hawaii). *Marine Chemistry*.

MacFarland, A.B., Walters, W.W., Hastings, M.G. Solid Phase Extraction Methodology for Robust Isotope Analysis of Atmospheric Ammonium. American Chemical Society, *Earth and Space Chemistry*. https://doi.org/10.1021/acsearthspacechem.3c00375.

MacFarland, A.B., Joyce, E.E., Wang, X., Walters, W.W., Altieri, K.E., Schiebel, H.N., Hastings, M.G. 2023. Investigation of coastal ammonium aerosol sources in the Northwest Pacific Ocean. *Atmospheric Environment* 312, 120034. https://doi.org/10.1016/j.atmosenv.2023.120034.

Presentations:

MacFarland, A.B., Walters, W.W., Altieri, K.E., Hastings, M.G. "Investigation of Open Ocean Ammonium Aerosol Sources in the North Pacific Ocean (Oahu, Hawaii)" American Geophysical Union (December 2024), Washington, DC.

MacFarland, A.B., Hastings, M.G. "Investigating Anthropogenic Atmospheric Deposition of Ammonium to the North Pacific Ocean" NASA RI Space Grant Symposium (March 2024), Providence, RI.

MacFarland, A.B., Walters, W.W., Hastings, M.G. "Purification Method for Robust Isotope Analysis of Atmospheric Ammonium" American Geophysical Union (December 2023), San Francisco, CA.

MacFarland, A.B., Joyce, E.E., Wang, X., Walters, W.W., Altieri, K.E., Schiebel, H.N., Hastings, M.G. "Comparison of Aerosol Ammonium Isotope Values in the North Pacific Ocean Atmosphere in China and Hawaii" Association for the Sciences of Limnology and Oceanography (June 2023), Mallorca, ES.

MacFarland, A., Joyce, E., Wang, X., Walters, W., Altieri, K., Schiebel, H., Hastings, M. "Investigation of Ammonium Aerosol Sources in the Northwest Pacific Ocean: Natural or Anthropogenic?" American Geophysical Union (December 2022), Chicago, IL.

MacFarland, A. "Nitrogen in the Ocean: Consequences of Human Activities and How to Trace Source Emissions" University of Massachusetts Boston (March 2022), Boston, MA.

MacFarland, A., Joyce, E., Wang, X., Walters, W., Altieri, K., Schiebel, H., Hastings, M. "Trends in Aerosol Ammonium Isotope Values off the Coast of China in the Northwest Pacific Ocean" Ocean Sciences Meeting (Virtual conference; March 2022), Honolulu, HI.

MacFarland, A., & Hastings, M. "Observations of Aerosol and Precipitation Ammonium Isotopes off the Coast of China in the Northwest Pacific Ocean" International Urban Ecological Security and Sustainability (virtual conference; June 2021), Boston, MA.

Professional Development:

- **Science of Science Communication Workshop** (ASLO 2023, OSM 2022)
    - Attended this full-day workshop where presentations and learning exercises were conducted in order to better present scientific work to different audiences; to better hone verbal, written, and visual presentation skills; and learn strategies to maximize impacts and engage an audience during presentations.
- **Leadership in Ocean Science Workshop** (ASLO 2023)
    - Engaged in various discussions centered around leadership in Ocean Science. Specifically, the importance of the use of interdisciplinary language, tackling problems effectively, and taking opportunities that will facilitate growth.
- **Teaching Introductory Aquatic Sciences Courses: Methods to Engage ALL Students Workshop** (ASLO 2023)
    - Attended and participated in discussions around strategies to overcome typical challenges of large introductory courses, as well as how to present information while making teaching engaging, relevant, and effective for all types of students.
- **Isocamp** (summer 2021)
    - Participated in an intensive two-week lecture and laboratory summer course at the University of New Mexico. Topics included the fundamental theories underlying isotope fractionation processes across a broad spectrum of ecological and environmental applications. Many experts discussed different isotopic techniques and how to apply them to various biogeochemical research questions. Students were given the opportunities to formulate questions, use lab instrumentation, and present ideas and findings.

Graduate Science Leadership Activities:

- **Earth Science Women's Network (ESWN)**, Member (2022 – Present)
    - A non-profit organization dedicated to increasing diversity across the geosciences with an emphasis on creating and supporting a nurturing community, working for cultural change to eliminate barriers to a diverse scientific workforce, and empowering scientists through professional development. Attendance of AGU ESWN banquets and talks in 2022, 2023, and 2024).

- **Graduate Women in Science and Engineering**, Department Representative (2022-2024)
    - Promoted inclusivity and gender equality in DEEPS, organized weekly coffee hours with colloquium speakers, and facilitated research and career related discussions.

- **GeoClub**, President (2021 – 2022)
    - Ran graduate student meetings, welcomed incoming first-year students, organized student events.

Acknowledgements

Completing this dissertation has been a long and rewarding journey, and I would not have made it to the end without the support and encouragement of many people. Earning this PhD was not a solitary achievement, it was built upon the time, energy, and generosity of a community. I'm incredibly grateful for the people who have stood by me during this process, offering guidance, inspiration, and motivation when I needed it most.

First and foremost, I would like to thank my advisor, Dr. Meredith Hastings, for your unwavering mentorship, thoughtful feedback, and continual support. Your knowledge, patience, and encouragement helped shape this work and allowed me to grow as both a researcher and a person. I also want to express my appreciation to my committee members, Dr. Timothy Herbert, Dr. Colleen Dalton, Dr. Christopher Horvat, and Dr. Autumn Oczkowski. Your insights, suggestions, and support throughout this project challenged me to think more critically.

To my family, thank you for your unwavering support and love. Your belief in me, even during the difficult moments, gave me strength and motivation. To my friends, your kindness, humor, and understanding have meant the world to me. Thank you for reminding me to take breaks, celebrating small and large victories, and always being there when I needed you.

Table of Contents

List of Figures

List of Tables

Chapter 1

Introduction

Alexandra B. MacFarland

Department of Earth, Environmental, and Planetary Sciences, Institute at Brown for Environment and Society, Brown University, Providence, RI 02912, USA

Excess nitrogen (N) entering the North Pacific Ocean (NPO) has affected oceanic biogeochemical cycles, but the origins of this excess N is unclear. N is a naturally occurring element and it is a growth-limiting macronutrient for photosynthesis. N gas in the atmosphere ($N_{2(g)}$) is converted to a usable form mainly through N-fixation, a process carried out only by certain bacteria. Readily available (e.g., usable) inorganic forms of N include nitrate (NO_3^-) and nitrite (NO_2^-; NO_x as an encompassing term for both), and ammonia (NH_3) and ammonium (NH_4^+; NH_x as an encompassing term for both). The oceanic N cycle has largely been viewed as in balance, with N predominantly entering the ocean via N-fixation and exiting via denitrification (bacteria converting usable N back into $N_{2(g)}$). Intermediate steps include nitrification (NH_4^+ → NO_2^- → NO_3^-) and ammonification (organic nitrogen (ON) → NH_3 → NH_4^+; Figure 1). At the same time, anthropogenic N entering the ocean from the atmosphere (i.e., atmospheric N deposition) has been rising steadily since preindustrial times (Galloway *et al*., 2004) and potentially rivals N-fixation in magnitude (Jickells *et al*., 2017).

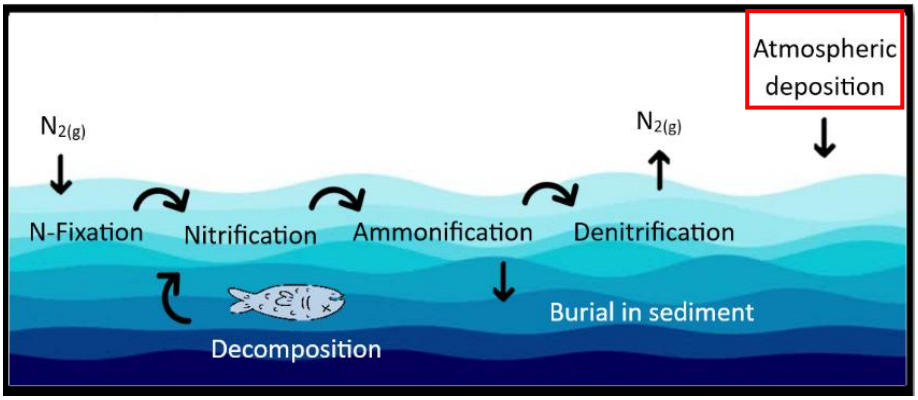

Figure 1: Oceanic N cycle. The cycle is balanced by N-fixation and denitrification, with the intermediate steps emitting into or out of the ocean depending on various factors (pH, temperature, etc). Atmospheric deposition is a newer external input, potentially disrupting this natural internal balance.

A vital tool to help answer questions related to source origins is N isotope analyses. Continental and marine aerosols have different observed compositions of $\delta^{15}N$ ($(\delta^{15}N\ (‰) = [(^{15}N/^{14}N)_{sample}/ (^{15}N/^{14}N)_{standard} - 1] \times 1000$), where the N isotopic reference is air-N_2; Jickells *et al*., 2003). The observed $\delta^{15}N$ allows higher precision for differentiating sources (e.g., marine vs continental), but isotopic fractionation must be properly accounted for to do so. Fractionation is defined as the relative partitioning of the heavier and lighter isotopes (^{15}N vs ^{14}N) between two coexisting phases, such as when NH_3 reacts and converts to NH_4^+. The two types of fractionation include kinetic fractionation, which is irreversible and when the lighter isotope is favored due to its faster reaction rate, and equilibrium fractionation, which is reversible and when the heavier isotope is preferentially distributed in a phase at equilibrium. Altieri *et al.* (2013, 2014) was able to distinguish between anthropogenic sources of atmospheric NH_4^+ and NO_3^- as well as observe seasonal patterns in $\delta^{15}N$ values at Bermuda in the Atlantic Ocean. It was further concluded that ~27% of total N wet deposition (inorganic + organic N in precipitation) was anthropogenic in origin (Altieri *et al*., 2016), which contrasts with global models that suggest as much as 75% of N deposition to the oceans represents an external/anthropogenic source of oceanic N (Jickells *et al*., 2017). This highlights the need for more observational air-sea exchange studies related to atmospheric N concentrations and $\delta^{15}N$ analyses. Many studies have focused on the deposition flux of NO_3^- and $\delta^{15}N$-NO_3^-, suggesting a further need for NH_4^+ concentration and $\delta^{15}N$-NH_4^+ analyses specifically, as it has been shown to hold vital information related to N deposition and source discrimination (Altieri *et al*., 2014, 2021).

Coastal studies have shown that increased N loading leads to damaging effects such as eutrophication (rapid photosynthetic growth and decay) and oxygen minimum zones (Paerl *et al*., 2002). Few studies have examined the major biogeochemical impacts of N entering the open

ocean despite the reported large increases in atmospheric deposition. Recently, however, there are reports of excess N in the NPO that suggest a rise in reactive N emissions from the Asian continent has contributed to a significant increase in anthropogenic atmospheric deposition, which is measurable as excess N (Kim *et al*., 2011) in the open ocean. Another study attributes excess N to nutrient dynamics such as marine N-fixation and/or lateral transport of nutrients (Letscher *et al*., 2016). Thus, the biogeochemical effects of increased atmospheric N deposition, evident in both terrestrial and coastal systems, is still unclear for the open ocean.

NH_3, a precursor to NH_4^+, is emitted into the atmosphere via both natural and anthropogenic sources, including lightning, fire, N-fixation, agriculture, industry, vehicles, etc. where it can convert to NH_4^+ and subsequently gets deposited, either in gas form (NH_3) or particulate form (NH_4^+) (Figure 2). This deposition, defined as the removal of particles and gases from the atmosphere onto a surface, can either be "dry" (i.e., aerosols) or "wet" (i.e., precipitation). Anthropogenic sources are considered external sources and are potentially affecting the overall N budget and balance of oceanic N. The rate of loading of NH_x into the atmosphere has been rising over time (Jickells *et al*., 2017) but can be difficult to track in the environment due to its short lifetime (hours to days; Xu and Penner, 2012) and its many emission sources and fates (cloud scavenging, formation of NH_4^+ aerosols, bidirectional exchange). Therefore, the questions remain: how far into the open ocean does atmospheric N deposition reach and in what quantity? What are its origins (e.g., natural or anthropogenic)?

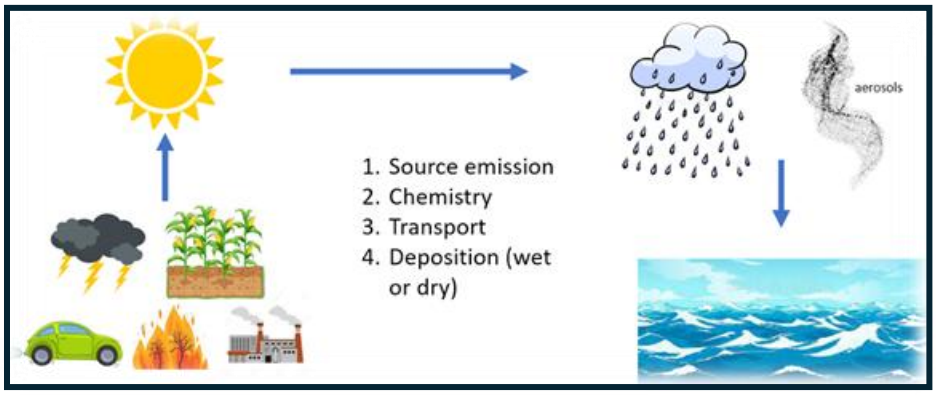

Figure 2: Steps to atmospheric deposition (1 = source emissions, 2 = N species react with sunlight or other species in the atmosphere, 3 = transport via wind, 4 = ultimate deposition from precipitation or aerosols).

There is controversy in the literature as to whether atmospheric deposition is a significant pathway for N to enter the ocean. Some studies consider contributions from atmospheric deposition to be negligible (Böttjer *et al*, 2017; Knapp *et al*., 2018; Zhang *et al*., 2019). Other studies, though, discuss a larger role that atmospheric N deposition could be playing both near the coast and further into the open ocean (Kim *et al*., 2011; Kim *et al*., 2014; Zhao *et al*., 2015; Letscher *et al*., 2016). Specifically, Kim *et al*. (2011, 2014) concluded that observed excess N in the northwest Pacific Ocean was due to deposition of anthropogenic reactive N emissions from the Asian continent. These findings do require that all N deposition is considered external to the ocean's N budget with a limited change in N-fixation over the same time period. However, differentiating between fixed N sources, particularly from atmospheric deposition, is needed in order to fully understand the effects of human activities and natural emissions on the marine environment (Jickells *et al*., 2003).

NH_4^+ is a major component of N deposited from the atmosphere to the ocean and is a readily bioavailable external source of N. NH_3 is not regulated in policy the same way as other species, and as a result, is the predominant inorganic N species increasing in emissions over

time. These two species are bidirectional, meaning they can switch back and forth between NH_3 and NH_4^+ depending on various environmental driving factors (Figure 3). The air-sea flux of NH_3 is determined by the concentration gradient between the surface ocean and atmosphere, and is sensitive to factors such as temperature, pH, and salinity, in decreasing order of significance (Altieri *et al*., 2021). For example, NH_3 fluxes out of the ocean and into the atmosphere at warmer temperatures, and fluxes into the ocean at cooler temperatures. Lower pH (i.e., higher acidity) promotes the conversion of NH_3 to NH_4^+ because of thermodynamic equilibrium processes. Due to this, fixed N is typically highly seasonal (Hansell *et al*., 2007, Zhao *et al*., 2015). This excess fixed N, potentially being affected by both internal and external sources (Figures 1 & 2), presents consequences to the biogeochemistry of the ocean.

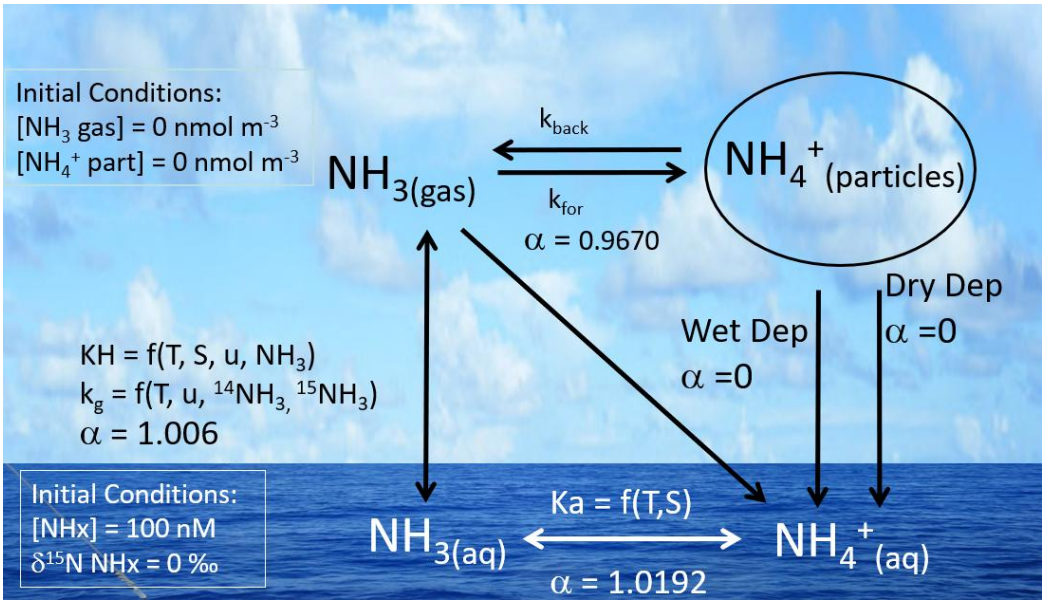

Figure 3: Diagram illustrating NH_x chemical and physical processes. Provided is the information needed to investigate the isotopic composition of ammonia gas and ammonium particles in the marine atmosphere. α = isotopic fractionation factor, K = reaction rate constant, KH = Henry's law constant, kg = gas transfer velocity, T= temperature, S = salinity, u = wind speed. Main takeaways: NH_x exists in gas an aerosol form, they undergo bi-directional reactions, fractionation occurs during these phase changes.

In this work, these studies aimed to better understand the deposition of inorganic N from the atmosphere to the ocean by investigating the amount and sources (naturally derived vs anthropogenically emitted) of these N species. Specifically, studies were conducted in two opposite but vital environments: (1) Changdao Island, China which represents a region strongly affected by anthropogenic pollution in Asia, and (2) Oahu, Hawaii which represents an open ocean marine system, with limited effects from anthropogenic activities (Figure 4). The projects discussed in this body of work contribute new data to quantify atmospheric deposition of dry inorganic N, which can be an influential stressor on the biogeochemistry of the ocean if it is external. Part of conducting this work resulted in novel method development in order to successfully obtain δ^{15}N-NH_4^+ values for atmospheric samples that display matrix interference issues, which is vital to aid in source determinations, and can potentially be applied to other types of environmental samples.

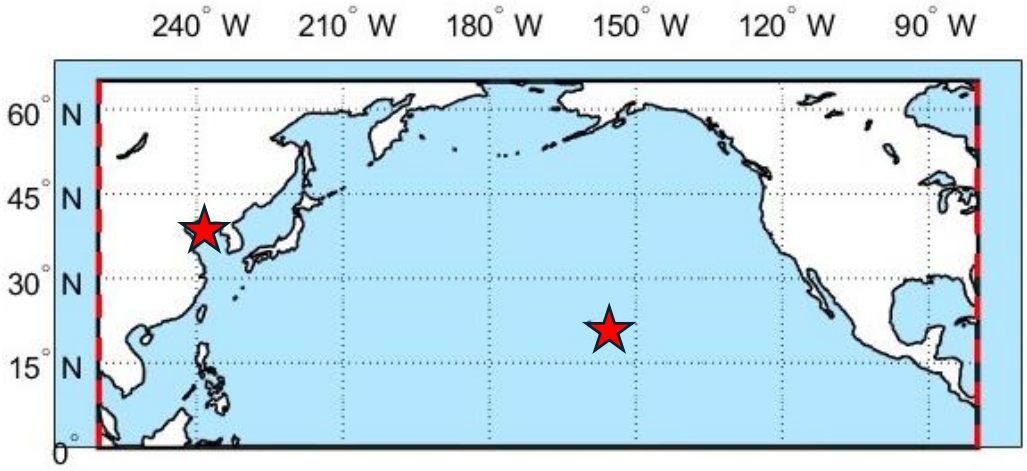

Figure 4: Study site locations in the North Pacific Ocean: Changdao Island, China (37.92° N, 120.73°E; coastal ocean) and Oahu, Hawaii (21.32°N, 157.67°W; open ocean).

The goals of the study presented in Chapter 2 included: (1) to understand and quantify the influence of anthropogenic emissions of reactive N on atmospheric NH_4^+ and (2) to determine

the atmospheric composition and sources of NH_4^+ to the NPO with a focus on seasonal trends. to investigate this, I analyzed atmospheric aerosol samples collected on Changdao Island, China via a high-volume aerosol sampler (Figure 5) from 2020-2021. This study site was used as a proxy for continental emissions that can be exported and subsequently deposited to the ocean. With the Kim *et al*. study as a basis, I tested the hypothesis that N deposition to the NPO is primarily anthropogenic based on continental versus marine sources of NH_3, the isotopic composition of NH_4^+, aerosol chemical composition, seasonal shifts in transport patterns, and partitioning of NH_3/NH_4^+ between the gas and particle phases.

Figure 5: Left: An image of the high-volume aerosol sampler at Changdao Island, which operates at 1.0 m^3/min (e.g., pumps the surrounding air onto the filter). Aerosol samples (bulk total suspended particles) were collected on pre-cleaned TE-G653 Glass Fiber Filters. Right: an example of a filter that has been collecting aerosols for 48 hours (filters started off white).

In Chapter 3, I present an analytical methodology to concentrate NH_4^+ and remove matrix interferences via a sample pre-treatment step utilizing a solid phase extraction technique involving cation exchange resins (Figure 6) that were evaluated via detailed laboratory experiments and tested against environmental aerosol samples. Motivation for this work

stemmed from the NH_4^+ extracted from my aerosol samples from Oahu, Hawaii (n = 57) that all failed to oxidize to NO_2^-, a necessary step in order to acquire $\delta^{15}N\text{-}NH_4^+$ values. This new sample pre-treatment step can be utilized for the concentration and purification of NH_4^+ for high throughput $\delta^{15}N$, which is significant due to many environments containing low concentrations of NH_4^+ and therefore can be below the threshold necessary to analyze $\delta^{15}N\text{-}NH_4^+$. Further, other types of samples, such as throughfall, have displayed matrix interference issues, so this pre-treatment step could allow for an increase in available samples to measure.

Figure 6: an image of the lab setup of the cation exchange resins. 10 separate resins were capable of being used at a time and could be flushed in between samples (e.g., they were reusable). A: funnel where eluent and filtered water was introduced, B: detachable column where sample was introduced, C: cation exchange resin that captured the NH_4^+ and removed anions and organics, D: waste containers that were switched out with vials when it was time to collect the purified NH_4^+.

In fact, this pre-treatment methodology was later used on surface water samples from an urban tropical estuary in San Juan, Puerto Rico as a collaborative project with the Environmental Protection Agency's (EPA) Atlantic Coastal Environmental Sciences Division (ACESD) in Narragansett, RI with Dr. Autumn Oczkowski. These samples were sent from her lab to ours at Brown University where they were analyzed for $\delta^{15}N\text{-}NH_4^+$ and $\delta^{15}N\text{-}NO_3^-$. More details can be found in the appendix as a measurement report.

In Chapter 4, I analyzed aerosol samples collected in Oahu, Hawaii from 2021-2022. This study site is used to represent a dominant marine environment where N is expected to be largely recycled as opposed to external excess N entering the system. The goals of this study included: (1) to characterize the aerosol composition at Oahu across the year, (2) determine the NH_4^+ source origins, and (3) calculate the rate of annual dry inorganic N deposition to the NPO. A multitude of tools were used including ion concentration measurements, $\delta^{15}N\text{-}NH_4^+$ analyses, species correlation calculations, air mass back trajectory calculations, k means clustering analysis, and isotope mixing models that include phase partitioning and fractionation.

In Chapter 5, I conclude this work while also utilizing the measurements made at Changdao Island and Oahu as a way to characterize the open and coastal ocean based on aerosol composition and N concentration, $\delta^{15}N\text{-}NH_4^+$ values, and airmass back trajectory origins. Further, dry inorganic N deposition rates were calculated using both NH_4^+ and NO_3^- concentration and $\delta^{15}N$ measurements and upscaled to the NPO. Air mass back trajectories were calculated to determine the percent of the ocean that receives continental influences, therefore characterizing it as the coastal ocean. Through the use of a three-endmember isotopic mixing model in Monte Carlo simulations, I also ran various tests to aid in determining the proportion that atmospheric deposition is contributing as an N input to the NPO, in conjunction with N-fixation and NO_3^- upwelling.

Therefore, all of my research was pursued in order to help fill this gap of knowledge when it comes to quantifying atmospheric N deposition to the NPO and its source origins. Analyzing and comparing Oahu, Hawaii to Changdao Island, China allowed for a better understanding of how much the marine system is contributing to observed excess N in regions where there is either a minimal or substantial export of pollution. Further, a new external source

of N was isotopically identified (seabird guano emissions; Chapter 4), which can have local impacts on the marine environment. Data from these sites allowed for the ability to scale up the deposition to the entire NPO as a way to predict how much atmospheric N deposition matters to the overall oceanic N budget. These observational records provided can be used in future studies to quantify biogeochemical impacts on the ocean system.

References

Altieri, K.E., Fawcett, S.E., Hastings, M.G. 2021. Reactive nitrogen cycling in the atmosphere and ocean. Annual Reviews, 49, 523-550.

Altieri, K.E., Hastings, M.G., Gobel, A.R., Peters, A.J. and Sigman, D.M. 2013. Isotopic composition of rainwater nitrate at Bermuda: The influence of air mass source and chemistry in the marine boundary layer. Journal of Geophysical Research: Atmospheres, 118(19).

Altieri, K.E., Hastings, M.G., Peters, A.J., Oleynik, S. and Sigman, D.M. 2014. Isotopic evidence for a marine ammonium source in rainwater at Bermuda. Global Biogeochemical Cycles, 28(10), 1066-1080.

Böttjer, D., Dore, J.E., Karl, D.M., Letelier, R.M., Mahaffey, C., Wilson, S.T., Zehr, J., Church, M.J. 2017. Temporal variability of nitrogen fixation and particulate nitrogen export at Station ALOHA. Limnology and Oceanography, 62(1), 200−216.

Galloway, J.N., Dentener, F.J., Capone, D.G., Boyer, E.W., Howarth, R.W., Seitzinger, S.P., Asner, G.P., Cleveland, C.C., Green, P.A., Holland, E.A., Karl, D.M., Michaels, A.F., Porter, J.H., Townsend, A.R., Vöosmarty, C.J., 2004. Nitrogen Cycles: Past, Present, and Future. Biogeochemistry 70, 153–226. https://doi.org/10.1007/s10533-004-0370-0.

Hansell, D.A., Olson, D.B., Dentener, F., Zamora, L.M. 2007. Assessment of excess nitrate development in the subtropical North Atlantic. Mar. Chem., 106(3), 562–79.

Jickells, T.D., Buitenhuis, E., Altieri, K., Baker, A.R., Capone, D., Duce, R.A., Dentener, F., *et al*. 2017. A reevaluation of the magnitude and impacts of anthropogenic atmospheric nitrogen inputs on the ocean. Global Biogeochem. Cycles 31(2), 289–305.

Jickells, T., Kelly, S., Baker, A., Biswas, K., Dennis, P., Spokes, L.J., Witt, M., Yeatman, S.G., 2003. Isotopic evidence for a marine ammonia source. Geophysical Research Letters 30. https://doi.o rg/10.1029/2 002GL016728.

Kim, I.-N., Lee, K., Gruber, N., Karl, D.M., Bullister, J.L., Yang, S., Kim, T.-W. 2014. Increasing anthropogenic nitrogen in the North Pacific Ocean. Science, 346(6213), 1102–1106.

Kim, T.-W., Lee, K., Najjar, R.G., Jeong, H.-D., Jeong, H.J. 2011. Increasing N Abundance in the Northwestern Pacific Ocean Due to Atmospheric Nitrogen Deposition. Science 334, 505–509. https://doi.org/10.1126/science.1206583.

Knapp, A.N., McCabe, K.M., Grosso, O., Leblond, N., Moutin, T., Bonnet, S. 2018. Distribution and rates of nitrogen fixation in the western tropical South Pacific Ocean constrained by nitrogen isotope budgets. Biogeosciences, 15, 2619–2628.

Letscher, R., Primeau, F., Moore, J. 2016. Nutrient budgets in the subtropical ocean gyres dominated by lateral transport. Nature Geosci 9, 815–819. https://doi.org/10.1038/ngeo2812.

Paerl, H.W., Dennis, R.L., Whitall, D.R., 2002. Atmospheric deposition of nitrogen: Implications for nutrient over-enrichment of coastal waters. Estuaries 25, 677–693. https://doi.org/10.1007/ BF02804899.

Sigman, D.M., Fripiat, F. 2019. Nitrogen Isotopes in the Ocean. Academia, Encyclopedia of Ocean Sciences (Third Edition), 263-278.

Takahashi, T., Broecker, W., Langer, S. 1985. Redfield ratio based on chemical data from isopycnal surfaces. JGR Oceans, 90, 6907-6924.

Xu, L., Penner, J. E. 2012. Global simulations of nitrate and ammonium aerosols and their radiative effects, Atmos. Chem. Phys., 12(20), 9479−9504.

Zhang, S., Stock, C.A., Curchitser, E.N., Dussin, R. 2019. A numerical model analysis of the mean and seasonal nitrogen budget on the Northeast U.S. Shelf. Journal of Geophysical Research. Oceans, 124, 2969–2991.

Zhao, Y., Zhang, L., Pan, Y., Wang, Y., Paulot, F., Henze, D.K., 2015. Atmospheric nitrogen deposition to the northwestern Pacific: seasonal variation and source attribution. Atmos. Chem. Phys, 15(9), 13657-13703. https://doi.org/10.5194/acp-15-10905.

Chapter 2

Investigation of Coastal Ammonium Aerosol Sources in the Northwest Pacific Ocean

Alexandra B. MacFarland[1], Emily E. Joyce[1], Xuchen Wang[2], Wendell W. Walters[1], Katye E. Altieri[3], Hayley N. Schiebel[4], Meredith G. Hastings[1]

[1] Institute at Brown for Environment and Society and
Department of Earth, Environmental, and Planetary Sciences
Brown University
324 Brook Street, Box 1846
Providence, RI 02912

[2] Marine Organic Geochemistry
Ocean University of China
238 Songling Road, Qingdao
China

[3] Department of Oceanography
University of Cape Town
Rondebosch, Cape Town
7700, South Africa

[4] Center for Urban Ecology and Sustainability
Suffolk University
8 Ashburton Place
Boston, MA 02108

Published in *Atmospheric Environment* (2023),
doi:10.1016/j.atmosenv.2023.120034.

Abstract

Determining the magnitude and origins of nitrogen (N) deposition in the open ocean is vital for understanding how anthropogenic activities influence oceanic biogeochemical cycles. Excess N in the North Pacific Ocean (NPO) is suggested to reflect recent anthropogenic atmospheric deposition from the Asian continent, changes in nutrient dynamics due to marine N-fixation, and/or lateral transport of nutrients. We investigate the impact of anthropogenic and marine sources on reactive N deposition in the NPO, with a focus on ammonium (NH_4^+), an important bioavailable nutrient, using aerosol samples (n=108) collected off the coast of China (Changdao Island). This study site is used as a proxy for continental emissions that can be exported and subsequently deposited to the ocean. The NH_4^+ concentration of aerosol samples varied seasonally ($p < 0.05$), with a higher average value in winter (2.77 ± 1.06 μg/m^3) and spring (1.93 ± 0.80 μg/m^3) compared to autumn (0.74 ± 0.55 μg/m^3) and summer (1.43 ± 0.41 μg/m^3). The isotopic composition of aerosol NH_4^+ varied seasonally, with higher averages in spring (13.3 ± 7.9‰) and summer (15.6 ± 6.2‰) compared to autumn (3.2 ± 2.5‰) and winter (3.8 ± 11.4‰). These seasonal patterns in the isotopic composition of NH_4^+ are investigated based on correlations of aerosol chemical species, seasonal shifts in transport patterns, partitioning of ammonia/ammonium between the gas and particle phase, and continental versus marine sources of ammonia. We find that anthropogenic activities, mainly agricultural practices (e.g., volatilization, fertilizer, animal husbandry), are the primary sources of NH_4^+ deposited to the NPO.

Introduction

Nitrogen (N) deposition in the ocean has been increasing since preindustrial times (Galloway *et al*., 2004). As a result, coastal studies have observed eutrophication (rapid growth and decay), algal blooms, and oxygen minimum zones. However, the consequences to the open ocean (characterized here as particulate matter that can be exported and deposited into the ocean) are less well-known. Global modeling suggests anthropogenic inputs have recently led to an overall increase in ocean carbon sequestration of ~0.4%, which is equivalent to an uptake of about 0.15 Pg C yr^{-1} (Jickells *et al*., 2017). Another study suggests that excess N could shift nutrient limitations from N to phosphorus, which could change the composition of phytoplankton species as well as the structure of ecosystems in the ocean (Elser *et al*., 2009). Additionally, an increase in primary productivity from excess N could expand low oxygen zones (Jickells *et al*., 2017). The continued addition of N from anthropogenic activities, mostly land-based activities, has the potential to alter oceanic, and even global, biogeochemical systems (Jickells *et al*., 2017), such that identifying potential N trends and source contributions over time could help influence emissions reduction policies and/or mitigation strategies.

Inorganic N (nitrate (NO_3^-), nitrite (NO_2^-), and ammonium (NH_4^+)) is the main form of N deposition in polluted (Cornell *et al*., 2003; Russell *et al*., 1998) as well as remote locations (Duce *et al*., 2008; Galloway *et al*., 1996, 1982, 1989). Distinguishing amongst the sources of N deposition to the open ocean is vital for discerning the effects of human activities on biogeochemical cycles (Altieri *et al*., 2021). If the deposition is a consequence of terrestrial/continental emissions, it signifies an outside input to the open ocean, and if that input is influenced largely by anthropogenic activities, it may continue to rise over time (Duce *et al*., 2008; Seinfeld and Pandis 2012; Jickells *et al*, 2017). On the other hand, if the N is coming from

the ocean itself and cycling through the atmosphere prior to (re)deposition, it would not be considered a net input of N to the ocean.

Excess N has been observed in the Northwest Pacific Ocean (Kim *et al*., 2011), but there are conflicts as to origin of this excess. Excess N is quantified as relative to the expected ratio of nitrogen to phosphorus in the open ocean (i.e., $N^* = N - (R_{N:P}) \times P$; where $R_{N:P}$ is the ratio of nitrogen to phosphorus; Gruber and Sarmiento, 1997). In the Northwest Pacific, excess N (i.e., +N*) has been reported and based on the geographical patterns, rates of change in N*, and the time frame of increases in oceanic N, it was concluded that the excess N was due to deposition of anthropogenic reactive N emissions from the Asian continent (Kim *et al*., 2011; Kim *et al*., 2014). However, this finding requires that all N deposition is considered external to the ocean's N budget and requires limited change in N-fixation over the same time period. At Station ALOHA in the North Pacific Ocean (NPO; 22.75°N, 158.00°W; Quay *et al*., 2010) only about 75% of the N measured could be accounted for via N-fixation (Karl *et al*., 2012) and mesoscale mixing (Johnson *et al*., 2010), and it is possible that atmospheric deposition may explain the remaining 25%. Additionally, a modeling study of gyres in the subtropics explains nutrient dynamics due to changes in marine N-fixation or lateral transport of nutrients (Letscher *et al*., 2016).

Stable isotopic composition of N holds promise as a valuable tool for identifying and detailing the sources and chemistry of reactive N. Different sources of NH_x (NH_4^+ and ammonia (NH_3)) exhibit unique isotopic signatures (Altieri *et al*., 2014; 2021). For example, continental and marine aerosol NH_4^+ have different observed compositions of $\delta^{15}N$ (Jickells *et al*., 2003). (The nitrogen stable isotopic composition is determined as follows: $\delta^{15}N$ (‰) = $[(^{15}N/^{14}N)_{sample}/(^{15}N/^{14}N)_{standard} - 1] \times 1000$, where the N isotopic reference is air-N_2). Physical,

chemical, and biological processes differentiate between the two isotopes (^{15}N and ^{14}N) which lead to small but measurable differences in the ratio of ^{15}N to ^{14}N among the forms of N found in the environment via various sources (Sigman and Fripiat, 2019). Many studies have focused on the deposition flux of NO_3^- and $\delta^{15}N\text{-}NO_3^-$, we seek to add to our understanding of NH_x since NH_x is readily bioavailable and its overall loading in the atmosphere has increased over time (Altieri *et al*., 2021). NH_4^+ is a bi-product of NH_3 emissions; natural sources of NH_3 to the atmosphere include N-fixation, organism waste, and decomposition, while anthropogenic sources include fertilizer, livestock, and industrial processes (Zhao *et al*., 2015).

Using stable isotopes, transport patterns, and the composition of wet deposition (rainwater) observations from Bermuda, Altieri *et al*. (2013, 2014) were able to distinguish sources of NH_4^+ and NO_3^- in the western North Atlantic Ocean. The island of Bermuda encounters continental as well as oceanic-influenced air masses. For NO_3^-, an anthropogenic imprint was determined via lower $\delta^{15}N$ values and higher concentrations in continental air masses. For NH_4^+, there was no correlation between $\delta^{15}N\text{-}NH_4^+$ and air mass history, and simple modeling was able to account for both the concentration and isotopic composition of NH_4^+ in precipitation with marine emissions as a primary source (Altieri *et al*., 2014). Overall, the Bermuda work determined that 27% of total N wet deposition (inorganic + organic; Altieri *et al*., 2016) was anthropogenic in origin, which contrasts with global models (Jickells *et al*., 2017) that suggest as much as 75% of N deposition to the oceans represents an external (anthropogenic) source of oceanic N.

This current study has two main objectives, (1) to understand and quantify the influence of anthropogenic emissions of reactive N on atmospheric NH_4^+ and (2) to determine the atmospheric composition and sources of NH_4^+ to the NPO with a focus on seasonal trends. Aerosol samples were collected on Changdao Island, China for the duration of one year from

2020-2021. This study site is used as a proxy for continental emissions that can be exported and subsequently deposited to the ocean. We test the hypothesis that N deposition to the NPO is primarily anthropogenic based on continental versus marine sources of NH_3, the isotopic composition of NH_4^+, aerosol chemical composition, seasonal shifts in transport patterns, and partitioning of NH_3/NH_4^+ between the gas and particle phases.

Methods

Study Site

The sampling site was located on the eastern windward side of Changdao Island (37.92°N, 120.73°E), positioned in the Yellow Sea roughly 64 km from the mainland of China (Figure 1). The Yellow Sea is bordered by the three peninsulas (the Liaodong peninsula, Shandong peninsula, and Korea peninsula), all well populated and industrialized, making the Northern Yellow Sea vulnerable to anthropogenic input, with minimal local emission sources (Kurokawa *et al*., 2013; Luo *et al*., 2014). Aerosol samples (n=108; bulk total suspended particles (TSP)) were collected on pre-cleaned TE-G653 Glass Fiber Filters (in compliance with the method of US EPA FRM 40 CFR Part 50 Appendix B) using a high-volume aerosol sampler operating at 1.0 m^3 min^{-1} (see further details in Ren *et al*. (2022)). The samples were collected for either 24, 48, or 72 hours. Lab blanks and field blanks were taken, the latter represented a filter placed in the sampler, then removed and processed as a sample. The ~1 m tall tower was placed on a flat cement floor atop a hill with no nearby obstructions (e.g., trees, buildings) and is solely used as an air monitoring station. All filter samples were frozen at -20 °C after collection and between all analyses. This has been demonstrated to be sufficient for upholding the original chemical composition of aerosol and rainwater samples in previous studies (Seitzinger *et al*., 2005; Knapp *et al*., 2010; Altieri *et al*., 2013, 2014; Gobel *et al*., 2013).

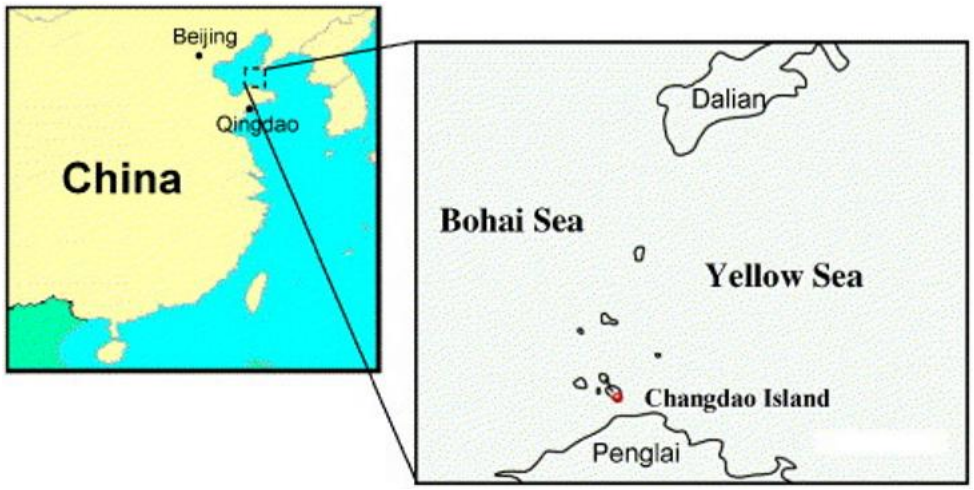

Figure 1: Map of eastern China and location of sampling on Changdao Island (37.92°N, 120.73°E, red dot).

After the frozen samples were received at Brown University, a 5 × 5 cm square was cut from the center of the filter at room temperature and extracted in a pre-cleaned bottle with ~100 mL of MQ water (exact amounts were recorded via weight) and then sonicated for one hour. After sonication, the filters were removed, and the samples were frozen at -20°C until further analyses.

Nitrogen concentration analysis

The concentration of ammonium ($[NH_4^+]$), nitrate ($[NO_3^-]$), and nitrite $[NO_2^-]$) were determined colorimetrically (indophenol blue) using a discrete UV–Vis analyzer (Westco Smartchem 200). U.S. EPA Compliant Methods 350.1 (O'Dell, 1993), 353.2 (Revision 2.0), and 354.1 were followed for NH_4^+, NO_3^-, and NO_2^-, respectively. Standard lab protocols were followed, including calibration to standards as well as blanks and in-house quality control measurements. The pooled standard deviation (1σ) for $[NH_4^+]$ was 0.6 µmol L^{-1}, and 0.3 µmol L^{-1} for $[NO_3^-]$ and $[NO_2^-]$. Liquid concentrations (µmol L^{-1}) were converted to air concentrations (µg m^{-3}) based on extraction volume (L) and average volume of air sampled through the filter (m^3).

Elemental Analyses

Concentrations of calcium (Ca^{2+}), magnesium (Mg^{2+}), sodium (Na^{+}), and potassium (K^{+}) were measured on an Inductively Coupled Plasma (ICP) atomic emission spectrometer. Samples (n = 103) were filtered with 0.45-micron filters and an aliquot of each sample solution was made 2% acidic with nitric acid. A commercial standard (IV-4) for each specific element was run roughly every 10 samples. The relative standard deviation for the standards was ≤ 3.3% for all four elements. All samples analyzed were corrected for drift, acidification, and blanks.

Ion analyses

Chloride (Cl^{-}) and sulfate (SO_4^{2-}) concentrations were measured on an Ion chromatography (IC) instrument (Dionex Integrion HPIC) using suppressed conductivity detection. (We note here that the aerosol samples were significantly influenced by sea salt and had very high chloride and sulfate content. Those concentrations were significantly higher than nitrate concentrations, making it difficult to accurately detect nitrate peaks on the IC, and we therefore report the UV-Vis analyzer results for nitrate concentrations). Anions were determined using a Dionex AS19-4µm guard (4 × 50 mm) and analytical column (4 × 250 mm) with 20 mM KOH as eluent with a flow rate of 1 mL min-1. All samples (n = 100) were filtered with 0.45-micron filters before being analyzed. In-house quality control standards (QCs) were run approximately every six samples. The pooled standard deviation for duplicates was 2.0 µmol for both Cl^{-} and SO_4^{2-} (n = 13 pairs and 12 pairs, respectively). The relative standard deviation for the low and high concentration QCs were ≤ 6.4% and < 3.4%, respectively. The samples analyzed were corrected for dilutions if applicable as well as blanks.

HYSPLIT air mass back trajectory analysis

Air mass back trajectories for each aerosol sample were calculated using NOAA's Hybrid Single-Particle Lagrangian Integrated Trajectory (HYSPLIT; Rolph *et al*., 2017; Stein *et al*., 2015). The plugin 'trajstat' (Wang *et al*., 2009) was used to calculate these trajectories to ultimately aid in the source determination of NH_4^+. Utilizing particle dispersion simulation and meteorological data, the model determines the trajectory of an air mass backward in time, starting from a specified point and time. Back trajectories were run at a height of 500 m above ground level every six hours for the length of the sample collection time as well as four additional days to account of the average lifetime of atmospheric NH_x (Paulot *et al*., 2016).

Potential Source Contribution Function Maps

Potential source contribution function (PSCF) maps were created for each season through the combined use of NH_4^+ concentrations and back trajectory calculations. These maps determine the most likely location of origin of a species (e.g., NH_4^+) relative to the study site. These calculations are based on the evaluation, for each grid cell (or area), of the ratio of the total number of marked trajectory segment endpoints to the total number of trajectory segment endpoints over that grid cell (Wang *et al*., 2009).

NH_4^+ isotope analysis

The determination of δ^{15}N-NH_4^+ follows the protocol of Zhang *et al*. (2007) based on a coupled off-line wet-chemistry technique involving hypobromite (BrO^-) oxidation and acetic acid/sodium azide reduction. Only samples with NH_4^+ concentrations greater than 5 μmol were analyzed for isotopic composition due to the high level of uncertainty for lower concentrations (Zhang *et al*., 2007). Samples above 5 μmol (n = 108) were diluted with ultraclean water (>18 MW) to either 5 μmol-NH_4^+ or 10 μmol-NH_4^+. NH_4^+ was then oxidized to nitrite (NO_2^-) using BrO^- in an alkaline solution, and further synthesized following the protocol by Zhang *et al*.

(2007). NO_2^- concentrations were analyzed to obtain oxidation yields, which were found to completely convert NH_4^+ to NO_2^- for all samples. The reaction was then stopped by the addition of sodium arsenite to extract the remaining BrO^-. Afterward, the samples were transferred into 20 mL vials, crimp-capped with PTFE/butyl septa, and flushed with helium gas for a minimum of 10 minutes. The NO_2^- was then reduced to nitrous oxide gas (N_2O) through the addition of 2 mL of 2 M sodium azide buffered in 40% acetic acid solution. After half an hour (minimum), the samples were neutralized using 6 M sodium hydroxide.

Samples were then analyzed for the $\delta^{15}N$-N_2O composition via an automated N_2O extraction system coupled with a continuous flow isotope ratio mass spectrometer for determination at *m/z* 44, 45, and 46. In each sample set, unknowns were calibrated to two internationally recognized NH_4^+ isotopic reference materials, IAEA-N_2 ($\delta^{15}N$ = 20.3‰) and USGS25 ($\delta^{15}N$ = −30.3‰; Böhlke *et al*., 1993; Böhlke and Coplen, 1995), and an internal QC ($\delta^{15}N$ = -1.5‰) that were run multiple times throughout each run. The isotopic standards underwent the same chemical processing as the unknowns and were used to correct for isotopic fractionation (i.e., from the chemical conversion of NH_4^+ to N_2O). The isotopic standards had a pooled standard deviation (1σ) of ± 0.6‰ for IAEA-N_2 (n = 32), ± 0.8‰ for USGS25 (n = 32), and ± 0.8‰ for the QC (n = 32). Additionally, the pooled standard deviation for duplicates (n = 13 pairs) and replicates (n = 20) was 0.3‰ and 0.5‰, respectively.

ISORROPIA-II Model Analysis

The ISORROPIA-II model performs aerosol thermodynamical equilibrium calculations and can partition NH_x between the gas and aerosol phases (Fountoukis and Nenes, 2007). Inputs to the partitioning routine include various elemental and ion concentrations as well as atmospheric temperature and relative humidity. The model was run in the 'reverse' mode under

'metastable' conditions and was done for each sample (n = 81) where all required concentration data were successfully measured (e.g., some samples had limited volume, and not all analyses could be completed). Concentrations for the following elements/ions were inputted: Na^+, SO_4^{2-}, NH_4^+, NO_3^-, Cl^-, Ca^{2+}, K^+, and Mg^{2+}. Additionally, average temperature and relative humidity values, measured during each collection period per sample, were used.

Calculating $\delta^{15}N\text{-}NH_{3(g)}$ from aerosol $\delta^{15}N\text{-}NH_4^+$

Outputs from ISORROPIA-II and the calculated ion balance of the samples both indicated that the aerosols were essentially completely neutralized by $NH_{3(g)}$. Under these conditions, a surplus of $NH_{3(g)}$ is assumed to stay in the atmosphere, resulting in isotopic fractionation between the aerosol and gas phases (Pan *et al*., 2018). To account for this, the $\delta^{15}N$ values of the original $NH_{3(g)}$ concentrations were determined using the following isotopic mass-balance model in a well-mixed closed system:

$$\delta_{gas} = \delta_{aerosol} - \varepsilon_{aerosol\text{-}gas}\,(1\text{-}f) \quad (1)$$

where δ_{gas} is the isotopic composition of the initial $NH_{3(g)}$, $\delta_{aerosol}$ is the isotopic composition of the final aerosol NH_4^+, and f is the fraction of the initial $NH_{3(g)}$ converted to the aerosol NH_4^+. Epsilon and alpha are related via the following equation:

$$\varepsilon = (\alpha - 1) \times 1000 \quad (2)$$

Therefore, the following formula (Walters *et al*., 2019) was used to determine δ_{gas}:

$$1000\,(^{15}\alpha_{NH4+(aq)/NH3(g)}\text{-}1)\,(\pm 3.5‰) = 14058/T - 12.20 \quad (3)$$

where T is temperature in Kelvin.

This formula was used for each sample (n=108), as opposed to a yearly average, to best account for any seasonal differences. To calculate f, concentrations of both NH_4^+ and $NH_{3(g)}$ are needed. Concurrent measurements of $NH_{3(g)}$ were not available in this study. Therefore, ISORROPIA-II

was used to reproduce gas phase chemistry as well as aerosol evolution during the timeframe of the study.

Stable Isotope Mixing Models in R (SIMMR)

The Bayesian mixing model executed in the R package SIMMR (stable isotopes mixing models in R; Parnell *et al*., 2013) was implemented. It determines a high number of plausible solutions of source contributions to each sample input by applying Bayes theorem. The model is equipped with a Monte Carlo Markov Chain algorithm that generates plausible solutions for each source's influence on each sample (Parnell *et al*., 2010, 2013; Cooper *et al*., 2014). From these *n* realizations, the best estimate (mean) and its uncertainty (standard deviation) can be obtained. SIMMR was used in this study to calculate the likely percentage that each given activity (volatilization/animal waste/fertilizer, industry/fuel combustion, vehicles, marine, biomass burning) was the origin of the NH_3 emissions. Ship emissions in the China region were not included in SIMMR, as the global anthropogenic emission inventory for NH_3 (1970-2017; McDuffie *et al*., 2020) shows that off-road/non-road transportation, including ship emissions, comprises less than 1% of the total emissions from 2015-2017. Additionally, the $\delta^{15}N\text{-}NH_3$ signature from ship emissions is currently unknown. Reported values used in SIMMR include: volatilization/animal waste/fertilizer (-19.2 ± 8.3‰; Freyer, 1978; Heaton, 1987; Frank *et al*., 2004; Hristov *et al*., 2009), fuel combustion/industry (-15.3 ± 3.6‰; Freyer, 1978; Heaton, 1987), vehicle emissions (6.6 ± 2.1‰; Walters *et al*., 2020, Song *et al*., 2021), marine sources (-6.5 ± 1.5‰; Jickells *et al*., 2003), and biomass burning (-6.1 ± 1.3‰; Freyer, 1978). The emission source ranges were chosen from sampling methodologies that used active sampling approaches, as it has been documented that passive samplers result in a $\delta^{15}N\text{-}NH_3$ bias and could potentially be unreliable (Pan *et al*., 2020; Walters *et al*., 2020; Kawashima *et al*., 2021). For the

marine signature, we utilize Jickells *et al*.'s (2003) values associated with aerosol samples collected in remote marine environments, though we note this is also consistent with a marine rainwater study (Altieri *et al*., 2014). The biomass burning signature is inferred from the ammonium aerosol data in Freyer (1978) who measured the nitrogen in coal that derives from biomass burning. There are no robust actively collected biomass burning signatures for δ^{15}N-NH_3.

Global anthropogenic NH_3 emission data retrieval

Anthropogenic NH_3 emission data was retrieved from McDuffie *et al*. (2020) who updated the open-source Community Emissions Data System (CEDS; Hoesly *et al*., 2019) to develop a new global emission inventory, CEDSGBD-MAPS (https://doi.org/10.5281/zenodo.3754964). It contains global anthropogenic emission data of atmospheric pollutants from sector- and fuel-specific sources from 1970–2017. Sector sources include agriculture, energy, industry, on road transportation, off road transportation, residential combustion, commercial combustion, other combustion, solvents, waste, and international shipping. Emissions were considered over an area of contribution based on the potential source contribution maps (see results section). This was done for 2015, 2016, and 2017 to calculate the percentage of different anthropogenic sources contributing to the study site.

Results

Species Concentrations

NH_4^+ concentrations varied seasonally ($p < 0.05$), with a high in winter (2.77 ± 1.06 $\mu g/m^3$) and a low in autumn (0.74 ± 0.55 $\mu g/m^3$; Figure 2). Winter had the largest variability, and summer had the least, with autumn and spring being transitions between the two. (Note that

blanks were below or near detection limits for N species and were not subtracted from the sample concentrations.).

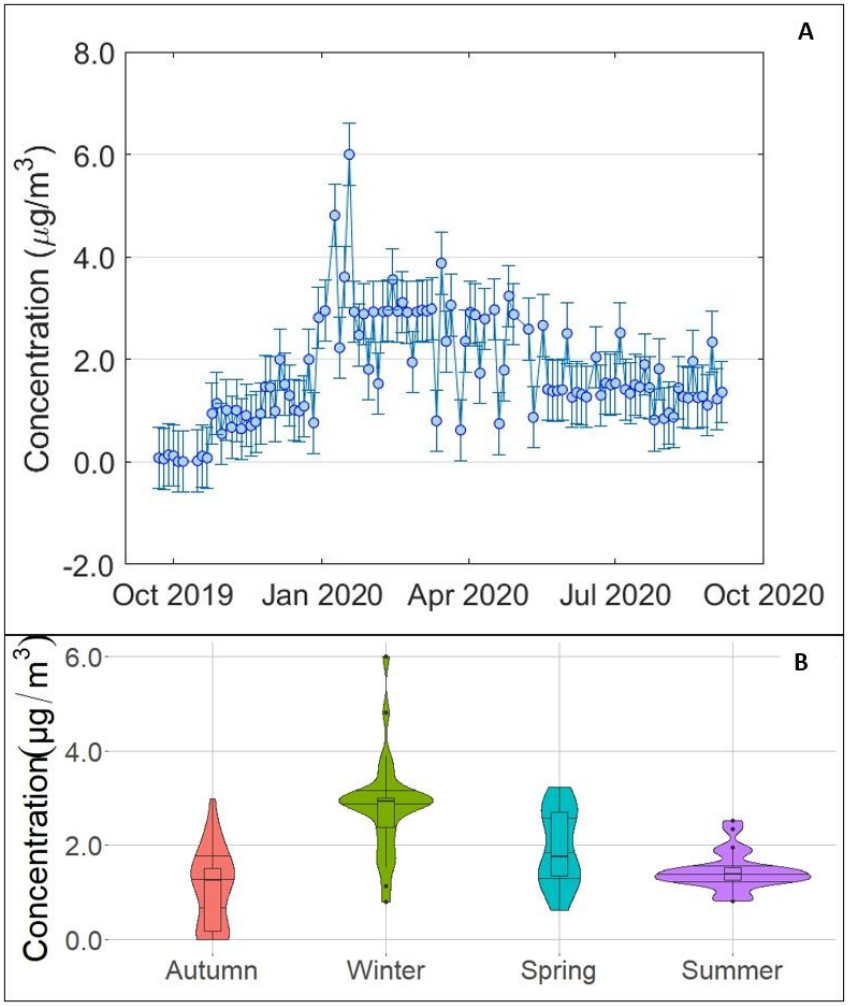

Figure 2: (A): Time series of NH_4^+ concentration (μg/m^3). Error bars (A) represent the pooled standard deviation for the concentration measurement technique. (B): Violin plot of NH_4^+ concentration (μg/m^3) by season (n = 28 (autumn), n = 30 (winter), n = 24 (spring), n = 26 (summer)).

All measured ions (Mg^{2+}, K^+, Na^+, NH_4^+, NO_3^-, Cl^-, SO_4^{2-}) had the highest average concentrations in the winter except Ca^{2+} which was highest in the spring (Table 1; Figure 3). Additionally, most measured ions (Ca^{2+}, Mg^{2+}, K^+, Na^+, Cl^-) had the lowest concentrations in the

summer except NH_4^+, NO_3^-, and SO_4^{2-}, which was lowest in the autumn. Overall, Mg^{2+} and K^+ had the lowest average annual concentrations compared to the rest (0.32 ± 0.36 µg/m^3 and 0.52 ± 1.10 µg/m^3, respectively), whereas NO_3^- and Na^+ had the highest annual average concentrations overall (3.82 ± 3.83 µg/m^3 and 3.40 ± 3.78 µg/m^3, respectively). Furthermore, all ions were significantly different amongst seasons ($p < 0.05$). A majority (> 55%) of the NO_2^- concentrations were at or below detection limit and therefore no NO_2^- data was included. For field blanks, %N was below the limits of detection; filter blanks were also run for the full suite of ions and chemical species where Ca^{2+}, Mg^{2+}, and SO_4^{2-} were found to be <5%. Na^+, K^+, and Cl^- appear to be contaminated as their "blank" values were unreasonably high compared to sample concentrations. Therefore, the samples were not blank-corrected.

Table 1: Average concentrations (µg/m^3 ±1σ) of measured elements and ions by season and annually.

	Autumn average (µg/m^3)	*n*	Winter average (µg/m^3)	*n*	Spring average (µg/m^3)	*n*	Summer average (µg/m^3)	*n*	Annual average (µg/m^3)
Ca^{2+}	0.77 ± 0.84	30	2.54 ± 3.34	31	2.66 ± 2.67	26	0.69 ± 0.37	16	1.76 ± 2.48
Mg^{2+}	0.23 ± 0.26	30	0.47 ± 0.43	31	0.37 ± 0.39	26	0.11 ± 0.07	16	0.32 ± 0.36
K^+	0.21 ± 0.23	30	1.03 ± 1.84	31	0.43 ± 0.36	26	0.20 ± 0.11	16	0.52 ± 1.10
Na^+	1.84 ± 2.28	30	5.39 ± 4.22	31	4.02 ± 4.44	26	1.35 ± 0.63	16	3.40 ± 3.78
NH_4^+	0.74 ± 0.55	28	2.77 ± 1.06	30	1.93 ± 0.80	24	1.43 ± 0.41	26	1.73 ± 1.07
NO_3^-	1.07 ± 1.03	30	6.20 ± 4.46	31	5.16 ± 4.38	29	2.64 ± 1.14	26	3.82 ± 3.83
Cl-	2.31 ± 3.05	28	4.72 ± 4.12	31	2.35 ± 4.49	26	0.68 ± 0.39	16	2.80 ± 3.83
SO_4^{2-}	0.80 ± 0.71	28	4.11 ± 2.85	31	3.11 ± 2.32	25	1.52 ± 0.29	16	2.52 ± 2.40

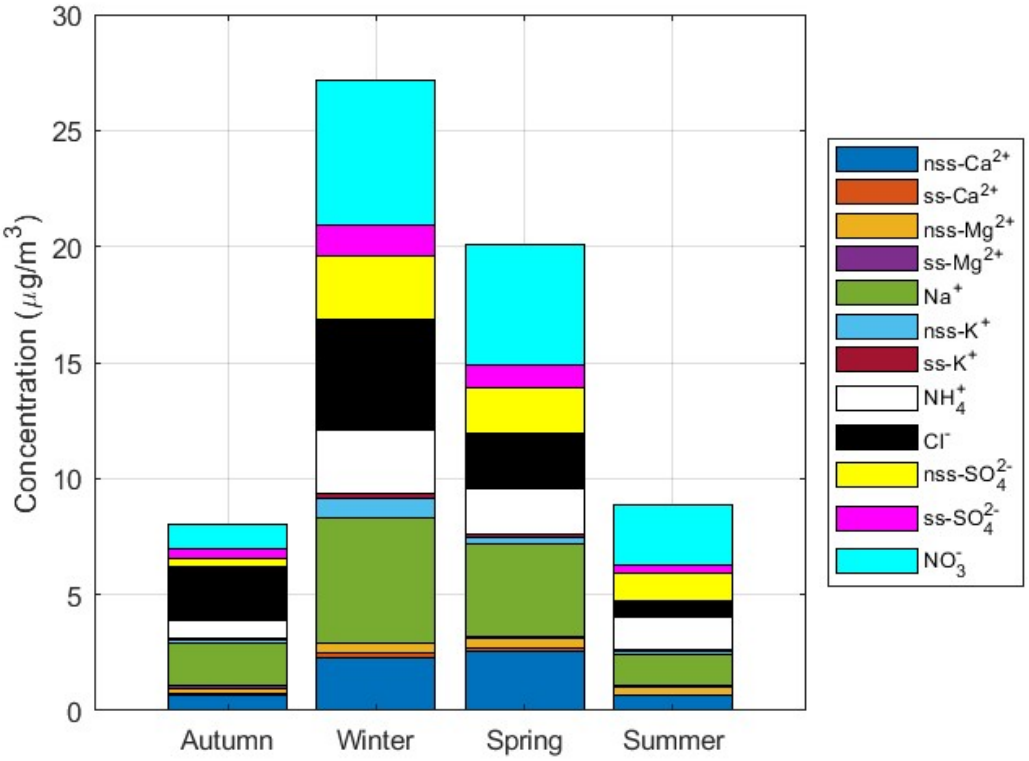

Figure 3: Stacked bar graph of species concentration changes among the four seasons (autumn, winter, spring, summer).

The NH_4^+ concentrations found in this study (annual average of 1.7 ± 1.1 µg/m^3; Table 1) are lower compared to Zhang *et al*. (2013), who studied aerosol NH_4^+ concentrations over the Yellow Sea and the East China Sea during autumn. They measured an average of 4.6 ± 2.2 µg/m^3 over the Northern Yellow Sea and 3.1 ± 2.8 µg/m^3 over the Southern Yellow Sea and East China Sea. In the open ocean of the Western North Pacific Ocean (as far east as ~140°E, 6°N), Xiao *et al*. (2018) reported an average NH_4^+ concentration of 0.2 ± 0.5 µg/m^3 in aerosol samples during the winter. Compared to our study, these values from Xiao *et al*. (2018) represent a higher percentage of marine air mass back trajectories and therefore showed more marine origins.

Non-sea salt values

Further indicative of terrestrial/anthropogenic inputs is the fraction of non-sea salt (nss) values for various ions. The nss values were calculated based on: $nss\text{-}X = X_{aerosol} - (X/Na)_{seawater} \times Na_{aerosol}$, where the mass ratios of $(X/Na)_{seawater}$ for SO_4^-, K^+, Ca^{2+}, and Mg^{2+} were 0.2515, 0.03701, 0.03821 and 0.012, respectively (Millero, 2006; Nah *et al*., 2021). All seasons were observed to have nss values > 55%, with the majority > 70% (Table 2).

Table 2: Average fraction of non-sea-salt values (% ±1σ) by season.

	Autumn	Winter	Spring	Summer
	Average (%)	Average (%)	Average (%)	Average (%)
fnss_Ca^{2+}	91.9 ± 5.4	89.8 ± 6.9	93.7 ± 4.1	92.0 ± 3.0
fnss_Mg^{2+}	90.6 ± 2.9	85.6 ± 5.0	85.9 ± 6.03	83.6 ± 5.5
fnss_K^+	69.0 ± 15.5	70.07 ± 16.6	68.24 ± 14.1	73.0 ± 7.2
fnss_SO_4^{2-}	56.2 ± 27.2	68.6 ± 13.6	70.8 ± 16.3	78.3 ± 7.4

Zhang *et al*. (2013) measured Ca^{2+}, K^+, and SO_4^{2-} in Ningbo, China, and calculated their nss values. Higher ratios of nss-SO_4^{2-}, nss-K^+, and nss-Ca^{2+} (all >70%) were detected in fine mode ($PM_{1.1-2.1}$), indicating that most particles originated from terrestrial sources (Zhang *et al*., 2013). Xiao *et al*. (2018) analyzed total suspended particulates (e.g., not size-segregated) and also calculated the nss values of Ca^{2+}, Mg^{2+}, K^+, and SO_4^{2-} during winter in the Western North Pacific Ocean. They found that nss-Mg^{2+} was only 13.1±6.9% of the total Mg^{2+}, with nss-Mg^{2+} typically being considered a crustal-derived ion in continental studies (Dueñas *et al*., 2012; Xiao *et al*., 2018). Nss-Ca^{2+} was higher at 41.8 ± 17.0% whereas the fraction of nss-SO_4^{2-}comprised 39.7% of total SO_4^{2-} in the samples. It was further observed that continental SO_4^{2-} can be carried to and impact the open ocean (Xiao *et al*., 2018).

Species Correlations

Pearson correlation values were calculated seasonally between each element and ion (Tables S1A-D) to investigate crustal versus marine sources. For all four seasons, Na^+ and Cl^-, Na^+ and ss-SO_4^{2-}, and Mg^{2+} (ss- and nss-) and ss-SO_4^{2-} were strongly positively correlated ($R \geq 0.70$). Na^+ and Mg^{2+} (ss- and nss-) were also strongly positively correlated during each season ($R > 0.85$), as well as Cl^- and ss-Mg^{2+} ($R \geq 0.70$). Furthermore, Cl^- and ss-SO_4^{2-} were strongly positively correlated for each season ($R > 0.70$). Overall, these strong relationships are not surprising, as they are ions derived from sea salt. Nss-K^+, nss-Ca^{2+} and nss-Mg^{2+} also are moderately or strongly correlated throughout the seasons (Tables S1A-D), which are indicative of crustal (terrestrial) sources (Dueñas *et al*.,2012; Xiao *et al*., 2013; Xiao *et al*., 2017; Xiao *et al*., 2018).

When looking at the nitrogen species, NH_4^+ and NO_3^- both had a strong correlation with nss-SO_4^{2-} in autumn ($R > 0.65$; Table S1A). Moderate correlations in autumn include NH_4^+ and nss-Ca^{2+} ($R = 0.45$) as well as NO_3^- with Ca^{2+} (ss- and nss-), Mg^{2+} (ss- and nss-), Na^+, Cl^-, and NH_4^+ ($R > 0.40$; Table S1A). No strong or moderate correlations were observed in winter, except NO_3^- and nss- Ca^{2+} ($R=0.41$; Table S1B). NH_4^+ and NO_3^- were strongly correlated in the spring ($R = 0.62$, Table S1C), and NH_4^+ was moderately correlated with nss-SO_4^{2-} ($R = 0.43$; Table S1C). The summer season is interesting due to the negative correlations observed that are not present in the other seasons. NH_4^+ was strongly negatively correlated with ss-Ca^{2+}, Mg^{2+} (ss- and nss-), ss-SO_4^{2-}, ss-K^+ and Na^+ ($R > -0.60$; Table S1D). Moderate correlations include NH_4^+ with nss-Ca^{2+}, nss-K^+, and Cl^- ($R > -0.40$). Additionally, NO_3^- was moderately negatively correlated with ss-K^+, ss-SO_4^{2-}, ss-Ca^{2+}, ss-Mg^{2+}, Na^+, and Cl^- ($R = -0.56$ to -0.59; Table S1D).

$\delta^{15}N\text{-}NH_4^+$ values were also checked for potential correlations between the measured species. During autumn, $\delta^{15}N\text{-}NH_4^+$ was strongly negatively correlated with nss-SO_4^{2-} ($R = -0.63$)

and NH_4^+ concentration (R = -0.67), and moderately negatively correlated with NO_3^- (R = -0.47). For every season besides autumn, $\delta^{15}N\text{-}NH_4^+$ remained moderately or strongly correlated with nss-Ca^{2+} (R > 0.50). For example, in Spring, $\delta^{15}N\text{-}NH_4^+$ was moderately positively correlated with nss-Ca^{2+} (R = 0.52) and moderately negatively correlated with NH_4^+ (R= -0.54). In summer, $\delta^{15}N\text{-}NH_4^+$ was strongly positively correlated with Na^+ and Cl^- (R > 0.60) and negatively correlated with NO_3^- (R = -0.65).

Air mass back trajectories

Although seasonally different, the air mass origins of the aerosol samples were predominantly continental (Figure S1A-D). For autumn, winter, and spring, the air masses were continental in origin, with both medium and long-range transport and a majority coming from the Northwest (Figure S1A-C). During the summer, a fraction of the air masses came from the marine system, with the remaining from the continent, both as medium and long-range transportation (Figure S1D).

The air mass back trajectories and concentration data were further used to create potential source contribution function (PSCF) maps per season (Figure 4A-D). The PSCF analysis shows that for all four seasons, the primary source region for NH_3 is fairly local to the study site, with autumn (Figure 4A) and summer (Figure 4D) showing a larger geographical footprint.

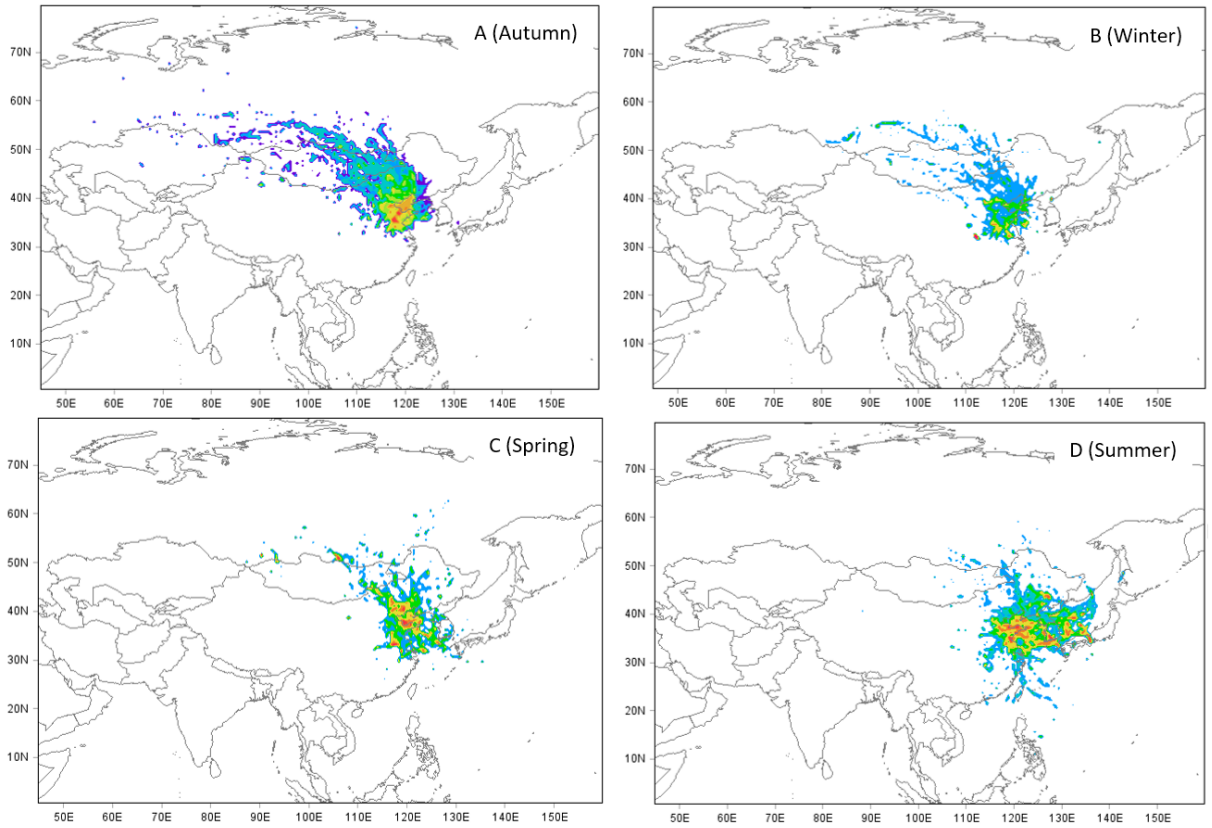

Figure 4: Potential source contribution function analysis by season (A = Autumn, B = Winter, C = Spring, D = Summer), with warmer colors (red, orange, yellow) representing greater relative impact of source locations versus cooler colors (green, blue, purple) representing lower relative contributions to the measured ammonium concentrations at Changdao Island.

Observed NH_4^+ isotopes.

The NH_4^+ isotope values fall in the range of -10.4‰ to 39.7‰ (Figure 5A). Very small variability is present in autumn but increases with the remaining seasons, with the largest in winter (Figure 5B). NH_4^+ isotope values were different seasonally ($P < 0.05$), with higher values in spring (13.3 ± 7.9‰) and summer (15.6 ± 6.2‰) compared to autumn (3.2 ± 2.5‰) and winter (3.8 ± 11.4‰).

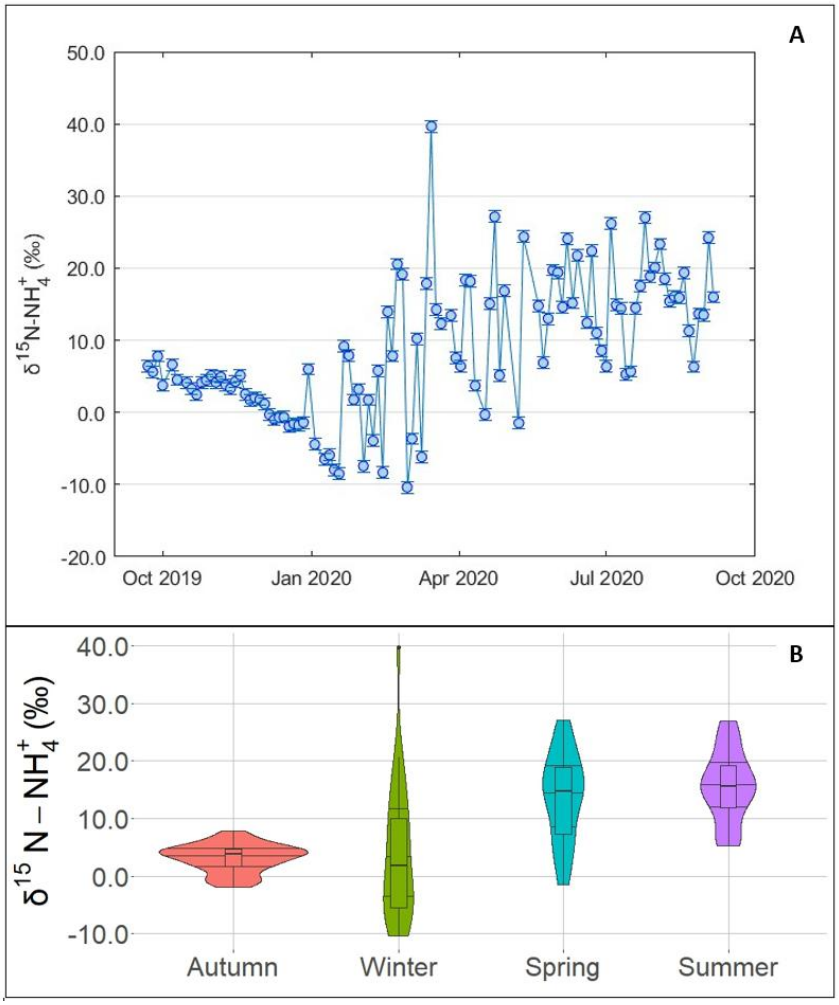

Figure 5: (A): Time series of NH_4^+ isotope values (‰). Error bars (A) represent the pooled standard deviation for the isotopic measurement technique. (B): Violin plot of NH_4^+ isotope values (‰) by season (n = 28 (autumn), n = 29 (winter), n = 25 (spring), n = 26 (summer)).

As stated, autumn has minimal variation compared to the other seasons. This could be due to the different sampling periods, as the aerosol samples in autumn were collected for 72 hours, whereas in the other seasons collection periods were either 48 or 24 hours. The shorter sampling periods are likely the cause for increased variation.

Calculated $NH_{3(g)}$ isotopes

Based on ISORROPIA-II, excess $NH_{3(g)}$ was always present (n=81), which is comparable to Nenes *et al*. (2021) who discusses the recent buildup of $NH_{3(g)}$ in China. Additionally, pH was calculated to fall between 6-8, which is consistent with a system that has a surplus of $NH_{3(g)}$. Given the excess of $NH_{3(g)}$, the influence of equilibrium isotopic fractionation on NH_4^+ is large. Seasonally, the average fractionation (ε; see eq. 1 and 3) was 37.35 ± 1.10 for autumn, 38.93 ± 0.78 for winter, 36.85 ± 0.93 for spring, and 35.36 ± 0.35 for summer. Calculated $NH_{3(g)}$ isotope values were different seasonally ($p < 0.05$) with higher values in summer (-19.73 ± 6.28‰) and spring (-23.67 ± 8.30‰) compared to winter (-35.16 ± 11.64‰) and autumn (-34.25 ± 3.41). However, individually calculated ε values were subtracted from each sample (e.g., not the seasonal average).

Isotope Mixing Model Results

Based on SIMMR, $NH_{3(g)}$ from agriculture was consistently the greatest source contribution in each season (all > 65%; Figure 6), with a maximum in the summer, and minimum in winter. Industrial fuel combustion was consistently the second highest source, with a maximum in winter, and minimum in summer. The remaining sources were all <10% individually for all seasons.

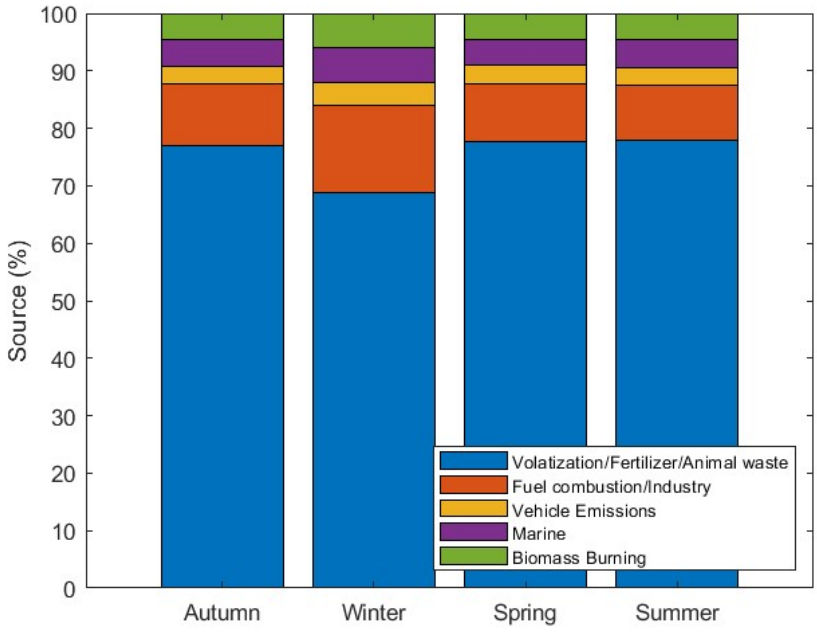

Figure 6: Stacked bar graph of probable NH_3 source contributions among the four seasons (calculated by SIMMR).

Discussion

NH_4^+ is an alkaline species known for forming haze, with the Northern China Plain (in close proximity to the current study site) being one of the greatest atmospherically polluted regions in China (NH_3, sulfuric acid, nitric acid, ammonium sulfate, ammonium hydrogen sulfate, etc; Xiang *et al*., 2022). During the 2020 expanded Chinese Lunar New Year celebration (January 24 to February 10), China was in a never-before-seen state of shutdown, due to the majority of people being contained in their homes to limit the spread of the novel coronavirus disease (COVID-19, Chang *et al*., 2020). Yet, widespread haze pollution still arose over Eastern China during this time (Chang *et al*., 2020). This time period overlapped with the current study, where [NH_4^+] was highest in the winter, supporting the strong relationship between NH_4^+ and haze formation and most likely explaining the winter maximum in the dataset. Additionally, the

higher nitrate and sulfate concentrations also found in winter (Figure 3) will favor more NH_4^+(p) formation relative to $NH_{3(g)}$ (Seinfeld and Pandis, 2016). Overall, our observations of the particulate matter exported to the ocean largely supports crustal/anthropogenic origins (species concentrations in Table 1, nss calculations in Table 2, and species correlations in Tables S1A-D).

The average δ^{15}N-NH_4^+ (and calculated δ^{15}N-NH_3) values were lowest in the winter (Figure 5) due to the high number of negative values present. Overall, the seasonal changes in the δ^{15}N values were not explained by changes in chemistry or the partitioning of ammonia/ammonium, based on the fractionation calculations and neutralization ratios (ISORROPIA output). These wintertime measurements roughly overlap with the COVID-19 lockdown in China, although different regions enacted different restrictive measures based on the number of cases in the area (Chen *et al*., 2020). It is suggested that agricultural activities did not slow down dramatically, but vehicles (including public transportation) greatly decreased and there was a slight reduction in industrial production (Chen *et al*., 2020), potentially explaining the lower δ^{15}N in the winter compared to other seasons since vehicles are the only positive δ^{15}N-NH_3 source. Therefore, one might expect in a different year, with no lockdown, that vehicles might be a greater contributor than observed in this study.

The SIMMR model results (Figure 6) predict a dominant signal from agricultural emissions (including volatilization, animal husbandry and use of fertilizers), however, the similarity in the isotopic ranges for industry and agriculture mean that these two sources are both strong levers on the predicted probability in a way that can be difficult to distinguish using this modeling technique. Another variable that is difficult to distinguish using this modeling technique is when two sources have similar ranges (e.g., marine and biomass burning). Therefore, the model cannot separate these sources well. However, marine sources and biomass

burning are shown to have minimal impact on our study site, both indicated by SIMMR as well as other tools used in this study (correlation tests, emission inventories, etc). Therefore, even though SIMMR cannot separate these two sources well, we are confident they are not major contributors to our site. This mixing model approach also does not consider changes in physical drivers of ammonia dynamics such as seasonal weather, soil pH, land/water type, etc. Still, several lines of evidence support agricultural emissions as an important driver of the NH_4^+ signals, particularly during our collection period.

He *et al*. (2021) implemented a machine learning technique to assess the effect of the Spring Festival and COVID-19 on NH_3 emissions in the North China Plain, where they estimated a larger decrease in NH_3 concentrations in urban areas compared to rural areas. Xu *et al*. (2022) studied changes in NH_3 due to the lockdown enforcements in China, where they used surface NH_3 measurements, satellite NH_3 observations, and GEOS-Chem simulations. Contrasting with He *et al*., Xu *et al*. reported an overall rise in NH_3 emissions, but with the increase being most distinct at rural sites, where concentrations were higher during COVID-19 in 2020 than the equivalent periods in earlier years. Specifically in northern China, the NH_3 increase is thought to be mainly driven by increased agricultural practices. Overall, the Chen *et al*., He *et al*., and Xu *et al*. studies lend support for decreased emissions from vehicles and industry relative to agricultural activities, including animal husbandry.

To test the sensitivity of the SIMMR results, which were dependent on the extent of fractionation factors calculated using the predicted ISORROPIA [NH_3] gas outputs from ISORROPIA, we changed the fraction of [NH_3] (and therefore the fractionation) by 10%, 20% and 30%. This changed the δ^{15}N-NH_3 that was then input into SIMMR. Even with a 20% error in fractionation, agricultural activities were still the dominant source in all seasons. Only with a

30% change in fractionation did we see an important change in results, with industry becoming a larger source contribution than agriculture in summer. While uncertainties in both the ISORROPIA results and SIMMR results remain, overall the sensitivity tests build confidence in the hypothesis that agricultural activities dominate NH_4^+ in the region.

Several additional lines of evidence support the importance of agriculture/agricultural emissions. Eastern China, near the study site, is a mix of farmland and urban areas. Pan *et al* (2018) identified different NH_3 hotspots (> 1 $\mu g/m^3$) in this area based upon a year-round observational network, utilizing a passive NH_3 monitoring network based on a diffusive technique with monthly integrated measurements at 53 locations. They considered the connections between hot spots and six different types of land use: desert, farmland, grassland, mountain and forest, urban, and waterbody. When comparing the PSCF (Figure 4A-D) results from this study to the hotspots identified by Pan *et al*. (2018) by season, we find that autumn and spring are most heavily influenced by farmlands, winter is a mix of farmlands and urban areas, and while summer overlaps with farmlands as well, it is the only season that includes noticeable transport from the ocean. (Note that airmasses from the ocean do not have to carry significant marine-based NH_4^+).

The majority of the aerosol composition of the samples is sourced from nss derived ions (Tables S1A-D), therefore, the marine air masses observed in the summer likely explain the lower concentrations seen during this season (Table 1). This is additionally consistent with the $CEDS_{GBD\text{-}MAPS}$ emissions inventory, which also identifies agriculture (non-combustion sources only (e.g., excludes open fires)) as the main NH_3 emission source to this region. For the years 2015-2017, agricultural activities comprised roughly 77.3 ± 0.2% of NH_3 emissions on an annual basis, with the greatest contributions observed in spring (86.4 ± 0.1%). The wintertime emissions

inventory only calculated a contribution of 51.2 ± 0.4% from agricultural emissions, which may be underestimated based on the isotopic results of the current study, which suggests agriculture accounts for roughly 65% of the NH_3 emissions in winter (Figure 6). However, it is possible that the discrepancy in these values stems from the timing of the current study, during the COVID-19 lockdown, which resulted in a decrease in transportation activities, and could have therefore resulted in a higher agricultural signal than other years.

The Yellow Sea is bordered by the three peninsulas (the Liaodong peninsula, Shandong peninsula, and Korea peninsula), all well populated and industrialized, making the Northern Yellow Sea vulnerable to anthropogenic input, which dominates based on the ion budgets year-round (e.g., nss values for the measured species are always > 55% (Table 2)). This is further supported by the calculated air mass back trajectories, in which the majority of samples originated from the continent (Figure S1A-D). The PSCF analysis (Figure 4A-D), SIMMR results (Figure 6), and the $CEDS_{GBD\text{-}MAPS}$ emissions inventory support agriculture as the primary source contribution compared to other potential sources.

Conclusion

Conflicts in the literature reveal uncertainty regarding source origins of N deposited to the open ocean, making it difficult to determine continental/anthropogenic or marine/natural sources as the dominant input. This study aims to help bridge that gap in understanding by quantifying the influence of anthropogenic emissions of reactive N on the atmospheric composition of aerosols and sources of aerosol NH_4^+, with a focus on seasonal trends.

Strong seasonal trends ($p < 0.05$) were found in the aerosol composition as well as the $\delta^{15}N\text{-}NH_4^+$ and $\delta^{15}N\text{-}NH_{3(g)}$ values. NH_4^+ concentrations varied with a high in winter (2.83 ± 1.00 $\mu g/m^3$) and low in autumn (1.11 ± 0.83 $\mu g/m^3$). The other measured elements and ions

(Mg^{2+}, K^+, Na^+, NH_4^+, NO_3^-, Cl^-, SO_4^{2-}) also had the highest concentrations in the winter except $Ca^{2+,}$ which was highest in the spring. Additionally, other measured elements and ions (Ca^{2+}, Mg^{2+}, K^+, Na^+, Cl^-) had the lowest concentrations in the summer except NO_3^-, and SO_4^{2-} which were lowest in the autumn. Furthermore, the annual fraction of nss values for Ca^{2+}, Mg^{2+}, K^+, and SO_4^{2-} were all high (> 65%). $\delta^{15}N\text{-}NH_4^+$ had higher values in spring (13.3 ± 7.9‰) and summer (15.6 ± 6.2‰) compared to autumn (3.2 ± 2.5‰) and winter (3.8 ± 11.4‰). $NH_{3(g)}$ isotope values also had higher values in summer (-19.7 ± 6.3‰) and spring (-23.67 ± 8.3‰) compared to winter (-35.2 ± 11.6‰) and autumn (-34.3 ± 3.4‰). This data, together with the air mass back trajectories, provide evidence for continental origins of NH_4^+ deposition primarily as a result of anthropogenic agricultural activities (volatilization/animal waste/fertilizer) throughout the year. Given the anthropogenic origin of NH_4^+ and its bioavailability, the results from this study should be further interpreted within the context of total inorganic and organic wet and dry N deposition to the NPO. It is crucial to bridge the gap in understanding of the impact of anthropogenic and marine sources on reactive N deposition to better determine the drivers of biogeochemical changes in the open ocean.

Acknowledgements

This research was funded by the National Science Foundation (NSF-OCE #1851343). Additionally, the authors thank Joe Orchardo at Brown University for his aid in running the ICP as well as Ruby Ho (lab manager for the Hastings lab) for instrumental support.

Competing interests

The authors acknowledge that there are no competing interests that conflict with this work.

Data availability

To obtain the data used in this study, go to https://doi.org/10.7910/DVN/P9ILX3. This data will be made public upon publication.

References

Altieri, K.E., Fawcett, S.E., Hastings, M.G. 2021. Reactive nitrogen cycling in the atmosphere and ocean. Annual Reviews, 49, 523-550.

Altieri, K.E., Fawcett, S.E., Peters, A.J., Sigman, D.M., Hastings, M.G. 2016. Marine biogenic source of atmospheric organic nitrogen in the subtropical North Atlantic. PNAS, 113(4), 925-930.

Altieri, K.E., Hastings, M.G., Gobel, A.R., Peters, A.J., Sigman, D.M. 2013. Isotopic composition of rainwater nitrate at Bermuda: The influence of air mass source and chemistry in the marine boundary layer. Journal of Geophysical Research: Atmospheres, 118(19).

Altieri, K.E., Hastings, M.G., Peters, A.J., Oleynik, S., Sigman, D.M. 2014. Isotopic evidence for a marine ammonium source in rainwater at Bermuda. Global Biogeochemical Cycles, 28(10), 1066-1080.

Böhlke, J.K., Coplen, T.B. 1995. Interlaboratory comparison of reference materials for nitrogen-isotope-ratio measurements, reference and intercomparison materials for stable isotopes of light elements. Vienna, Austria, 1993. In: Proceedings of the IAEA-TECDOC-825 Consultants Meeting.

Böhlke, J.K., Gwinn, C.J., Coplen, T.B. 1993. New reference materials for nitrogen-isotope-ratio measurements. Geostand. Geoanal. Res., 17, 159–164.

Chang, Y., Huang, R.-J., Ge, X., Huang, X., Hu, J., Duan, Y., Zou, Z., Liu, X., Lehmann, F. 2020. Puzzling Haze Events in China During the Coronavirus (COVID-19) Shutdown. Geophysical Research Letters, 47.

Chen, H., Huo, J., Fu, Q., Duan, Y., Xiao, H., Chen, J. 2020. Impact of Quarantine Measures on Chemical Compositions of PM2.5 during the COVID-19 Epidemic in Shanghai, China. Science of The Total Environment, 743.

Cooper, R.J., Krueger, T., Hiscock, K.M., Rawlins, B.G. 2014. Sensitivity of fluvial sediment source apportionment to mixing model assumptions: a Bayesian model comparison. Water Resour Res, 50, 9031–9047.

Cornell, S.E., Jickells, T.D., Cape, J.N., Rowland, A.P., Duce, R.A. 2003. Organic nitrogen deposition on land and coastal environments: A review of methods and data. Atmos. Environ., 37(16), 2173–2191.

Duce, R.A., LaRoche, J., Altieri, K., Arrigo, K.R., Baker, A.R., Capone, D.G., Cornell, S., *et al*. 2008. Impacts of Atmospheric Anthropogenic Nitrogen on the Open Ocean. Science, 320(5878), 893–897.

Dueñas, C., Fernández, M.C., Gordo, E., Cañete, S., Pérez, M. 2012. Chemical and radioactive composition of bulk deposition in Málaga (Spain). Atmos. Environ., 62, 1–8.

Elser, J., Andersen, T., Baron, J., Bergstrom, A.-K., Jansson, M., Kyle, M., Nydick, K., Steger, L., Hessen, D. 2009. Shifts in Lake N:P Stoichiometry and Nutrient Limitation Driven by Atmospheric Nitrogen Deposition. Science, 326(5954), 835-837.

Fountoukis, C., Nenes, A. 2007. ISORROPIA II: a computationally efficient thermodynamic equilibrium model for K+–Ca2+–Mg2+–NH+4 –Na+–SO2−4 –NO−3 –Cl−–H2O aerosols. Atmos. Chem. Phys., 7, 4639–4659.

Frank, D.A., Evans, R.D., Tracy, B.F. 2004. The role of ammonia volatilization in controlling the natural 15N abundance of a grazed grassland. Biogeochemistry, 68, 169–178.

Freyer, H. D. 1978. Seasonal trends of NH4+ and NO3− nitrogen isotope composition in rain collected at Jülich, Germany. Tellus, 30, 83–92.

Galloway, J.N., Dentener, F.J., Capone, D.G., Boyer, E.W., Howarth, R.W., Seitzinger, S.P., Asner, G.P., *et al*. 2004. Nitrogen Cycles: Past, Present, and Future. Biogeochemistry, 70(2), 153–226.

Galloway, J.N., Keene, W.C., Artz, R.S., Miller, J.M., Church, T.M., Knap, A.H. 1989. Processes controlling the concentrations of SO4=, NO3-, NH4+, H+, HCOOT and CH3COOT in precipitation on Bermuda. Tellus B, 41B(4), 427–443.

Galloway, J. N., Keene, W.C., Likens, G.E. 1996. Processes controlling the composition of precipitation at a remote southern hemispheric location: Torres del Paine National Park, Chile. J. Geophys. Res., 101(D3), 6883–6897.

Galloway, J.N., Likens, G.E., Keene, W.C., Miller, J. M. 1982. The composition of precipitation in remote areas of the world. J. Geophys. Res., 87(NC11), 8771–8786.

Gobel, A.R., Altieri, K.E., Peters, A.J., Hastings, M.G. and Sigman, D.M. 2013. Insights into anthropogenic nitrogen deposition to the North Atlantic investigated using the isotopic composition of aerosol and rainwater nitrate. Geophysical Research Letters, 40(22), 5977-5982.

Gruber, N., Sarmiento, J.L. 1997. Global patterns of marine nitrogen fixation and denitrification. Global Biogeochemical Cycles, 11(2), 235-266.

Heaton, T.H.E. 1987. 15N14N ratios of nitrate and ammonium in rain at Pretoria, South Africa. Atmos. Environ., 21, 843–852.

He, Y., Pan, Y., Gu, M., Sun, Q., Zhang, Q., Zhang, R., Wang, Y. 2021. Changes of ammonia concentrations in wintertime on the North China Plain from 2018 to 2020. Atmospheric Research, 253, 105490.

Hristov, A.N., Zaman, S., Vander Pol, M., Ndegwa, P., Campbell, L., Silva, S. 2009. Nitrogen losses from dairy manure estimated through nitrogen mass balance and chemical markers. J. Environ. Qual., 38, 2438–2448.

Hoesly, R., O'Rourke, P., Braun, C., Feng, L., Smith, S. J., Pitkanen, T., Siebert, J., Vu, L., Presley, M., Bolt, R., Goldstein, B., Kholod, N. 2019. CEDS: Community Emissions Data System (Version Dec-23-2019), Zenodo.

Jickells, T.D., Buitenhuis, E., Altieri, K., Baker, A.R., Capone, D., Duce, R.A., Dentener, F., et al. 2017. A Reevaluation of the Magnitude and Impacts of Anthropogenic Atmospheric Nitrogen Inputs on the Ocean. Global Biogeochemical Cycles, 31(2), 289–305.

Jickells, T.D., Kelly, S.D., Baker, A.R., Biswas, K., Dennis, P.F., Spokes, L.J., Witt, M., Yeatman, S.G. 2003. Isotopic Evidence for a Marine Ammonia Source. Geophysical Research Letters, 30(7).

Johnson, K.S., Riser, S.C., Karl, D.M. 2010. Nitrate supply from deep to near-surface waters of the North Pacific subtropical gyre. Nature, 465(7301), 1062–1065.

Karl, D.M., Church, M.J., Dore, J.E., Letelier, R.M., Mahaffey, C. 2012. Predictable and efficient carbon sequestration in the North Pacific Ocean supported by symbiotic nitrogen fixation. Proceedings of the National Academy of Sciences, 109(6), 1842–1849.

Kim, I.-N., Lee, K., Gruber, N., Karl, D.M., Bullister, J.L.,Yang, S., Kim, T.-W. 2014. Increasing anthropogenic nitrogen in the North Pacific Ocean. Science, 346(6213), 1102-1106.

Kim, T.W., Lee, K., Najjar, R.G., Jeong, H.D., Jeong, H.J. 2011. Increasing N abundance in the northwestern Pacific Ocean due to atmospheric nitrogen deposition. Science, 334(6055), 505-509.

Knapp, A.N., Hastings, M.G., Sigman, D.M., Lipschultz, F., Galloway, J.N. 2010. The flux

and isotopic composition of reduced and total nitrogen in Bermuda rain. Marine Chemistry, 120(1), 83-89.
Kawashima, H., Ogata, R., Gunji, T. 2021. Laboratory-based validation of a passive sampler for determination of the nitrogen stable isotope ratio of ammonia gas. Atmos. Environ., 245, 118009.
Kurokawa, J., Ohara, T., Morikawa, T., Hanayama, S., Janssens- Maenhout, G., Fukui, T., Kawashima, K., Akimoto, H. 2013. Emissions of air pollutants and greenhouse gases over Asian regions during 2000–2008: Regional Emission inventory in Asia (REAS) version 2. Atmos. Chem. Phys., 13, 11019–11058.
Letscher, R.T., Primeau, F., Moore, J.K. 2016. Nutrient budgets in the subtropical ocean gyres dominated by lateral transport. Nature Geoscience, 9(11), 815-819.
Luo, X.S., Tang, A.H., Shi, K., Wu, L.H., Li, W.Q., Shi, W.Q., Shi, X.K., Erisman, J.W., Zhang, F.S., Liu, X.J. 2014. Chinese coastal seas are facing heavy atmospheric nitrogen deposition. Environ. Res. Lett., 9, 095007.
McDuffie, E.E., Smith, S.J., O'Rourke, P., Tibrewal, K., Venkataraman, C., Marais, E.A., Zheng, B., Crippa, M., Brauer, M., Martin, R.V. 2020. A global anthropogenic emission inventory of atmospheric pollutants from sector- and fuel-specific sources (1970–2017): an application of the Community Emissions Data System (CEDS). Earth Syst. Sci. Data, 12, 3413–3442.
Millero, F.J. 2006. Chemical Oceanography. 3rd ed. CRC Press, 496.
Nah, T., Yang, J., Wang, J., Sullivan, A.P., Weber, R.J. 2021. Fine Aerosol Acidity and Water during Summer in the Eastern North Atlantic. Atmosphere, 12(1040).
Nenes, A., Pandis, S.N., Kanakidou, M., Russell, A.G., Song, S., Vasilakos, P., Weber, R.J. 2021. Aerosol acidity and liquid water content regulate the dry deposition of inorganic reactive nitrogen. Atmos. Chem. Phys., 21, 6023–6033.
O'Dell, J.W. 1993. In: Method 350.1, Revision 2.0: Determination of Ammonia Nitrogen by Semi-automated Colorimetry. US EPA.
Pan, Y., Tian, S., Liu, D., Fang, Y., Zhu, X., Gao, M., Gao, J., Michalski, G., Wang, Y. 2018. Isotopic evidence for enhanced fossil fuel sources of aerosol ammonium in the urban atmosphere. Environmental Pollution, 238, 942–947.
Pan, Y., Gu, M., Song, L., Tian, S., Wu, D., Walters, W. W., Yu, X., Lü, X., Ni, X., Wang, Y. 2020. Systematic low bias of passive samplers in characterizing nitrogen isotopic composition of atmospheric ammonia. Atmos. Res., 243, 105018.
Pan, Y., Tian, S., Zhao, Y., Zhang, L., Zhu, X., Gao, J., Huang, W., Zhou, Y., Song, Y., Zhang, Q., Wang, Y. 2018. Identifying Ammonia Hotspots in China Using a National Observation Network. Environ. Sci. Technol., 52, 3926−3934.
Parnell A.C., Inger, R., Bearhop, S., Jackson, A.L. 2010. Source partitioning using stable isotopes: coping with too much variation. PLoS One (5),1–6.
Parnell, A.C., Phillips, D.L., Bearhop, S., Semmens, B.X., Ward, E.J., Moore, J.W., Jackson, A.L., Grey, J., Kelly, D.J., Inger, R. 2013. Bayesian stable isotope mixing models. Environmetrics, 24(6), 387-399.
Paulot, F., Ginoux, P., Cooke, W.F., Donner, L.J., Fan, S., Lin, M.-Y., Mao, J., Naik, V., Horowitz, L.W. 2016. Sensitivity of nitrate aerosols to ammonia emissions and to nitrate chemistry: implications for present and future nitrate optical depth. Atmos. Chem. Phys., 16, 1459–1477.
Quay, P., Peacock, C., Bjorkman, K., Karl, D. 2010. Measuring primary production rates in the

ocean: Enigmatic results between incubation and non-incubation methods at Station ALOHA. Global Biogeochemical Cycles, 24(3).
Ren, P., Luo, C., Zhang, H., Schiebel, H., Hastings, M.G., Wang, X. 2022. Atmospheric Particles Are Major Sources of Aged Anthropogenic Organic Carbon in Marginal Seas. Environ. Sci. Technol., 56, 14198−14207.
Rolph, G., Stein, A., Stunder, B. 2017. Real-time environmental applications and display sYstem: READY. Environ. Model. Software, 95, 210–228.
Russell, K.M., Galloway, J.N., Macko, S.A., Moody, J.L., Scudlark, J.R. 1998. Sources of nitrogen in wet deposition to the Chesapeake Bay region. Atmos. Environ., 32(14–15), 2453–2465.
Seinfeld J.H., Pandis, S.N. 2012. Atmospheric Chemistry and Physics: From Air Pollution to Climate Change. Hoboken, NJ: Wiley.
Seinfeld, J.H., Pandis, S.N., 2016. Atmospheric Chemistry and Physics: From Air Pollution to Climate Change. John Wiley & Sons.
Seitzinger, S.P., Harrison, J.A., Dumont, E., Beusen, A., Bouwman, A.F. 2005. Sources and delivery of carbon, nitrogen, and phosphorus to the coastal zone: An overview of Global Nutrient Export from Watersheds (NEWS) models and their application. Global Biogeochemical Cycles, 19(4).
Sigman, D.M., Fripiat, F. 2019. Nitrogen Isotopes in the Ocean. Academia, Encyclopedia of Ocean Sciences (Third Edition), 263-278.
Song, L., Walters, W.W., Pan, Y., Li, Z., Gu, M., Duan, Y., Lü, X., Fang, Y. 2021. 15N natural abundance of vehicular exhaust ammonia, quantified by active sampling techniques. Atmos. Environ., 255, 118430.
Stein, A.F., Draxler, R.R., Rolph, G.D., Stunder, B.J.B., Cohen, M.D., Ngan, F. 2015. NOAA's HYSPLIT atmospheric transport and dispersion modeling system. Bull. Am. Meteorol. Soc., 96, 2059–2077.
Walters, W.W., Chai, J., Hastings, M.G. 2019. Theoretical Phase Resolved Ammonia−Ammonium Nitrogen Equilibrium Isotope Exchange Fractionations: Applications for Tracking Atmospheric Ammonia Gas-to-Particle Conversion. ACS Earth Space Chem., 3, 79-89.
Walters, W.W., Song, L., Chai, J., Fang, Y., Colombi, N., Hastings, M.G. 2020. Characterizing the Spatiotemporal Nitrogen Stable Isotopic Composition of Ammonia in Vehicle Plumes. Atmospheric Chemistry and Physics, 20(19), 11551–11567.
Wang, Y. Q., Zhang, X. Y., Draxler, R. 2009. TrajStat: GIS-based software that uses various trajectory statistics analysis methods to identify potential sources from long-term air pollution measurement data. Environmental Modelling Software, 24, 938–939.
Xiang, Y.-K., Dao, X., Gao, M., Lin, Y.-C., Cao, F., Yang, X.-Y., Zhang, Y.-L. 2022. Nitrogen isotope characteristics and source apportionment of atmospheric ammonium in urban cities during a haze event in Northern China Plain. Atmospheric Environment, 269, 118800.
Xiao, H.-W., Xiao, H.-Y., Shen, C.-Y., Zhang, Z.-Y., Long, A.-M. 2018. Chemical Composition and Sources of Marine Aerosol over the Western North Pacific Ocean in Winter. Atmosphere, 9(298).
Xiao, H.W., Xiao, H.Y., Long, A.M., Wang, Y.L., Liu, C.Q. 2013. Chemical composition and source apportionment of rainwater at Guiyang, SW China. J. Atmos. Chem., 70, 269–281.

Xiao, H.W., Xiao, H.Y., Luo, L., Shen, C.Y., Long, A.M., Chen, L., Long, Z.H., Li, D.N. 2017. Atmospheric aerosol compositions over the South China Sea: temporal variability and source apportionment. Atmos. Chem. Phys., 17, 3199–3214.

Xu, W., Zhao, Y., Wen, Z., Chang, Y., Pan, Y., Sun, Y., Ma, X., Sha, Z., Li, Z., Kang, J., Liu, L., Tang, A., Wang, K., Zhang, Y., Guo, Y., Zhang, L., Sheng, L., Zhang, X., Gu, B., Song, Y., Damme, M.V., Clarisse, L., Coheur, P.-F., Collett, J.L., Goulding, K., Zhang, F., He, K., Liu, X. 2022. Increasing importance of ammonia emission abatement in PM2.5 pollution control. Science Bulletin, 67, 1745–1749.

Zhang, H.-H., Yang, G.-P., Liu, C.-Y., Su, L.-P. 2013. Chemical Characteristics of Aerosol Composition over the Yellow Sea and the East China Sea in Autumn. Journal of the Atmospheric Sciences, 70, 1784-1794.

Zhang, L., Altabet, M., Wu, T., Hadas, O. 2007. Sensitive Measurement of NH4+ 15N/14N (*d*15NH4+) at Natural Abundance Levels in Fresh and Saltwaters. Anal. Chem., 79, 5297-5303.

Zhao, Y., Zhang, L., Pan, Y., Wang, Y., Paulot, F., Henze, D.K. 2015. Atmospheric nitrogen deposition to the northwestern Pacific: seasonal variation and source attribution. Atmos. Chem. Phys, *15*(9), 13657-13703.

Supporting Information

Table S1A: Pearson correlation among species and isotopes (autumn dataset; P < 0.05 are bolded, * indicates P < 0.10).

	nss-Ca^{2+}	ss-Ca^{2+}	nss-Mg^{2+}	ss-Mg^{2+}	nss-K^{+}	ss-K^{+}	nss-SO_4^{2-}	ss-SO_4^{2-}	Na^{+}	Cl^{-}	NO_2^{-}	NO_3^{-}	NH_4^{+}	$\delta^{15}N$-NH_4^{+}
nss-Ca^{2+}	-	-	-	-	-	-	-	-	-	-	-	-		-
ss-Ca^{2+}	**0.85**	-	-	-	-	-	-	-	-	-	-	-	-	-
nss-Mg^{2+}	**0.88**	**0.97**	-	-	-	-	-	-	-	-	-	-	-	-
ss-Mg^{2+}	**0.80**	**0.96**	**0.97**	-	-	-	-	-	-	-	-	-	-	-
nss-K^{+}	**0.43**	**0.41**	**0.57**	**0.62**	-	-	-	-	-	-	-	-	-	-
ss-K^{+}	**0.80**	**0.96**	**0.97**	**1.00**	**0.62**	-	-	-	-	-	-	-	-	-
nss-SO_4^{2-}	0.29	0.18	0.24	0.18	**0.40**	0.18	-	-	-	-	-	-	-	-
ss-SO_4^{2}	**0.57**	**0.84**	**0.79**	**0.80**	0.25	**0.80**	*0.36**	-	-	-	-	-	-	-
Na^{+}	**0.80**	**0.96**	**0.97**	**1.00**	**0.62**	**1.00**	0.18	**0.80**	-	-	-	-	-	-
Cl^{-}	**0.82**	**0.93**	**0.90**	**0.93**	**0.77**	**0.93**	**0.42**	**0.93**	**0.93**	-	-	-	-	-
NO_2^{-}	0.02	-0.24	-0.20	-0.30	-0.13	-0.30	0.17	-0.23	-0.30	-0.28	-	-	-	-
NO_3^{-}	**0.49**	**0.46**	**0.54**	**0.41**	0.24	**0.41**	**0.68**	**0.49**	**0.41**	**0.44**	-0.03	-	-	-
NH_4^{+}	**0.45**	*0.37**	**0.39**	0.31	0.20	0.31	**0.77**	*0.34**	0.31	*0.34**	0.36	**0.59**	-	-
$\delta^{15}N$-NH_4^{+}	0.02	0.08	0.07	0.09	-0.03	0.09	**-0.63**	0.02	0.09	0.05	-0.15	**-0.47**	**-0.67**	-

Table S1B: Pearson correlation among species and isotopes (winter dataset; P < 0.05 are bolded, * indicates P < 0.10).

	nss-Ca^{2+}	ss-Ca^{2+}	nss-Mg^{2+}	ss-Mg^{2+}	nss-K^{+}	ss-K^{+}	nss-SO_4^{2-}	ss-SO_4^{2-}	Na^{+}	Cl^{-}	NO_2^{-}	NO_3^{-}	NH_4^{+}	$\delta^{15}N$-NH_4^{+}
nss-Ca^{2+}	-	-	-	-	-	-	-	-	-	-	-	-		-
ss-Ca^{2+}	**0.56**	-	-	-	-	-	-	-	-	-	-	-	-	-
nss-Mg^{2+}	**0.83**	**0.88**	-	-	-	-	-	-	-	-	-	-	-	-
ss-Mg^{2+}	**0.56**	**1.00**	**0.88**	-	-	-	-	-	-	-	-	-	-	-
nss-K^{+}	0.13	0.05	0.13	0.05	-	-	-	-	-	-	-	-	-	-
ss-K^{+}	**0.56**	**1.00**	**0.88**	**1.00**	0.05	-	-	-	-	-	-	-	-	-
nss-SO_4^{2-}	*0.31**	**0.56**	**0.48**	**0.56**	0.05	**0.56**	-	-	-	-	-	-	-	-
ss-SO_4^{2}	**0.56**	**1.00**	**0.88**	**1.00**	0.05	**1.00**	**0.56**	-	-	-	-	-	-	-
Na^{+}	**0.56**	**1.00**	**0.88**	**1.00**	0.05	**1.00**	**0.56**	**1.00**	-	-	-	-	-	-
Cl^{-}	**0.54**	**0.94**	**0.87**	**0.94**	0.03	**0.94**	**0.43**	**0.94**	**0.94**	-	-	-	-	-
NO_2^{-}	-0.00	0.05	-0.02	0.05	0.01	0.05	0.07	0.05	0.05	0.00	-	-	-	-
NO_3^{-}	**0.41**	0.05	0.20	0.05	**0.37**	0.05	0.28	0.05	0.05	0.00	0.23	-	-	-
NH_4^{+}	0.11	-0.08	0.01	-0.08	-0.02	-0.08	0.27	-0.08	-0.08	0.00	0.11	**0.39**	-	-
$\delta^{15}N$-NH_4^{+}	**0.77**	**0.41**	**0.63**	**0.41**	0.24	**0.41**	0.05	**0.41**	**0.41**	**0.39**	0.13	*0.32**	-0.16	-

Table S1C: Pearson correlation among species and isotopes (spring dataset; P < 0.05 are bolded, * indicates P < 0.10).

	nss-Ca^{2+}	ss-Ca^{2+}	nss-Mg^{2+}	ss-Mg^{2+}	nss-K^{+}	ss-K^{+}	nss-SO_4^{2-}	ss-SO_4^{2-}	Na^{+}	Cl^{-}	NO_2^{-}	NO_3^{-}	NH_4^{+}	$\delta^{15}N$-NH_4^{+}
nss-Ca^{2+}	-	-	-	-	-	-	-	-	-	-	-	-		-
ss-Ca^{2+}	**0.56**	-	-	-	-	-	-	-	-	-	-	-	-	-
nss-Mg^{2+}	**0.71**	**0.95**	-	-	-	-	-	-	-	-	-	-	-	-
ss-Mg^{2+}	**0.56**	**1.00**	**0.95**	-	-	-	-	-	-	-	-	-	-	-
nss-K^{+}	**0.96**	**0.49**	**0.63**	**0.49**	-	-	-	-	-	-	-	-	-	-
ss-K^{+}	**0.56**	**1.00**	**0.95**	**1.00**	**0.49**	-	-	-	-	-	-	-	-	-
nss-SO_4^{2-}	**0.80**	*0.38**	**0.41**	*0.38**	**0.84**	*0.38**	-	-	-	-	-	-	-	-
ss-SO_4^{2}	**0.56**	**1.00**	**0.94**	**1.00**	**0.48**	**1.00**	*0.38**	-	-	-	-	-	-	-
Na^{+}	**0.56**	**1.00**	**0.95**	**1.00**	**0.49**	**1.00**	*0.38**	**1.00**	-	-	-	-	-	-
Cl^{-}	0.23	**0.88**	**0.84**	**0.88**	0.14	**0.88**	-0.08	**0.87**	**0.88**	-	-	-	-	-
NO_2^{-}	0.33	0.05	0.16	0.05	0.25	0.05	0.11	0.05	0.05	-0.02	-	-	-	-
NO_3^{-}	0.14	-0.04	-0.06	-0.04	0.20	-0.04	0.19	-0.03	-0.04	-0.15	0.31	-	-	-
NH_4^{+}	0.14	-0.24	-0.26	-0.24	0.38	-0.24	*0.43**	-0.23	-0.24	-0.33	-0.11	**0.62**	-	-
$\delta^{15}N$-NH_4^{+}	**0.52**	0.29	*0.41**	0.29	0.27	0.29	-0.08	0.27	0.29	0.28	0.27	-0.16	**-0.54**	-

Table S1D: Pearson correlation among species and isotopes (summer dataset; P < 0.05 are bolded, * indicates P < 0.10).

	nss-Ca^{2+}	ss-Ca^{2+}	nss-Mg^{2+}	ss-Mg^{2+}	nss-K^{+}	ss-K^{+}	nss-SO_4^{2-}	ss-SO_4^{2-}	Na^{+}	Cl^{-}	NO_2^{-}	NO_3^{-}	NH_4^{+}	$\delta^{15}N$-NH_4^{+}
nss-Ca^{2+}	-	-	-	-	-	-	-	-	-	-	-	-		-
ss-Ca^{2+}	**0.66**	-	-	-	-	-	-	-	-	-	-	-	-	-
nss-Mg^{2+}	**0.74**	**0.84**	-	-	-	-	-	-	-	-	-	-	-	-
ss-Mg^{2+}	**0.66**	**1.00**	**0.84**	-	-	-	-	-	-	-	-	-	-	-
nss-K^{+}	**0.85**	**0.65**	**0.54**	**0.65**	-	-	-	-	-	-	-	-	-	-
ss-K^{+}	**0.66**	**1.00**	**0.84**	**1.00**	**0.65**	-	-	-	-	-	-	-	-	-
nss-SO_4^{2-}	**0.54**	0.36	**0.59**	0.36	0.17	0.36	-	-	-	-	-	-	-	-
ss-SO_4^{2}	**0.66**	**1.00**	**0.84**	**1.00**	**0.65**	**1.00**	0.36	-	-	-	-	-	-	-
Na^{+}	**0.66**	**1.00**	**0.84**	**1.00**	**0.65**	**1.00**	0.36	**1.00**	-	-	-	-	-	-
Cl^{-}	0.28	**0.73**	**0.51**	**0.73**	0.34	**0.73**	0.09	**0.73**	**0.73**	-	-	-	-	-
NO_2^{-}	-0.08	-0.09	-0.05	-0.09	-0.19	-0.09	0.30	-0.09	-0.09	-0.26	-	-	-	-
NO_3^{-}	-0.29	**-0.59**	-0.19	**-0.59**	-0.41	**-0.59**	-0.19	**-0.59**	**-0.59**	**-0.56**	0.33	-	-	-
NH_4^{+}	*-0.45**	**-0.81**	**-0.62**	**-0.81**	*-0.43**	**-0.81**	-0.33	**-0.81**	**-0.81**	**-0.51**	-0.04	0.05	-	-
$\delta^{15}N$-NH_4^{+}	**0.51**	**0.67**	*0.47**	**0.67**	**0.56**	**0.67**	-0.07	**0.67**	**0.67**	**0.63**	*-0.37**	**-0.65**	-0.09	-

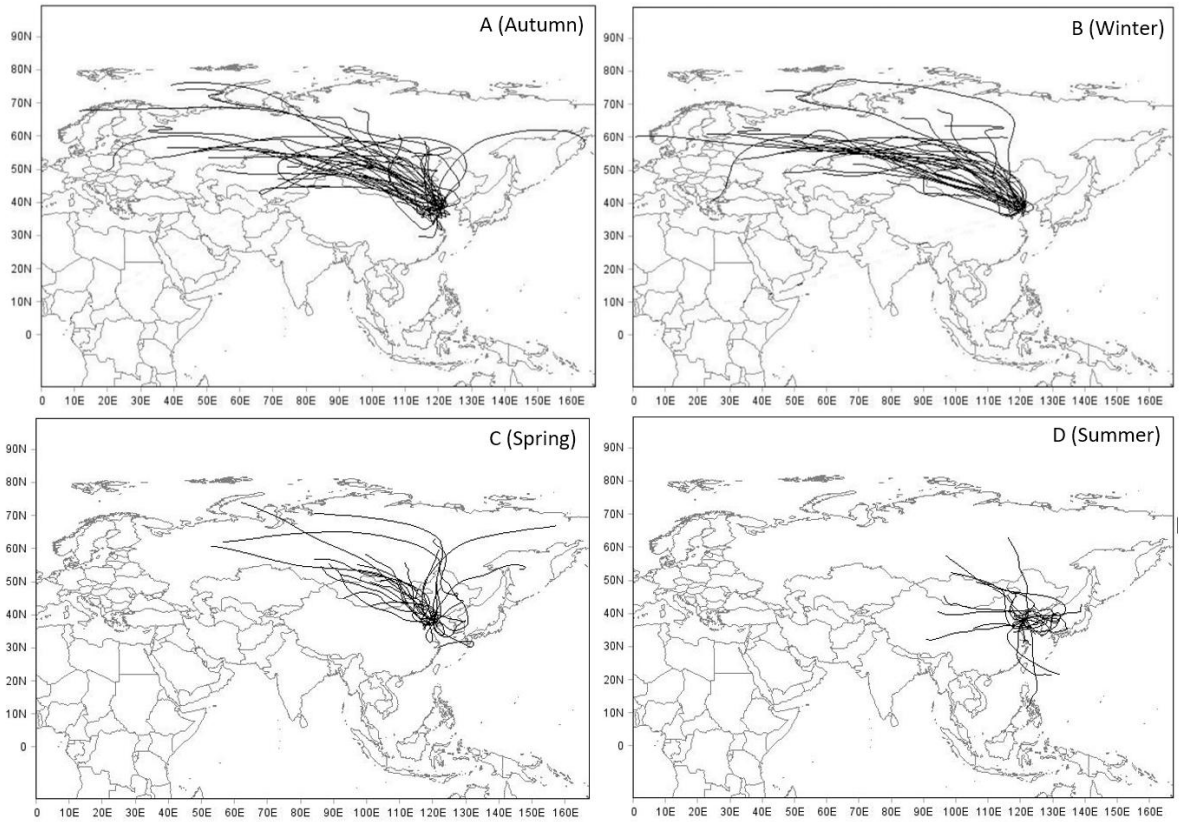

Figure S1: Seasonal air mass back trajectories using HYSPLIT showing transport patterns for aerosol samples over the sample collection time plus four additional days (A = Autumn (n = 29), B = Winter (n = 29), C = Spring (n = 25), D = Summer (n = 26)).

Chapter 3

Solid Phase Extraction Methodology for Robust Isotope Analysis of Atmospheric Ammonium

Alexandra B. MacFarland[1,2], Wendell W. Walters[2,3], Meredith G. Hastings[1,2]

[1]Department of Earth, Environmental, and Planetary Sciences
Brown University
324 Brook Street, Box 1846
Providence, RI 02912

[2]Institute at Brown for Environment and Society
Brown University
85 Waterman St
Providence, RI 02912

[3]Department of Chemistry and Biochemistry
University of South Carolina
631 Sumter Street
Columbia, SC 29208

Published in *ACS Earth and Space Chemistry* (2024),
doi:10.1021/acsearthspacechem.3c00375.

Abstract

The stable nitrogen isotope composition ($\delta^{15}N$) of atmospheric ammonia (NH_3) and ammonium (NH_4^+) has emerged as a potent tool for improving our understanding of the atmospheric burden of reduced nitrogen. However, current chemical oxidation methodologies commonly utilized for characterizing $\delta^{15}N$ values of NH_4^+ samples have been found to lead to low precision for low concentration (i.e., < 5 μmol L^{-1}) samples and often suffer from matrix interferences. Here, we present an analytical methodology to extract and concentrate NH_4^+ from samples through use of a sample pre-treatment step using a solid phase extraction technique involving cation exchange resins. Laboratory control tests indicated that 0.4 g of cation exchange resin (Biorad AG-50W) and 10 mL of 4 M sodium chloride extraction solution enabled the complete capture and removal of NH_4^+. Using this sample pre-treatment methodology, we obtained accurate and precise $\delta^{15}N$ values for NH_4^+ reference materials and an in-house quality control sample at concentrations as low as 1.0 μM. Additionally, the sample pre-treatment methodology was evaluated using atmospheric aerosol samples previously measured for $\delta^{15}N$-NH_4^+ (from Changdao Island, China), which indicated an excellent $\delta^{15}N$-NH_4^+ match between sample pre-treatment and no treatment ($y = (0.98 \pm 0.05)x + (0.11 \pm 0.6)$, $R^2 = 0.99$). Further, this methodology successfully extracted NH_4^+ from aerosol samples and separated it from present matrix effects (samples collected from Oahu, Hawaii; pooled standard deviation $\delta^{15}N$-NH_4^+ = ± 0.5‰, n = 16 paired samples) that without pre-treatment originally failed to quantitatively oxidize to nitrite for subsequent $\delta^{15}N$ isotope analysis. Thus, we recommend applying this sample pre-treatment step for all environmental NH_4^+ samples to ensure accurate and precise $\delta^{15}N$ measurement.

Introduction

Reduced inorganic nitrogen (NH_x = ammonia (NH_3) + ammonium (NH_4^+)) is a readily bioavailable form of nitrogen (N), with its rate of loading into the atmosphere increasing over time[1]. NH_x can be difficult to track in the environment due to its short lifetime (e.g., hours to days)[2] and its multitude of emission sources and fates (dry deposition, cloud scavenging, formation of NH_4^+ aerosols, bidirectional exchange). However, distinguishing between NH_3 sources from atmospheric deposition is essential to understanding the effects of human activities and natural emissions on various environments[1].

The stable nitrogen isotope composition of NH_4^+ has been shown to be a useful tool for categorizing and detailing the sources and chemistry of reactive nitrogen in the environment[3-7]. This is because different sources of NH_4^+ tend to have unique nitrogen isotope compositions[1,4]. The stable nitrogen isotope composition is typically reported using delta notation ($\delta^{15}N$) and is determined as follows:

$$\delta^{15}N\ (‰) = [(^{15}N/^{14}N)_{sample}/(^{15}N/^{14}N)_{reference} - 1] \times 1000 \quad (1)$$

where the $(^{15}N/^{14}N)_{reference}$ is air-N_2. Physical, chemical, and biological processes discern between the two isotopes (^{15}N and ^{14}N) which result in small but measurable differences in the ratio of ^{15}N:^{14}N among the inorganic forms of N (e.g., NH_4^+) observed in the environment emitted by various sources[8]. For example, continental and marine aerosol NH_4^+ have different observed $\delta^{15}N$ values, making the tracking of anthropogenic and natural emissions of NH_3 possible (e.g., marine sources are typically lower in $\delta^{15}N$ compared to continental sources)[1,3,9,10]. Previous work has indicated that aerosols collected from the remote Atlantic Ocean had low $\delta^{15}N$-NH_4^+ values that ranged from -8 to -5‰ associated with marine activity and high $\delta^{15}N$-NH_4^+ up to 10‰ associated with the transport of air masses deriving from continental regions[3].

Due to the low concentrations of NH_4^+ in many environments, it has been historically difficult to measure $\delta^{15}N$ of environmental NH_4^+ samples. A significant development in our ability to utilize $\delta^{15}N$ of NH_4^+ was the methodology advancement of quantitatively oxidizing NH_4^+ to nitrite (NO_2^-) using chemical methods, coupled to an established protocol for the conversion of NO_2^- to nitrous oxide gas (N_2O) for routine $\delta^{15}N$ analysis for as little as 10 nmol of NH_4^+[11]. This method had been suggested to be a robust technique to quantify $\delta^{15}N$ of NH_4^+ for sample concentrations as low as 0.5 μM. However, recent work has reported a significant reagent blank associated with the chemical method used to oxidize NH_4^+ to NO_2^-; thus, recommending that this method can only be applied for NH_4^+ concentrations above 2 μmol L^{-1}, limiting our ability to accurately measure $\delta^{15}N$ for diluted NH_4^+ concentrations[5,9].

Further, the chemical method for $\delta^{15}N$-NH_4^+ determination was developed for and tested on freshwater and saltwater samples and was found to have no significant matrix interferences during the conversion of NH_4^+ to NO_2^- to N_2O[11]. Since this method's development, it has been applied to a range of NH_4^+ samples including precipitation, aerosols, and denuded gas[7,12,13]. Many studies assume successful NH_4^+ oxidation to NO_2^- without direct confirmation, but when these checks are performed, quantitative oxidation is often not found. Further, incomplete oxidation of NH_4^+ to NO_2^- can induce isotope fractionation resulting in a $\delta^{15}N$ bias. For example, it was recently shown that NH_4^+ extracted from NH_3 collected on an acid-coated denuder failed to quantitatively oxidize for 7.2% of samples[6]. More alarmingly, aerosol NH_4^+ extracted from aerosol filters failed to oxidize for 38% of samples[6]. This oxidation failure is likely not caused because of the media and/or acid matrices used for NH_3 or NH_4^+ collection as previously works have indicated no interference when collecting pure NH_3 or particulate NH_4^+ from laboratory investigations[12,13], but instead likely reflect the collection of other interferences from the

environment complicating the analysis of $\delta^{15}N$. Recently in our lab, NH_4^+ extracted from aerosol samples (n = 57) from Oahu, Hawaii, and NH_4^+ extracted from throughfall and soils all failed to oxidize to NO_2^-, motivating our search for a sample pre-treatment step that can be utilized for the concentration and purification of NH_4^+ for high throughput $\delta^{15}N$ analysis.

Sample pre-treatment may therefore be necessary for accurate and robust measurements of $\delta^{15}N\text{-}NH_4^+$. One common approach has been using the micro-diffusion method, which attempts to quantitatively isolate NH_3 from solution via volatilization from solution and collection on an acid-coated filter[14]. While this could be a suitable approach for concentration of NH_4^+ in atmospheric samples, it is time consuming (requires weeks to complete), labor intensive and can require significant sample volumes. Additionally, this method requires extensive filter wrapping/taping which can introduce a higher likelihood of human error[14,15]. Recently, a solid phase extraction technique utilizing cation exchange resins was developed with a focus on concentrating low [NH_4^+] samples for $\delta^{15}N\text{-}NH_4^+$ analysis in ice cores by Lamothe *et al*. (2023)[16]. Here, we have expanded upon this solid phase extraction methodology with a focus on concentrating laboratory standards and an in-house quality control (QC) solution as well as evaluated the method's ability to extract NH_4^+ from marine aerosol samples that exhibit matrixes that impede the chemical conversion of NH_4^+ to N_2O when using the well-established chemical method for $\delta^{15}N\text{-}NH_4^+$ analysis created by Zhang *et al*. (2007)[11]. These matrix interference issues were not addressed in the Lamothe *et al*. (2023) study. We focused on optimizing the various parameters of the solid phase extraction technique (resin amount, extraction volume, extraction concentration) to achieve the highest possible precision and accuracy of $\delta^{15}N$ for atmospheric samples. This work may also be a crucial step in developing robust methodologies for accurate and precise $\delta^{15}N$ characterization of NH_4^+ from other types of environments.

Experimental Section

Protocol Development

We targeted a 10 μM solution of NH_4^+ once samples were extracted from the resin columns because previous work has suggested that at this concentration, we can acquire precise $\delta^{15}N$ measurements[5,11,12]. Additionally, we targeted 10 mL of final eluent solution, such that we aim to bind 100 nmol of NH_4^+. Previous work has suggested that Bio-Rad AG-50W can be used for concentrating dilute NH_4^+ samples using 0.6 g of resin and 5 mL of 1 M sodium chloride (NaCl) extraction solution[16]. Here, we evaluated the amount of resin and amount/concentration of NaCl for the complete capture and removal of NH_4^+ on the resin. Our evaluation criteria were (1) consistent production of generated N_2O from samples and reference materials following the chemical conversion of NH_4^+ to N_2O, (2) high precision/low standard deviations of the $\delta^{15}N$ measurements of isotope reference materials and in house quality control sample (QC), and (3) a $\delta^{15}N$-NH_4^+ calibration slope of the isotope reference materials close to 2.0, as expected for conversion of NO_2^- with sodium azide to N_2O [11,17]. The slope is calculated between the observed average NH_4^+ blank of the international standards to their $\delta^{15}N$ reference values.

Note that in the initial protocol development phase, concentrations of NH_4^+ and NO_2^- were determined using a discrete UV–Vis analyzer (colorimetrically via a Westco Smartchem 200; U.S. EPA Compliant Methods 350.1 and 353.2, respectively (Revision 2.0))[18,19]. Reproducibility calculated from replicate measurements of quality control standards are typically ±2% and ±1% for NH_4^+ and NO_2^- respectively, while limits of detection are approximately 0.3 and 0.2 μM for NH_4^+ and NO_2^-, respectively[13]. With the established protocol, oxidized sample concentrations were checked via expected peak areas of N_2O on the isotope ratio mass spectrometer (IRMS).

Cation Exchange Resin Preparation

Bio-Rad AG-50W cation exchange resin (AG-50W-X2 Cation Exchange Resin, analytical grade, 50–100 mesh, hydrogen form, 0.6 Meq/mL) were utilized for concentrating NH_4^+ (aq). Resin columns were prepared by transferring the targeted resin mass to 10 mL Bio-Rad Poly-Prep Columns, which were attached to 250 mL funnels (Econo-Column Funnels). The control tests consisted of both 0.8 g and 0.4 g resins tested with different NaCl concentrations such as 0.5, 1.0, 2.0, 3.0, and 4.0 M. (Prior to the publication of the Lamothe *et al*. (2023)[16] study, we initially chose 0.8g due to the 0.8g/mL density of the resin; further testing (see below) revealed more accurate and consistent isotope values with 0.4 g (see below)). The resin was hydrated by gravity dripping ~15-20 mL of ultraclean MilliQ water (>18 MΩ) through the resin columns. The resin is initially in the hydron (H^+) form and is converted to sodium (Na^+) by gravity dripping ~250 mL 1 M NaCl (Thermo Scientific Sodium Chloride, ACS, Ultrapure) through the columns. The Bio-Rad AG 50W cation exchange resin has a higher relative selectively to NH_4^+ (1.95) compared to Na^+ (1.5), such that the targeted NH_4^+ analyte will be effectively collected on the resin. The final 5 – 10 mL of eluent outflow from the columns is checked with pH strips to ensure a pH near 7, indicating Na^+ has replaced all H^+ ions in the resin. If the pH remains acidic (pH < 5), an additional 50 mL of 1 M NaCl is passed through the resins. Once the pH of the outflow is close to neutral, 300 mL of MilliQ water is then passed through the columns to thoroughly rinse them and expel excess Na^+ (aq). Following these steps, the columns are then ready for use (Figure 1A). When not in use, the columns are stored in 5 mL of MilliQ water and the ends of the columns are capped (Poly-Prep Column Stack Cap and End Caps, Micro Bio-Spin chromatography columns) to keep the resin beds hydrated.

Concentration Protocol

Once the resin columns were prepared and conditioned in the Na^+ form they were then utilized for the concentration of NH_4^+ (aq) samples in an alternating sample load and extraction/regeneration phase (Figure 1B). Prior to use, the stored resin columns were uncapped and the MilliQ used to keep the resins hydrated was removed by gravity dripping. Next, 10 mL of targeted NaCl concentrations were dripped through the columns, followed by 10 mL of MilliQ water which were both collected and disposed of as waste. For the control tests we targeted 0.5, 1.0, 2.0, 3.0 and 4.0 M NaCl, where we found 4.0 M NaCl to be the optimal concentration and utilized this concentration for the sample pretreatment of environmental samples.

The resins were then in the sample load phase (Figure 1B). Briefly, samples were allowed to gravity drip through the resin columns, and the outflow was collected and disposed of as waste. During the dripping process, the column funnels were covered with aluminum foil to limit contamination. After the samples finished passing through the resins, the resins moved into the sample extraction/regeneration phase (Figure 1B). Briefly, 10 mL of 4 M NaCl was passed through the resin, which extracted the sample NH_4^+ initial bound to the resin and in the process regenerated the resin in the Na^+ form. The NaCl eluent outflow containing the sample NH_4^+ was collected for subsequent $\delta^{15}N$ analysis. After the NaCl extraction solution finished dripping, 10 mL of MilliQ water gravity-dripped through the columns to remove excess NaCl. The resins were then ready for the next sample loading phase. The sample loading and extraction/regeneration phases were repeated until all samples for a particular batch of analyses were completed. In line with the identical treatment principle, for each batch analysis, NH_4^+ isotope reference materials (IAEA-N2 and USGS-25), a laboratory NH_4^+ quality-control (QC), and MilliQ blanks were passed through the resin columns and processed the same way. The

reference values for IAEA-N2 and USGS-25 were then used to calibrate the final $\delta^{15}N$ of the samples. Typically, the isotope reference materials, QC, and blanks were processed in quintet for each batch analysis. The standard deviations of repeated measures of the reference materials or samples are used as an indicator of precision, whereas the average QC values are used as an indicator for accuracy (i.e., the QC is treated as a sample and its $\delta^{15}N$ values are compared within and across batch analyses). Once all samples, standards, and blanks were processed through the resins, the columns were capped and hydrated, and stored (room temperature environment or refrigerator is acceptable) for subsequent use.

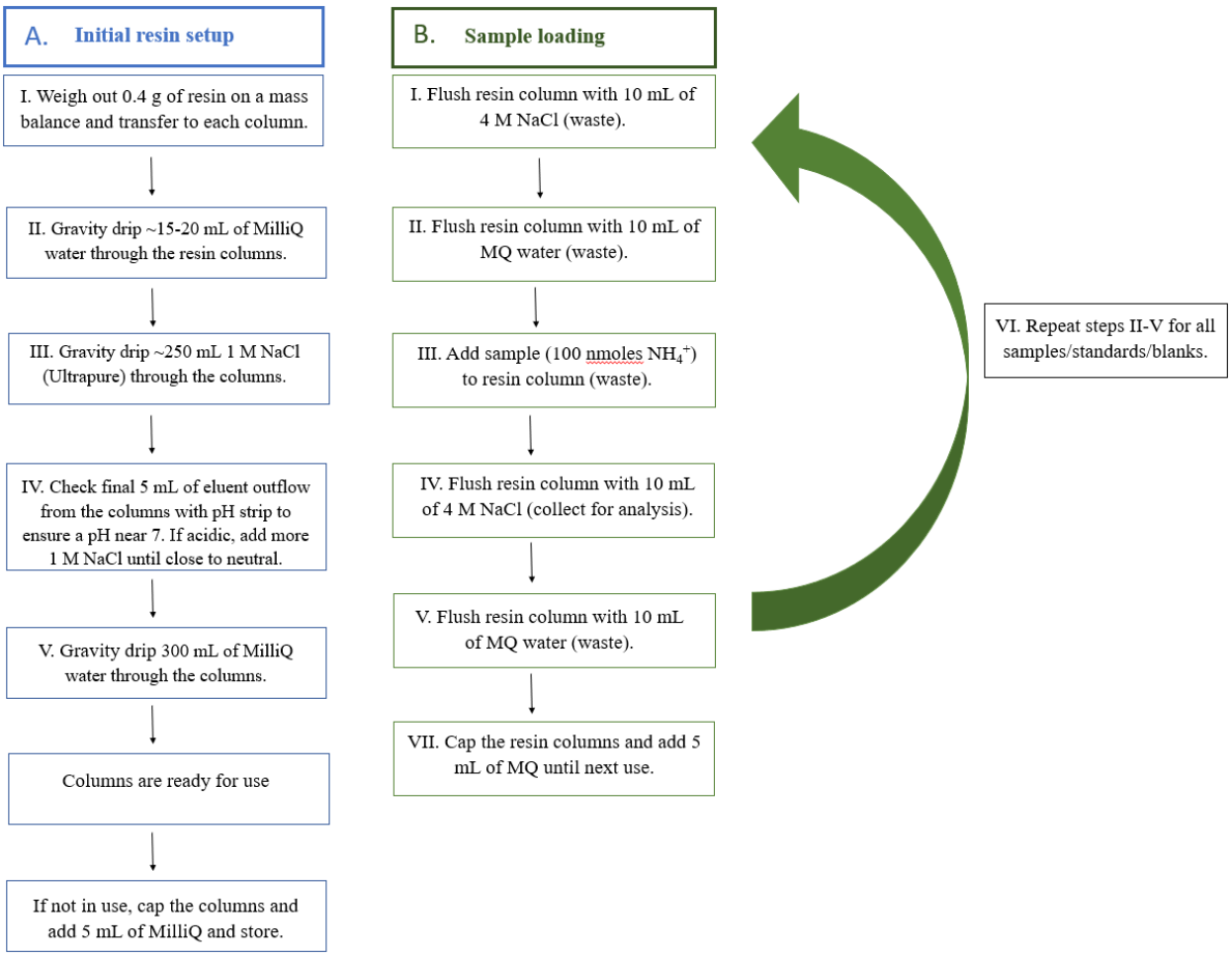

Figure 1: Flowchart of steps for (A) initial resin column setup and (B) use of cation exchange columns to concentrate or purify NH_4^+ samples.

Control Tests

We first evaluated the various parameters of the solid phase extraction method to ensure accurate $\delta^{15}N\text{-}NH_4^+$ values for the NH_4^+ isotope reference materials and laboratory QC at an initial [NH_4^+ (aq)] of 10 μM. Different combinations of the NaCl eluent concentrations (0.5, 1, 2, 3, and 4 M) and resin amounts (0.4 and 0.8 g) were tested. Once the optimal combination of resin amount and eluent concentration was determined, we evaluated the ability of the method to concentrate NH_4^+ (aq) for accurate and precise $\delta^{15}N\text{-}NH_4^+$ of the isotope reference materials and laboratory QC with initial [NH_4^+ (aq)] concentrations of 7.5, 5.0, 2.5, and 1.0 μM. For each concentration, 100 nmol of NH_4^+(aq) was captured such that the volume of the standards and QC that passed through the resin ranged from 10 to 200 mL. Additionally, blanks were determined using MilliQ water passed through the resin at the same volume as the standard and QC sets. The NH_4^+ standards and QC were also analyzed for $\delta^{15}N\text{-}NH_4^+$ at 7.5, 5.0, 2.5, and 1.0 μM without the use of the pre-treatment step (i.e., the cation exchange resin) to compare and further investigate the effectiveness of this resin method.

Environmental Samples

Once the parameters of the solid-phase extraction protocol (resin bead volume, NaCl eluent concentration) were optimized, the method was applied to environmental samples. The method was initially utilized to compare with previously reported $\delta^{15}N\text{-}NH_4^+$ from aerosol samples collected from Changdao Island, China[7]. These samples were previously analyzed for $\delta^{15}N\text{-}NH_4^+$ without the use of the resin concentration method because these samples exhibited no matrix interference upon NH_4^+ oxidation and had sufficiently elevated [NH_4^+ (aq)] (i.e., typically greater than 10 μM)[7]. These samples were analyzed in three different ways: (1) no pre-treatment such that samples were thawed and represented their initial matrix (MilliQ water extracts from aerosol filters), (2) no resin treatment but with samples made up in a 4 M NaCl matrix (e.g.,

samples diluted with a 4 M NaCl solution instead of pure MilliQ water), and (3) complete processing of samples using the described pre-treatment resin method. These tests were conducted to separately evaluate the impact of the 4 M NaCl matrix as well as potential resin effects on the $\delta^{15}N$ analysis of aerosol samples.

Aerosol samples collected in Oahu, Hawaii and extracted in MilliQ water, were also analyzed for $\delta^{15}N\text{-}NH_4^+$ using this exchange resin methodology. Without the use of the sample pre-treatment resin method, these samples failed to quantitatively oxidize to NO_2^- (e.g., all samples were < 60% oxidized) using the standard alkaline hypobromite solution, a critical first step for $\delta^{15}N\text{-}NH_4^+$ analysis using a coupled chemical oxidation and reduction methodology that converts NH_4^+ to N_2O[11]. The poor oxidation yields were confirmed from measurement of NO_2^- after the NH_4^+ oxidation step using a discrete UV–Vis analyzer. The ability of the resin concentration method to remove the apparent matrix effect limiting NH_4^+ oxidation was evaluated from analyzing the N_2O peak areas on a continuous flow IRMS. Since we are injecting the same amount of material (i.e, 10 nmol of NO_2^-) for samples and standards, we would expect consistent N_2O peak areas using the IRMS (around 20 Vs in our case but could differ between labs depending on the sensitivity of the IRMS instrument).

Determination of $\delta^{15}N\text{-}NH_4^+$

All NH_4^+ samples, standards, QCs, and laboratory blanks were oxidized to NO_2^- using a chemical method involving hypobromite (BrO^-) in an alkaline solution, which was synthesized as previously described[11]. It is noted that the BrO^- solution typically experiences minimal interference from dissolved organic nitrogen (DON)[11]. Though we do note that the role of DON as a potential interference in the $\delta^{15}N$ analysis of NH_4^+ could be dependent on the environment the samples are collected. This requires attention due to the potential for DON oxidation to NO_2^-,

similar as the intended target of NH_4^+ oxidation. Thus, we recommend careful evaluation of the product NO_2^- and/or N_2O to evaluate the role of DON oxidation as a potential interference. If greater than expected NO_2^- or N_2O is observed, this could potentially implicate the role of DON. For the considered aerosol samples, we never encountered more than expected NO_2^- and/or N_2O and thus assume the presence of DON is negligible for these types of samples. This chemical method was shown to be more accurate for $\delta^{15}N\text{-}NH_4^+$ analysis compared to the microdiffusion method[20]. Briefly, samples and standards were transferred into 50 mL vials that are acid washed, rinsed with MilliQ water, and baked at 500 °C for 4 h prior to use. Next, 2 mL of the BrO^- oxidizing reagent was added to each of the sample and standard 50 mL vials, capped, and allowed to react overnight. Then 0.5 mL of 1 M sodium arsenite is added to each vial to remove the remaining BrO^-. After oxidation, 10 nmol of the generated NO_2^- were then transferred into 20 mL vials, crimp-capped with PTFE/butyl septa, and flushed with helium gas for a minimum of 10 minutes. The NO_2^- was then reduced to N_2O through the addition of 2 mL of 2 M sodium azide buffered in 40% acetic acid solution[11]. After a minimum of 0.5 h, the samples were neutralized using 6 M sodium hydroxide. Samples were then analyzed for the $\delta^{15}N\text{-}N_2O$ composition via an automated N_2O extraction system coupled with a continuous flow IRMS for determination at *m/z* 44, 45, and 46. Two internationally recognized $\delta^{15}N\text{-}NH_4^+$ reference materials (composed of ammonium sulfate), IAEA-N2 ($\delta^{15}N = 20.4 \pm 0.2‰$) and USGS-25 ($\delta^{15}N = -30.3 \pm 0.3‰$)[21,22], and an internal QC ($\delta^{15}N = -1.0 \pm 0.5‰$) were analyzed during every run. The final $\delta^{15}N\text{-}NH_4^+$ is determined by correction for isobaric influences, blank contribution and calibrating the unknown samples and QC to the internationally recognized standards, as previously described[12,13]. The authors note that no unexpected safety hazards were encountered while using this method.

Results and Discussion

Optimizing NaCl Extraction Concentration

For all tested resin amounts and NaCl extraction concentrations, besides 0.5 M NaCl, the standard deviations of the NH_4^+ standard solutions (i.e., IAEA-N2 and USGS25) were generally within 1‰ (Table 1). However, we found that the accuracy of the calibrated $\delta^{15}N\text{-}NH_4^+$ of the QC was strongly dependent on the solid-phase extraction parameters (Figure 2). Only the combinations that utilized 0.4 g resin resulted in a $\delta^{15}N\text{-}NH_4^+$ of the QC that overlapped with its expected value, with two out of three of those combinations producing an average that fits the expected range (2 M and 4 M NaCl; Figure 2).

Table 1: Average standard (IAEA-N2 and USGS25) and QC $\delta^{15}N\text{-}NH_4^+$ values post cation exchange resin with varying concentrations of NaCl extraction solution and resin amount ($\bar{x} \pm 1\sigma$ (n)). Combined average standard & QC peak areas (Vs), blank peak averages (Vs), and calculated corrected slopes are included. All standards and QCs were targeted at 10 μM NH_4^+.

NaCl (M)	Resin (g)	$\delta^{15}N$ (IAEA-N2) (‰)	$\delta^{15}N$ (USGS-25) (‰)	$\delta^{15}N$ (QC) (‰)	Standards & QC peak area (Vs)	Blank peak area (Vs)	Slope*
0.5	0.8	20.4 ± 3.3 (8)	-30.3 ± 2.5 (10)	-18.5 ± 1.6 (10)	15.0 ± 1.7	3.2 ± 0.2 (5)	2.7 ± 0.07
1	0.8	20.4 ± 0.7 (10)	-30.3 ± 1.1 (10)	-10.4 ± 0.6 (10)	15.3 ± 1.3	2.4 ± 0.3 (5)	2.4 ± 0.02
2	0.8	20.4 ± 0.5 (10)	-30.3 ± 0.9 (10)	-6.0 ± 0.3 (10)	16.1 ± 0.8	3.6 ± 0.3 (5)	2.1 ± 0.01
3	0.8	20.4 ± 0.5 (10)	-30.3 ± 0.8 (10)	-3.4 ± 0.6 (10)	14.7 ± 0.8	2.7 ± 0.3 (5)	2.2 ± 0.01

4	0.8	20.4 ± 0.7 (10)	-30.3 ± 0.7 (10)	-3.3 ± 0.6 (8)	14.5 ± 1.6	2.9 ± 0.4 (4)	2.0 ± 0.01
2	0.4	20.4 ± 0.6 (10)	-30.3 ± 0.7 (10)	-1.2 ± 0.6 (10)	16.3 ± 1.3	2.8 ± 0.1 (5)	2.1 ± 0.01
3	0.4	20.4 ± 1.0 (10)	-30.3 ± 1.4 (10)	-2.2 ± 1.4 (10)	14.3 ± 1.0	2.4 ± 0.2 (5)	2.1 ± 0.02
4	0.4	20.4 ± 1.0 (9)	-30.3 ± 0.6 (9)	-1.0 ± 0.3 (10)	16.3 ± 1.8	3.5 ± 1.0 (5)	2.0 ± 0.02

*a slope of 2.0 is expected due to the conversion of NO_2^- with sodium azide to N_2O.

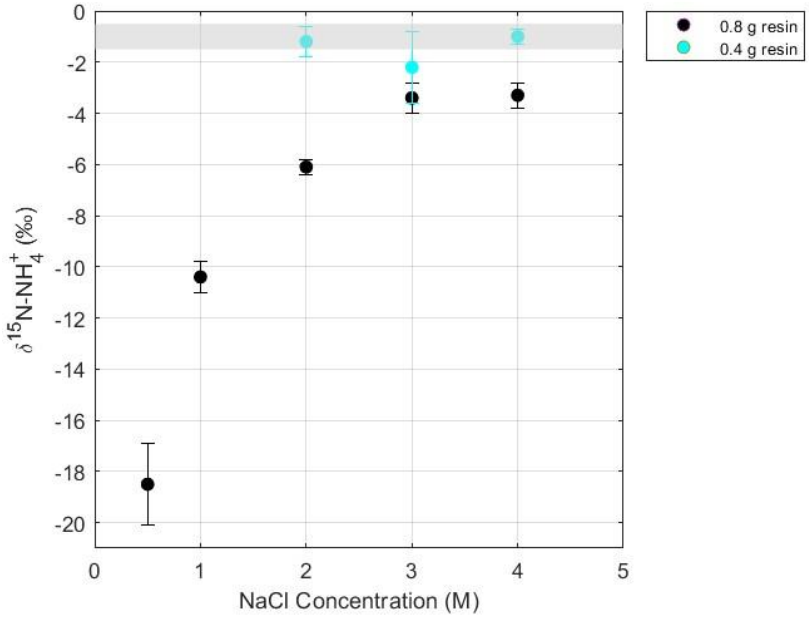

Figure 2: Average QC δ^{15}N-NH_4^+ values post cation exchange resin with varying concentrations of NaCl extraction solution (*n* = 10). Black circles are average δ^{15}N-NH_4^+ using 0.8 g resin, and blue circles are average δ^{15}N-NH_4^+ using 0.4 g resin. Shaded region indicates expected QC δ^{15}N-NH_4^+ range. Error bars represent ± 1σ.

The $\delta^{15}N\text{-}NH_4^+$ of the QC for the 3 M NaCl set was the most variable ($1\sigma = \pm 1.4‰$; $n = 10$), compared with the 2 M NaCl ($1\sigma = \pm 0.6‰$; $n = 10$) and 4 M NaCl ($1\sigma = \pm 0.3‰$; $n = 9$) sets. While the 2 M NaCl extraction solution produced an accurate and reasonably precise $\delta^{15}N\text{-}NH_4^+$ of the QC, we recommend utilizing 0.4 g resin and 4 M NaCl as the optimal extraction solution concentration for the NH_4^+ solid phase extraction methodology as these parameters resulted in the highest accuracy and best precision for $\delta^{15}N\text{-}NH_4^+$. Additionally, the use of 4 M NaCl will provide a buffer (e.g., an excess of Na^+ without impeding subsequent oxidation).

Not only are these optimal parameters different from Lamothe *et al*. (2023)[16], who utilize 0.6 g resin and 5 mL 1 M NaCl, but the concentration of NaCl required in this study is higher than expected based off the Biorad cation exchange resin instruction manual[23]. The manual suggests that changing the resin from NH_4^+ (relative selectivity of 1.95) to Na^+ (relative selectivity of 1.5) should require no more than two bed volume of 1 M NaCl and converting the resin volume from Na^+ to NH_4^+ should require two to three bed volumes. However, this study indicated that 1 M NaCl is too low of a concentration to successfully extract the NH_4^+ from the resin for accurate $\delta^{15}N\text{-}NH_4^+$ measurement, which instead required 10 mL (~ 20 bed volumes) of 4 M NaCl to obtain accurate isotopic results (Table 1, Figure 2).

Concentrating NH_4^+

Utilizing the optimized resin volume and extraction parameters, the solid-phase extraction method was evaluated for its ability to concentrate NH_4^+ samples for $\delta^{15}N\text{-}NH_4^+$ analysis. Overall, the standard deviations of $\delta^{15}N\text{-}NH_4^+$ values for the isotope reference materials and QC were below 1.3‰, with most being below 1.0‰ (Table 2; Figure 3). - Additionally, there were consistent IRMS responses (e.g., $\delta^{15}N\text{-}NH_4^+$ peak areas) for the various concentration targets (Table 2), indicating a complete oxidation of NH_4^+ to N_2O. The calibration

slope between the observed NH_4^+ values and the expected reference values was expected to be near ~2.0 (as one N atom in the product of N_2O is from the azide reagent)[17], which was observed for each [NH_4^+] set (Table 2). This criterion was used to evaluate the performance of solid phase extraction method conditions along with low standard deviations of the isotope reference materials. Further, outliers in the dataset were tested using an outlier test for peak areas and samples were removed if peak areas were significantly high or low (± 2σ). For all sets, average peak areas of blanks were < 22% of average sample and standard peak areas. Although a blank was present, it was consistent, reproducible, and correctable.

The blank did not increase with increasing NaCl concentration, indicating that this blank is not derived from the NaCl extraction solution (either as NH_4^+ or NO_2^-). As MilliQ water injections (without the alkaline hypobromite oxidation reagent) were below detection limits, it was determined that the sodium/azide/acetic acid reagent also did not contribute significantly to the blank. Further, the reagent blank did not increase for lower initial NH_4^+ concentrations that required an increased volume of MilliQ water passing through the resin, which indicated a lack of significant NH_4^+ blank in the laboratory MilliQ water. Therefore, the most likely source of the blank is associated with the alkaline hypobromite reagent.

Table 2: Average corrected standard (IAEA-N2 and USGS-25) and QC $\delta^{15}N$-NH_4^+ values post cation exchange resin (0.4 g) extracted with 10 mL of 4 M NaCl all concentrated to 10 μM ($\bar{x}$ ± 1σ (n)). Combined average standard & QC peak areas (Vs), blank peak averages (Vs), and calculated corrected slopes are included.

NH_4^+ (μM)	$\delta^{15}N$ (IAEA-N2) (‰)	$\delta^{15}N$ (USGS-25) (‰)	$\delta^{15}N$ (QC) (‰)	Standard & QC peak area (Vs)	Blank peak area (Vs)	Slope
7.5	20.4 ± 0.5 (10)	-30.3 ± 0.7 (10)	-0.2 ± 0.4 (10)	17.9 ± 1.5	2.7 ± 0.3 (5)	2.2 ± 0.01
5.0	20.4 ± 1.2	-30.3 ± 1.0 (10)	-1.3 ± 0.5 (9)	19.1 ± 1.8	3.5 ± 0.3 (5)	2.0 ± 0.02

	(10)					
2.5	20.4 ± 0.4 (9)	-30.3 ± 0.3 (10)	-1.1 ± 0.2 (10)	17.5 ± 2.1	2.6 ± 0.03 (5)	2.1 ± 0.01
1.0	20.4 ± 0.7 (10)	-30.3 ± 0.6 (10)	-1.4 ± 1.1 (10)	21.3 ± 3.2	2.9± 1.5 (4)	2.5 ± 0.02

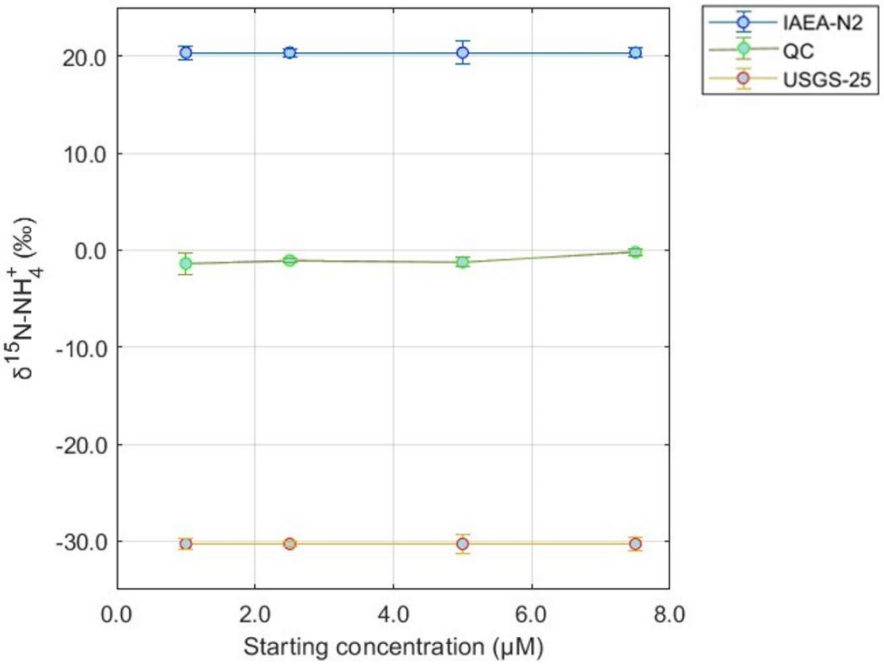

Figure 3: Standard (IAEA-N2 and USGS-25) and QC δ^{15}N-NH_4^+ averages at different concentrations that were concentrated to 10 μM through a cation exchange resin (0.4 g) and extracted with 10 mL of 4 M NaCl. Error bars represent ± 1σ. Data from Table 2.

Low [NH_4^+] samples without resins

The δ^{15}N measurements for NH_4^+ concentrations below 10 µM without the use of the cation resin sample pre-treatment revealed QC δ^{15}N-NH_4^+ outside of the expected range (-1.0 ± 0.5‰) for 2.5 and 5.0 µM, and within the expected range for 7.5 µM (Table 3, Figure 4).

Table 3: Average corrected standard (IAEA-N2 and USGS-25) and QC δ^{15}N-NH_4^+ values at various [NH_4^+] without use of the pre-treatment resin step ($\bar{x}$ ± 1σ (n)). Combined average standard & QC peak areas (Vs), blank peak averages (Vs), and calculated corrected slopes are included.

NH_4^+ (μM)	$\delta^{15}N$ (IAEA-N2) (‰)	$\delta^{15}N$ (USGS-25) (‰)	$\delta^{15}N$ (QC) (‰)	Standard & QC peak area (Vs)	Blank peak area (Vs)	Slope
7.5	20.4 ± 1.1 (3)	-30.3 ± 0.6 (5)	-1.4 ± 0.3 (5)	22.8 ± 1.5	3.7 ± 0.4 (5)	2.0 ± 0.03
5.0	20.4 ± 0.5 (5)	-30.3 ± 1.5 (4)	-2.4 ± 0.1 (3)	21.7 ± 1.5	4.7 ± 0.5 (5)	2.0 ± 0.03
2.5	20.4 ± 0.5 (5)	-30.3 ± 3.4 (4)	-2.7 ± 0.7 (3)	18.0 ± 2.7	2.9 ± 0.5 (5)	2.1 ± 0.07
1.0	N/A (5)	N/A (5)	N/A (5)	N/A	3.6 ± 0.8 (5)	0.0 ± 0.1

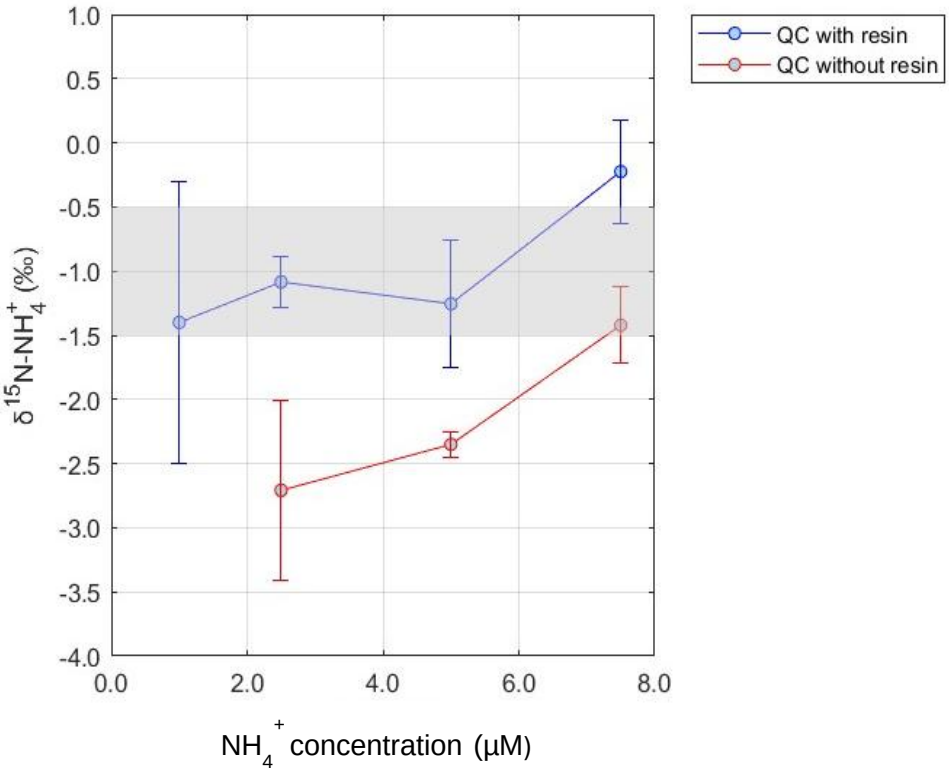

Figure 4: QC $\delta^{15}N$-NH_4^+ averages at different concentrations that were concentrated to 10 µM through a cation exchange resin (0.4 g) and extracted with 10 mL of 4 M NaCl (blue line) compared to QC $\delta^{15}N$-NH_4^+ averages at different concentrations that did not get concentrated and did not use the pre-treatment resin step (red line). Shaded region indicates expected QC $\delta^{15}N$-NH_4^+ range. Error bars represent ± 1σ. Data from Tables 2 and 3.

As concentration decreases, the uncertainty in calibration increases. This is most likely what drove the QC to have a different calibrated value compared to its expected value (Table 3).

It is noted that for the 1.0 μM set, failure to oxidize was consistent across the run (Table 3). This 1.0 μM set was replicated a second time with similar results leading to oxidation failures (average combined standard peak area of 4.4 ± 1.8 (n = 25) and average blank peak area of 2.4 ± 0.8 (n = 4)). Therefore, opting to not use the cation exchange resins for samples below 7.5 μM can lead to potential $\delta^{15}N$ biases and in some cases (i.e., concentration below 1 μM) an inability to measure $\delta^{15}N$ (Table 3, Figure 4). The cation exchange resin sample pre-treatment enabled accurate concentration of 1.0, 2.5, 5.0, and 7.5 μM NH_4^+ standards and QCs for precise and accurate $\delta^{15}N$ determination and is recommended to be applied for NH_4^+ samples with concentrations below 10 μM (Figures 3 and 4).

Application to Marine Ammonium Aerosol Samples

Here we evaluated the resin methods ability to accurately reproduce previously reported $\delta^{15}N\text{-}NH_4^+$ in marine aerosol samples from Changdao Island, China[7]. These samples, during and after original analyses, were stored in a freezer to preserve chemical composition. When analyzing the four previously measured aerosol samples, all three methods were shown to determine $\delta^{15}N\text{-}NH_4^+$ values with excellent comparison to their expected $\delta^{15}N\text{-}NH_4^+$ values (Table 4). Note that the measured NH_4^+ concentrations were > 100 μM for each sample. The excellent reproducibility of $\delta^{15}N\text{-}NH_4^+$ from the samples previously reported as sample re-run after storage in a freezer for approximately 3.5 years indicates cryostorage is suitable for preserving aerosol NH_4^+ samples for $\delta^{15}N$ analysis.

Table 4: $\delta^{15}N\text{-}NH_4^+$ values (± 1σ where applicable) of four previously measured aerosol samples (sample ID China 1-4) from Changdao Island, China along with corrected QC $\delta^{15}N\text{-}NH_4^+$ values (± 1σ) all diluted to 10 μM NH_4^+. These samples and QC were run three separate ways: same method as the previously reported isotope values (MilliQ matrix and no resin), with a 4 M NaCl matrix and no resin, and with a MilliQ matrix and extracted from the resin columns with 10 mL of 4 M NaCl.

Sample ID	Previously reported $\delta^{15}N$ (‰)	*n*	Re-measured $\delta^{15}N$ (‰)	*n*	$\delta^{15}N$ (NaCl Matrix) (‰)	*n*	$\delta^{15}N$ (pre-treatment resin step) (‰)	*n*
China 1	2.5 ± 0.0	2	3.3	1	3.7	1	3.7	1
China 2	-8.8 ± 0.3	2	-8.6	1	-7.6 ± 0.1	2	-9.1	1
China 3	14.6 ± 0.0	2	14.4 ± 0.2	2	14.2 ± 0.6	2	14.0 ± 0.2	2
China 4	15.4 ± 0.3	2	15.4 ± 0.1	2	15.8 ± 0.03	2	15.0 ± 0.1	2
QC	-1.2 ± 0.3	12	-1.1 ± 0.3	3	-0.6 ± 0.2	3	-1.2 ± 0.2	3

China samples 1, 3, and 4 are duplicates (analyzed twice in the same run) and sample 2 is a replicate (analyzed twice over two separate runs). These four samples were run over three separate runs in total and QCs from all three runs were averaged (n = 12; Table 4; "previously reported $\delta^{15}N$ (‰)" column). For the treated samples that utilized the resin methodology, the pooled standard deviation for sample duplicates is < 0.3‰. Additionally, average peak areas of blanks (n = 3) were consistently low (< 17% of average sample and standard peak areas). Overall, the expected values versus the measured values were very strongly linear (Figure 5), and the average differences between the expected (previously reported) $\delta^{15}N\text{-}NH_4^+$ and the measured $\delta^{15}N\text{-}NH_4^+$ with the pre-treatment resin step is ≤ 0.6‰ (n = 4 pairs). This comparison indicates that treatment via the resin method and the extraction matrix do not induce significant $\delta^{15}N$ biases to the environmental samples.

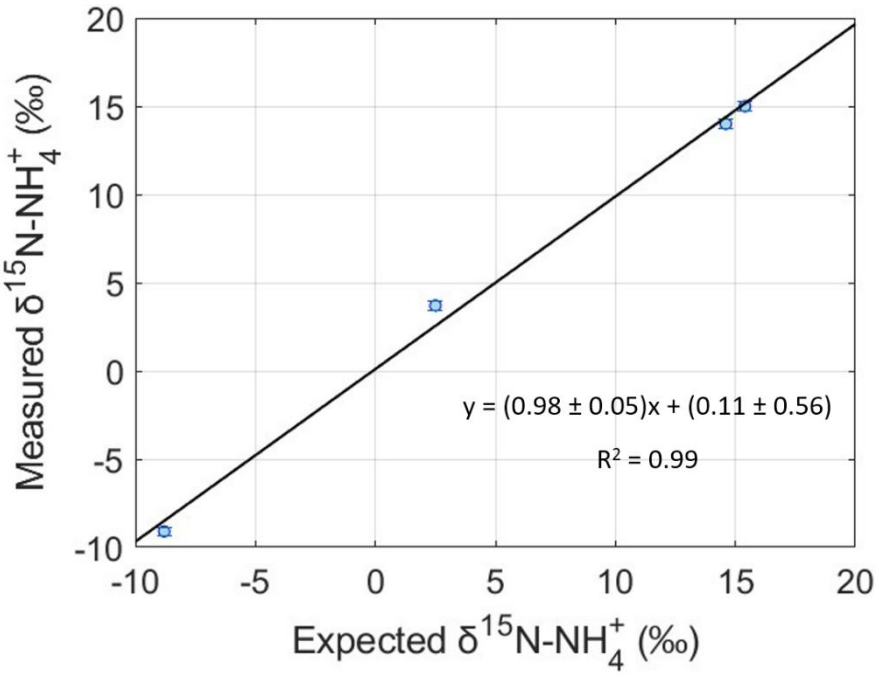

Figure 5: Expected vs measured δ^{15}N-NH_4^+ values of four aerosol samples collected on Changdao Island, China. Measured values represent treated samples post resin and extracted with 10 mL of 4 M NaCl. Error bars represent ± 1σ.

Utilizing the Resin Method to Separate NH_4^+ from Samples with Matrix Interferences

Previous marine NH_4^+ aerosol samples from Hawaii demonstrated significant difficulties in being oxidized to NO_2^- without using the resin sample pre-treatment methodology. These samples had sufficiently high NH_4^+ concentrations that ranged from 9 - 306 μM. These samples were processed with the hypobromite alkaline reagent where the NH_4^+ failed to completely oxidize to NO_2^-. For example, 14 samples that yielded lower than expected [NO_2^-] (<60% converted) were processed for their isotopic composition. In addition to revealing incomplete oxidation through lower than anticipated [NO_2^-], they were further shown to be only partially oxidized based on the low N_2O IRMS peak areas where conversion ranged from 28-72% of that expected. Additionally, poor isotope accuracy and precision was found with the lower than expected conversion to NO_2^-, such that a direct comparison between the results with and without

the resin yielded a slope of 0.63 and an R^2 of 0.67 (n = 14). However, when processing these Hawaii samples (n = 57) using the solid phase extraction methodology, 96% successfully oxidized (Figure 6A).

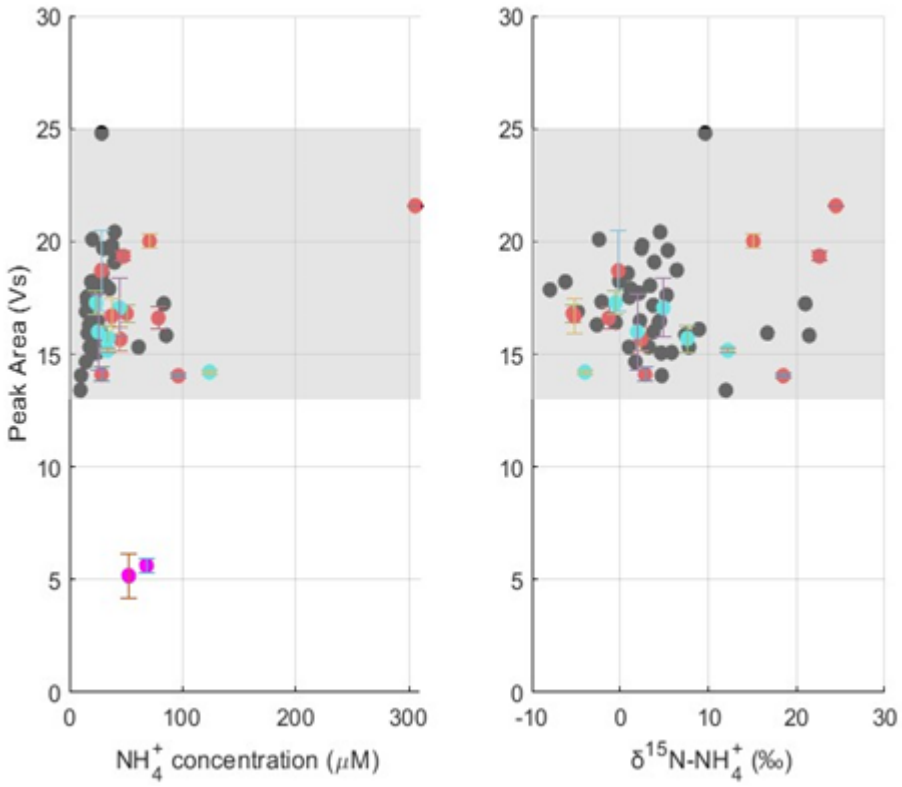

Figure 6: (A): NH_4^+ concentration (µM) of Hawaii marine aerosol samples vs peak area (Vs) from the IRMS. (B): δ^{15}N-NH_4^+ (‰) of Hawaii marine aerosol samples vs peak area (Vs) from the IRMS. For both A and B: Shaded region depicts the acceptable peak range for proper oxidation for these samples. The legend refers to peak area analyses where black circles = single samples, blue circles = replicate samples, red circles = duplicate samples, pink circles = samples run as a duplicate and replicate. Error bars represent ± 1σ for peak area.

Duplicates (n = 10 pairs) and replicates (n = 6 pairs) had a pooled standard deviation of 0.4‰ and 0.5‰, respectively, which is comparable to the standard deviation values of δ^{15}N for the international standards (Table 5). Additionally, average peak areas of blanks (n = 3 per run) were consistently low enough to be adequately corrected for (< 29% of average sample and standard peak areas). Furthermore, the standard/QC averages and low standard deviations in each

run, along with the consistent sample peak areas (Table 5), provide confidence that the resin sample pre-treatment method enabled the successful measurement of accurate and precise δ^{15}N-NH_4^+ for the Hawaii aerosol samples with a difficult sample matrix that originally impeded oxidation (Figure 6B).

Identifying the exact role of the cation exchange in separating out potential matrix interferences is beyond the scope of this work. While it is difficult to know what interferences impact NH_4^+ oxidation and how treating samples through the cation exchange resin removes these interferences, we speculate that it may be related to the presence of organics. The elevated concentration of the eluent extraction (4 M NaCl), which does not appear to impact oxidation, implies that inorganic ions do not have a significant impact on NH_4^+ oxidation. The cation exchange resin should only bind the sample cations and it would be expected that most of the organic material (barring organic cations such as amines) within the sample should pass through the resin without being bound and subsequently extracted. We note that two samples still did not yield the expected N_2O peak areas (Figure 6A). These samples were re-processed through the resin methodology using a higher sample volume to potentially account for an incorrect starting NH_4^+ concentration, but this still yielded lower than expected N_2O peak areas. It is unclear why these samples still were unable to be run successfully for δ^{15}N-NH_4^+, though potentially a separate interference that the cation exchange resins were not able to remove is responsible, such as elevated levels of organic cations. Still, the resin sample pre-treatment method significantly expands the ability to utilize the hypobromite/sodium azide chemical method for δ^{15}N-NH_4^+ analysis of low concentration samples or samples with matrix interferences.

Table 5: Average corrected standard and QC δ^{15}N-NH_4^+ values post cation exchange resin (0.4 g) extracted with 10 mL of 4 M NaCl for unknown Hawaii marine aerosol sample runs

($\bar{x}$ ± 1σ (n)). Combined average standard & QC peak areas (Vs), blank peak averages (Vs), and calculated corrected slopes are included.

Run	$\delta^{15}N$ (IAEA-N2) (‰)	$\delta^{15}N$ (USGS-25) (‰)	$\delta^{15}N$ (QC) (‰)	Standard & QC peak area (Vs)	Blank peak area (Vs)	Slope
1	20.4 ± 0.3 (2)	-30.3 ± 0.4 (3)	-1.4 ± 0.6 (3)	19.2 ± 0.9	5.0 ± 0.9 (3)	1.9 ± 0.02
2	20.4 ± 0.7 (6)	-30.4 ± 0.5 (6)	-1.2 ± 0.3 (6)	22.0 ± 1.1	5.3 ± 0.1 (3)	2.0 ± 0.02
3	20.4 ± 1.1 (4)	-30.3 ± 0.6 (4)	-0.7 ± 0.2 (4)	21.0 ± 1.2	3.7 ± 0.1 (3)	2.1 ± 0.03
4	20.4 ± 0.7 (4)	-30.3 ± 0.8 (4)	-2.0 ± 0.5 (4)	21.0 ± 1.9	4.3 ± 0.2 (3)	2.1 ± 0.03

Conclusion

The $\delta^{15}N$-NH_4^+ of environmental samples can be difficult to analyze due to low concentrations, and potential matrix interferences that prevent necessary oxidation of NH_4^+ to N_2O using widely employed chemical oxidation methods (e.g., a BrO^- oxidizing reagant). To combat some of these issues, we present a purification methodology for robust $\delta^{15}N$ analyses of atmospheric NH_4^+ samples. This is achieved via a sample pre-treatment step utilizing a solid phase extraction technique with cation exchange resins. In this method, 0.4 g of cation exchange resin (AG-50W) was used per column and samples/standards/blanks were extracted with 10 mL of 4 M NaCl, parameters that were optimized through a series of control tests. These resins were able to successfully concentrate samples from 1.0 μM to 10 μM, which was tested on two international standards (IAEA-N2 and USGS-25) and an in-house quality control (QC) solution. Without use of this pre-treatment step, the $\delta^{15}N$ analysis of NH_4^+ samples below 7.5 μM were shown to be unreliable.

Additionally, samples from Changdao Island, China (n = 4), which were previously measured for $\delta^{15}N$-NH_4^+ and experienced no matrix interference issues, yielded excellent and comparable results with and without use of the resins (R^2 = 0.99). The average differences

between the expected (previously reported) $\delta^{15}N\text{-}NH_4^+$ and the measured $\delta^{15}N\text{-}NH_4^+$ with the pre-treatment resin step is ≤ 0.6‰. Importantly, this new methodology was successful on marine aerosol samples from Oahu, Hawaii (n = 57), that displayed matrix interference issues where the NH_4^+ could not previously be oxidized. Using this cation exchange resin methodology, 96% of samples successfully oxidized, and the pooled standard deviations for duplicate (n = 10) and replicate (n = 6) pairs were 0.4‰ and 0.5‰, respectively. Therefore, we recommend utilizing this sample pre-treatment methodology for all environmental NH_4^+ samples to obtain accurate and precise $\delta^{15}N$ measurement.

Funding Sources

This research was funded by the National Science Foundation (NSF-OCE #1851343). We also acknowledge support from an Institute at Brown for Environment and Society Seed Grant.

Data Availability

To obtain the data used in this study, go to https://doi.org/10.7910/DVN/ZQFLOJ. This data will be made public upon publication. Isotopic correction sheet available upon request.

References

1. Altieri, K.E., Fawcett, S.E., Hastings, M.G. 2021. Reactive nitrogen cycling in the atmosphere and ocean. Annual Reviews, 49, 523-550.
2. Xu, L., Penner, J.E. 2012. Global simulations of nitrate and ammonium aerosols and their radiative effects, Atmos. Chem. Phys., 12(20), 9479– 9504.
3. Jickells, T.D., Kelly, S.D., Baker, A.R., Biswas, K., Dennis, P.F., Spokes, L.J., Witt, M., Yeatman, S.G. 2003. Isotopic Evidence for a Marine Ammonia Source. Geophysical Research Letters, 30(7).
4. Altieri, K.E., Hastings, M.G., Peters, A.J., Oleynik, S., Sigman, D.M. 2014. Isotopic evidence for a marine ammonium source in rainwater at Bermuda. Global Biogeochemical Cycles, 28(10), 1066-1080.
5. Le Roy, E., Walters, W.W., Joyce, E.E., Hastings, M.G. 2021. Sources of ammonium in seasonal wet deposition at a coastal New England city. Atmospheric Environment, 260, 118557.
6. Walters, W.W., Karod, M., Willcocks, E., Baek, B.H., Blum, D.E., Hastings, M.G. 2022. Quantifying the importance of vehicle ammonia emissions in an urban area of northeastern USA utilizing nitrogen isotopes. Atmos. Chem. Phys., 22, 13431–13448.
7. MacFarland, A.B., Joyce, E.E., Wang, X., Walters, W.W., Altieri, K.E., Schiebel, H.N., Hastings, M.G. 2023. Investigation of coastal ammonium aerosol sources in the Northwest Pacific Ocean. Atmospheric Environment 312, 120034.
8. Sigman, D.M., Fripiat, F. 2019. Nitrogen Isotopes in the Ocean. Academia, Encyclopedia of Ocean Sciences (Third Edition), 263-278.
9. Walters, W.W., Song, L., Chai, J., Fang, Y., Colombi, N., Hastings, M.G. 2020. Characterizing the spatiotemporal nitrogen stable isotopic composition of ammonia in vehicle plumes. Atmos. Chem. Phys., 20, 11551–11567.
10. Song, L., Walters, W.W., Pan, Y., Li, Z., Gu, M., Duan, Y., Lü, X., Fang, Y. 2021. 15N natural abundance of vehicular exhaust ammonia, quantified by active sampling techniques. Atmos. Environ., 255, 118430.
11. Zhang, L., Altabet, M., Wu, T., Hadas, O. 2007. Sensitive Measurement of NH4+ 15N/14N (*d*15NH4+) at Natural Abundance Levels in Fresh and Saltwaters. Anal. Chem., 79, 5297-5303.
12. Walters, W.W., Hastings, M.G. 2018. Collection of Ammonia for High Time-Resolved Nitrogen Isotopic Characterization Utilizing an Acid-Coated Honeycomb Denuder. *Anal. Chem.*, 90(13), 8051–8057.
13. Walters, W.W., Blum, D.E., Hastings, M.G. 2019. Selective Collection of Particulate Ammonium for Nitrogen Isotopic Characterization Using a Denuder–Filter Pack Sampling Device. *Anal. Chem.*, 91(12), 7586–7594.
14. Stark, J.M., Hart, S.C. 1996. Diffusion Technique for Preparing Salt Solutions, Kjeldahl Digests, and Persulfate Digests for Nitrogen-15 Analysis. Soil Science Society of American Journal, 6(60), 1846-1855.
15. Zhang, S., Fang, Y., Xi, D. 2015. Adaptation of micro-diffusion method for the analysis of 15N natural abundance of ammonium in samples with small volume. Rapid Commun. Mass Spectrom., 29, 1297–1306.
16. Lamothe, A., Savarino, J., Ginot, P., Soussaintjean, L., Gautier, E., Akers, P.D., Caillon, N., Erbland, J. 2023. An extraction method for nitrogen isotope measurement of ammonium in low concentrated environment. Atmos. Meas. Tech., 16, 4015–4030.

17. Mcllvin, M.R., Altabet, M.A. 2005. Chemical Conversion of Nitrate and Nitrite to Nitrous Oxide for Nitrogen and Oxygen Isotopic Analysis in Freshwater and Seawater. Anal. Chem., 77, 5589-5595.
18. O'Dell, J.W. 1993. In: Method 353.2, Revision 2.0: Determination of Nitrate-Nitrite by Automated Colorimetry. US EPA.
19. O'Dell, J.W., 1993. In: Method 350.1, Revision 2.0: Determination of Ammonia Nitrogen by Semi-automated Colorimetry. US EPA.
20. Biasi, C., Jokinen, S., Prommer, J., Ambus, P., Dorsch, P., Yu, L., Granger, S., Boeckx, P., Nieuland, K.-V., Bruggemann, N., Wissel, H., Voropaev, A., Zilberman, T., Jantti, H., Trubnikova, T., Welti, N., Voigt, C., Gebus-Czupty, B., Czupty, Z., Wanek, W. 2022. Challenges in measuring nitrogen isotope signatures in inorganic nitrogen forms: An interlaboratory comparison of three common measurement approaches. Rapid Communications in Mass Spectrometry, 36(22).
21. Böhlke, J.K., Coplen, T.B. 1995. Interlaboratory comparison of reference materials for nitrogen-isotope-ratio measurements, reference and intercomparison materials for stable isotopes of light elements. Vienna, Austria, 1993. In: Proceedings of the IAEA-TECDOC-825 Consultants Meeting.
22. Böhlke, J.K., Gwinn, C.J., Coplen, T.B. 1993. New reference materials for nitrogen-isotope- ratio measurements. Geostand. Geoanal. Res., 17, 159–164.
23. https://www.biorad.com/webroot/web/pdf/lsr/literature/LIT203.pdf

Chapter 4

Investigation of Open Ocean Ammonium Aerosol Sources in the North Pacific Ocean (Oahu, Hawaii)

Alexandra B. MacFarland[1], Wendell W. Walters[2], Katye E. Altieri[3], Meredith G. Hastings[1]

[1] Department of Earth, Environmental, and
Planetary Sciences and Institute at Brown for Environment and Society
Brown University
324 Brook Street, Box 1846
Providence, RI 02912

[2] Department of Chemistry and Biochemistry
University of South Carolina
631 Sumter Street
Columbia, SC 29208

[3] Department of Oceanography
University of Cape Town
Rondebosch, 7700, South Africa

Under review in *Marine Chemistry*

Abstract

Anthropogenic nitrogen (N) deposition entering the ocean from the atmosphere has increased over time. Ammonia (NH_3), a precursor to ammonium (NH_4^+), is released into the atmosphere via both natural and anthropogenic sources, such as ammonification, biomass burning, decomposition of waste, agriculture, industry, sewage, vehicle emissions, and the surface ocean. Studies disagree on the quantity of anthropogenic N deposition to the ocean, as well as the consequences this excess N poses to the biogeochemistry of the open ocean, particularly in the Pacific Ocean. Understanding the current role that the open ocean is playing in the N cycle and budget is essential to determine the sources of N (e.g., internal or external, recycled or excess) and to further distinguish the relationships between atmospheric and oceanic N. Therefore, in the current study, ion concentrations and ammonium isotope values ($\delta^{15}N\text{-}NH_4^+$) were measured for aerosol samples collected on the coast of Oahu, Hawaii from 2021-2022 (n=67). This location was chosen based on low anthropogenic activity, access to the open ocean, and the premise of a dominant marine signal. Particulate NH_4^+ concentrations ($[NH_4^+]$) averaged 3.7 ± 7.3 ng/m^3, with no distinct seasonality ($p > 0.05$). The $\delta^{15}N\text{-}NH_4^+$ values also did not exhibit distinct seasonality ($p > 0.05$), but did fall into three unique clusters (using a k-means clustering analysis): cluster one = 19.0 ± 3.9‰ (n=8), cluster two = 4.1 ± 2.3‰ (n=31), and cluster three = -3.3 ± 2.4‰ (n=13). Cluster three was best explained as an ocean emissions signature, which was determined via a phase partitioning model that incorporated N isotope fractionation associated with NH_3 conversion to NH_4^+. Cluster one had higher than average $[NH_4^+]$ along with air mass origins from two seabird sanctuaries and was hypothesized to be a seabird emission signature. Cluster two was considered a mix of these two sources (67% marine, 33% seabird emissions). 6% of [IN] is from $[NH_4^+]$, with 35% resulting from seabird emissions.

The annual inorganic N (IN; NO_3^- + NH_4^+) dry deposition value for this site was 1.3 ± 1.1 Tg $N \cdot y^{-1}$.

1. Introduction

There has been a steady rise in atmospheric nitrogen (N) deposition over the last several decades (Galloway *et al*., 2008), specifically in coastal oceans (Jickells *et al*., 2017). Consequences include algal blooms, oxygen minimum zones, reduced biodiversity, and shifts in ecosystem structures (Cosper *et al*.,1989; Smetacek *et al*., 1991; Nixon, 1995; Paerl *et al*., 2002; Rabalais, 2002). The amount of anthropogenic N entering the ocean from the atmosphere potentially rivals the amount from N-fixation (Jickells *et al*., 2003; Jickells *et al*, 2017). Ammonia (NH_3), a precursor to ammonium (NH_4^+), is released into the atmosphere via both natural and anthropogenic sources, such as: lightning, biomass burning, N-fixation, agriculture, industry, and vehicle emissions (Zhao *et al*., 2015). Anthropogenic external sources are likely affecting the overall oceanic N budget and the balance of N in the ocean (Altieri *et al*., 2021). This excess N is defined as relative to the expected ratio of N to phosphorus (P; $R_{N:P}$) in the open ocean (i.e., $N^* = N - (R_{N:P}) \times P$; Gruber and Sarmiento, 1997). Although the effects of +N* are well understood in coastal ecosystems, the consequences associated with the open ocean are less well constrained. Additionally, the deposition rates and specific source origins of this +N* are not agreed upon in the literature.

A region where this issue is especially unresolved is the North Pacific Ocean (NPO) where studies suggest opposing conclusions based on N*-rates and observed rates of atmospheric N deposition. Marine N-fixation is a prominent source of bio-available N to the ocean's surface, especially seasonally, according to long-term studies at station ALOHA, which sits in the North Pacific Subtropical Gyre. Studies at Station ALOHA, however, concluded that only roughly 75%

of the N measured could be explained through N-fixation and mesoscale mixing, implying that the remaining 25% could be explained by atmospheric deposition (Johnson *et al*., 2010; Quay *et al*., 2010; Karl *et al*., 2012). Another study observed nitrate (NO_3^-) fluxes in and out of the euphotic zone near Hawaii and utilized isotopic measurements to characterize variations in thermocline concentrations of NO_3^- as both N-fixation and diagenetic alteration of sinking material (Casciotti *et al*., 2011). Using a box model, Böttjer *et al*. (2017) concluded that N-fixation accounts for 26-47% of total N export in waters in the late summer/early fall (when the upper ocean is warm and stratified), which is when the majority of N-fixation takes place. This method, however, excluded the potential input of N through atmospheric deposition as well as advection of new N to the upper ocean layer due to their poor constraints. Letscher *et al*. (2016) employed an oceanic model that incorporated both ocean circulation and ecosystem dynamics and concluded that lateral transport and biological uptake of organic and inorganic N and phosphorus from gyres matches, and sometimes surpasses, vertical delivery of nutrients. In this work, Letscher *et al*. combined atmospheric N deposition and N-fixation as external inputs, with this supplying a quarter of the yearly available N. A study of N isotopic measurements in corals suggested that the observed lower isotopic values were the result of anthropogenic atmospheric deposition, but this claim is dependent on open ocean studies that proposed that N-fixation rates have not varied significantly over the last few decades. Zhao *et al*. (2015) discussed how monsoonal flow and seasonal emission sources also affect N deposition to the North Pacific Ocean, but Letscher *et al*. (2016) was able to justify nutrient dynamics without those variables. Further, parameters on N-fixation in various models are inconsistent, and can be quite sensitive to atmospheric inputs (Casciotti *et al*., 2024), increasing their uncertainty. Therefore, more in-

depth atmospheric and ocean studies are vital to better understand atmospheric N deposition, which could have a large impact on the biogeochemistry of the open ocean (Kim *et al*., 2014).

NH_x (NH_3 + NH_4^+) is a readily bioavailable form of N, with an increased rate of loading into the atmosphere over the last several decades (Altieri *et al*., 2021). However, it can be challenging to track due to its short lifetime (hours to days; Xu and Penner, 2012) and its numerous emission sources and fates (e.g., dry deposition, cloud scavenging, formation of NH_4^+ aerosols, bidirectional exchange). Additionally, year-round atmospheric NH_x concentrations are very limited. Distinguishing amongst NH_3 emission sources is needed to understand the effects of human activities and natural emissions on various environments, particularly the open ocean (Altieri *et al*., 2021).

The stable N isotopic composition of NH_4^+ can be an informative tool to analyze the chemistry and emission sources of reactive N (Jickells *et al*., 2003; Altieri *et al*., 2014; Le Roy *et al*., 2021; Altieri *et al*., 2021; Walters *et al*., 2022; MacFarland *et al*., 2023). The composition of stable N isotopes is stated using delta notation ($\delta^{15}N$) and is established as follows: $\delta^{15}N$ (‰) = $[(^{15}N/^{14}N)_{sample}/(^{15}N/^{14}N)_{standard} - 1] \times 1000$, where air-$N_2$ is the N isotopic reference. Small but measurable changes in the ratio of ^{15}N:^{14}N among the different N forms (e.g., NH_x) are detectible among chemical, biological, and physical processes as well as varying source origins (Sigman and Fripiat, 2019). Marine and terrestrial atmospheric NH_4^+, for example, have distinct observed $\delta^{15}N$ values, therefore allowing the tracing of natural and anthropogenic NH_3 emissions (e.g., marine origins are usually lower in $\delta^{15}N$ compared to terrestrial origins; Jickells *et al*., 2003; Walters *et al*., 2020; Altieri *et al*., 2021; Song *et al*., 2021). For example, aerosols collected from a remote region of the Atlantic Ocean had low $\delta^{15}N$-NH_4^+ values (−8 to −5‰) that were linked to marine activity whereas high $\delta^{15}N$-NH_4^+ values (up to +10‰) were linked to the transport of air

masses from the continents (Jickells *et al*., 2003). Another study in the Atlantic Ocean analyzed the isotopic composition of seasonal atmospheric NH_4^+ in precipitation and concluded the input of a year-round marine source (Altieri *et al*., 2014). Later, it was calculated that only ~ 27% of total N deposition (organic and inorganic) to the North Atlantic Ocean was anthropogenic in origin (Altieri *et al*., 2016), revealing a larger role for recycling of oceanic N in the marine boundary layer than expected.

Understanding the current role that the open ocean is playing in the N cycle and budget is essential to determine the sources of N (e.g., internal or external, recycled or excess) and to further distinguish the relationships between atmospheric and oceanic N. Therefore, we aimed to study the influence of reactive inorganic N aerosol deposition (NH_x, NO_x) in the North Pacific Ocean (Oahu, Hawaii), where we expected to observe a dominant marine input. The objectives of this study were to (1) characterize the aerosol composition at Oahu across the year, (2) determine the NH_4^+ source origins, and (3) calculate the rate of annual dry inorganic N deposition to the NPO. A suite of tools was used including ion concentration measurements, $\delta^{15}N\text{-}NH_4^+$ analyses, species correlation calculations, air mass back trajectory calculations, cluster analysis, and isotope mixing models that include phase partitioning and fractionation.

2. Methods

2.1. Study Locations

A stationary sampling site was located on the eastern windward side of Oahu, Hawaii (21.32°N, -157.67°W), with the Hawaiian archipelago sitting roughly 3,200 km southwest of the contiguous United States (Figure 1). Aerosol samples (*n*=67, bulk total suspended particles (TSP))) were collected using a high-volume aerosol sampler operating at about 1,200 L min^{-1}. The samples were collected, on average, over seven days (exact number of hours were recorded)

from March 2021 – June 2022. Laboratory blanks and field blanks were taken to assess potential contamination from laboratory and field procedures. Laboratory blanks include prepared filters that were sealed and kept in the laboratory. Field blanks are generated by placing a filter in the sampler and then removing and processing it as a sample and were collected bi-weekly (*n*=26). The aerosol sampler, roughly ~1 m tall, was placed on the eastern most side of the Makai Research Pier. Weather data were collected concurrently, including atmospheric temperature (°C), relative humidity (%), wind direction (360°), and wind speed (m/s) every minute. All filter samples and field blanks were frozen at -20°C after collection and shipped frozen to Brown University. This has been demonstrated to be adequate for maintaining the original chemical composition of aerosol samples (Knapp *et al*., 2010; Altieri *et al*., 2013, 2014; Gobel *et al*., 2013).

Open ocean aerosol samples (*n*=4) and blanks were also collected via a Hawaii Ocean Time series (HOTs) research cruise from 7/29/22 – 8/1/22. The research cruise left from Honolulu, Oahu and made stops at Station Kahe (21°20.6'N, 158°16.4'W), Station Aloha (22°45.0'N, 158°00.0'W), and Station Kaena (21°50.8'N, 158°21.8'W) before returning to Honolulu, Oahu (Figure 1). The air sampler was set up at the hull of the ship on the top deck, with the exhaust pipe near the sampler shut off during collection to avoid collecting ship emissions. Two samples were collected while stationery at Station Aloha, and two samples were collected while the ship was moving (one from Kahe to Aloha and another from Aloha to Kaena). Aerosol samples were collected, stored frozen, and then processed via the same procedures as the stationary samples.

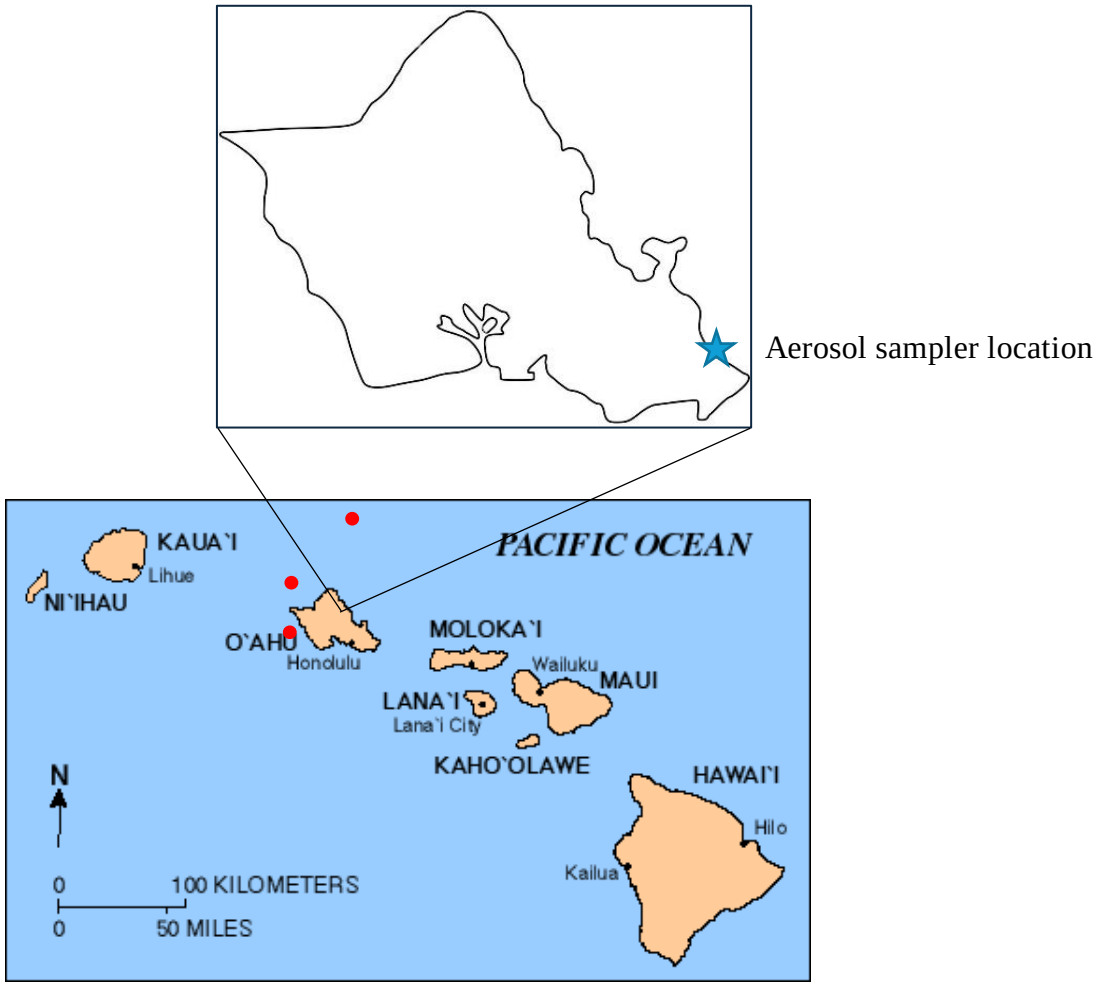

Figure 1: Map of Hawaiian Islands (bottom) and location of sampling on Oahu (top; 21.32°N, -157.67°W, yellow star). Red dots, from bottom to top, represent Station Kahe (21°20.6'N, 158°16.4'W), Station Kaena (21°50.8'N, 158°21.8'W), and Station ALOHA (22°45.0'N, 158° 00.0'W).

2.2. Filter preparation

For stationary sampling, glass fiber filters (TE-G653; in compliance with the method of US EPA FRM 40 CFR Part 50 Appendix B) were baked at 500°C for 4 h and kept in aluminum foil prior to use. For the HOTs cruise samples (section 2.2), the filters were coated in 5% citric acid before being baked in order to collect total NH_x (Walters *et al*., 2019a).

2.3. Filter digestion

After the frozen samples were received at Brown University, 5.1 cm diameter circles were cut from each filter (exact number of circular extracts varied between filters and was recorded). These filter cut-outs were extracted in a pre-cleaned bottle with ~50 mL of ultraclean water (>18 MΩ ; MilliQ; exact amounts were recorded via weight) and then sonicated for three hours. The contents were then filtered via a vacuum pump system (Omicron nylon membrane 0.2 µm filter) and the solution was collected into separate clean bottles. The vacuum pump system was cleaned with MilliQ water between each sample.

2.4. Nitrogen Concentration Analysis

The concentration of ammonium ($[NH_4^+]$), nitrate ($[NO_3^-]$), and nitrite $[NO_2^-]$) were obtained colorimetrically (indophenol blue) via a discrete UV–Vis analyzer (Westco Smartchem 200). U.S. EPA Compliant Methods 350.1, 353.2 (Revision 2.0), and 354.1 were followed for NH_4^+, NO_3^-, and NO_2^- (O'Dell, 1993a, O'Dell, 1993b), respectively. Standard lab protocols were followed, including calibration to standards as well as blanks and repeated measures of an in-house quality control. $[NO_2^-]$ was low, on average, at ~2 µmol L^{-1} (near detection limit), with similar concentrations for field blanks. Therefore, NO_2^- measurements were not utilized during any further analyses. Liquid concentrations (µmol L^{-1}) were converted to air concentrations (µg m^{-3}) based on extraction volume (L) and average volume of air sampled through the filter (m^3). Relative standard deviations for NH_4^+ (n=11) and NO_3^- (n=10) QCs were both < 5%. Average field blanks for NH_4^+ had a relative standard deviation of 9%, so the average blank value was subtracted from sample measurements. NO_3^- had a relative standard deviation of < 5% of sample averages, so no blanks were subtracted.

2.5. Ion Concentration Analyses

Sodium (Na^+), potassium (K^+), calcium (Ca^{2+}), magnesium (Mg^{2+}), chloride (Cl^-) and sulfate (SO_4^{2-}) concentrations were measured on an Ion Chromatography (IC) instrument (Dionex Integrion HPIC) using suppressed conductivity detection. Anions were determined using a Dionex AS19-4 μm guard (4 × 50 mm) and analytical column (4 × 250 mm) with 20 mM KOH as eluent with a flow rate of 1 mL min^{-1}. Cations were analyzed using a Dionex CS-16 guard column (5 × 50 mm) analytical column (5 × 250 mm). Eluent of 30 mM methane sulfonic acid was used to detect cations with a pump flow rate of 1 mL min^{-1}. All samples were filtered with 0.20-μm filters before being analyzed. In-house QCs were run approximately every 10 samples. The relative standard deviation for QCs of Na^+ (*n*=8), K^+ (*n*=8), Ca^{2+} (*n*=8), and SO_4^{2-} (*n*=7) were < 5% whereas Cl^- was 5.2% (*n*=7) and Mg^{2+} was 7.3% (*n*=8). Average field blanks for K^+ had a relative standard deviation of 9%, so the average blank value was subtracted from sample measurements. The remaining ions had a blank relative standard deviation of < 5% of sample averages, so no blanks were subtracted.

2.6. HYSPLIT Air Mass Back Trajectory Analysis

Air mass back trajectories for each aerosol sample were calculated using NOAA's Hybrid Single-Particle Lagrangian Integrated Trajectory (HYSPLIT; Rolph *et al*., 2017; Stein *et al*., 2015). The plugin 'trajstat' (Wang *et al*., 2009) was utilized to compute these trajectories in order to assist in the source determination of NH_4^+. Employing particle dispersion simulation and meteorological data, the model calculates the trajectory of an air mass backward in time, starting from a given point and time. Back trajectories were run at a height of 500 m above ground level

every 6 h for the length of the sample collection time plus an additional 72 hours to account for the average lifetime of atmospheric NH_x (Paulot *et al*., 2016).

2.7. Potential Source Contribution Function Maps

Potential source contribution function (PSCF) maps were produced seasonally through the combined use of NH_4^+ concentrations and back trajectory calculations. Seven and ten-day trajectories were calculated, with very similar results, so the seven-day trajectories were utilized during PSCF analyses as the day-day trajectories overlap with other samples and would skew PSCF results when concentrations were added. These maps establish the most likely location of origin of NH_4^+, or other species of interest, relative to the study site. These calculations are based on the evaluation, for each grid cell (or area), of the ratio of the total number of marked trajectory segment endpoints to the total number of trajectory segment endpoints over that grid cell (Wang *et al*., 2009).

2.8. $\delta^{15}N$-NH_4^+ Analysis

The determination of $\delta^{15}N$–NH_4^+ followed the protocol of Zhang *et al*. (2007) based on a coupled off-line wet-chemistry technique using hypobromite (BrO) oxidation and acetic acid/sodium azide reduction. This was combined with a pre-treatment step developed by MacFarland *et al*., (2024) that used a solid phase extraction technique involving cation exchange resins to concentrate samples and remove potential matrix interferences (anions, organics, etc). Samples were diluted with MilliQ water to 10 μmol-NH_4^+. NH_4^+ was then oxidized to NO_2^- using BrO in an alkaline solution, and further synthesized following the protocol by Zhang *et al*. (2007). The reaction was then stopped by the addition of sodium arsenite to extract the remaining

BrO. The samples were then transferred into 20 mL vials, crimp-capped with PTFE/butyl septa, and flushed with helium gas for a minimum of 10 min. The NO_2^- was then reduced to nitrous oxide gas (N_2O) through the addition of 2 mL of 2 M sodium azide buffered in 40% acetic acid solution. After half an hour (minimum), the samples were neutralized using 6 M sodium hydroxide. Samples were then analyzed for the $\delta^{15}N$–N_2O composition via an automated N_2O extraction system coupled with a continuous flow Isotope Ratio Mass Spectrometer (IRMS) for determination at m/z 44, 45, and 46. Successful oxidation was based on expected sample peak areas measured by the IRMS. In each sample set, unknowns were calibrated to two internationally recognized NH_4^+ isotopic reference materials, IAEA-N2 ($\delta^{15}N$ = 20.4‰) and USGS-25 ($\delta^{15}N$ = 30.3‰; Böhlke *et al*., 1993; Böhlke and Coplen, 1995). An internal QC ($\delta^{15}N$ = –1.0 ± 0.5‰) was also run multiple times throughout each run to check the accuracy of the instrument against a known sample that underwent the same corrections as the unknown samples. The isotopic standards underwent the same chemical processing as the unknowns and were used to correct for isotopic fractionation (i.e., from the chemical conversion of NH_4^+ to N_2O). The isotopic standards had a standard deviation (1σ) of ± 0.8‰ for IAEA-N2 (*n*=16), ± 0.6‰ for USGS-25 (*n*=17), and ± 0.6‰ for the QC (*n*=17). Additionally, the pooled standard deviation for duplicates (n = 10 pairs) and replicates (*n*=6) was 0.4‰ and 0.5‰, respectively.

2.9. Oceanic Phase Partitioning Model

A phase partitioning model was implemented in *R*, following Altieri *et al*. (2014) with modifications described in the Supplemental Text. Inputs included ocean pH, ocean salinity, ocean temperature, surface water [NH_4^+], surface water $\delta^{15}N$-NH_4^+, atmospheric temperature, and wind speed. Briefly, this model calculates the $\delta^{15}N$-$NH_{3(g)}$ assuming the flux of NH_3 from

the ocean to the atmosphere is the sole NH_3 source. A range of $\delta^{15}N\text{-}NH_4^+$ aerosol values are then calculated using three different gas-to-aerosol formation scenarios and the isotope effects associated with each process. Scenario one assumes equilibrium between NH_3 and NH_4^+ (Eq1 and Eq2). Eq1 is from Walters *et al*. (2019b) in which the gas to aerosol equilibrium fractionation is due to atmospheric temperature.

$$^{15}\alpha_{NH4+(s)/\,NH3(g)} = (((12522 / T(K)) - 11.31) /1000) +1 \quad \text{(Eq1)}$$

where T(K) is temperature in kelvin.

α is then inputted into the following equation.

$$\delta^{15}N\text{-}NH_4^+ = 1000\alpha + (\alpha \times \delta^{15}N\text{-}NH_3) - 1000‰ \quad \text{(Eq2)}$$

Scenario two (Eq 3) assumes that NH_x is in phase equilibrium with the atmosphere and ocean, and that NH_3 is absorbed in H_2O followed by the formation of $NH_4^+{}_{(aq)}$ (from Walters *et al*., 2019b).

$$^{15}\alpha_{NH4+(aq)/\,NH3(g)} = (((2275/T(K)) - 3.47)/ 1000) +1 \quad \text{(Eq3)}$$

where α was input into Eq2.

Scenario three (Eq 4) tests non-equilibrium conditions, where NH_3 observes unidirectional neutralization reactions involving $H_2SO4_{(g)}$ during nucleation, so $NH_{3(g)}$ and aerosol NH_4^+ equilibrium is not achieved and results in a kinetic isotope effect of –28‰. Equation (4) considers a 28‰ fractionation value based on diffusion rates of $^{15}NH_3$ relative to $^{14}NH_3$ (Pan *et al*., 2016).

(4) $\delta^{15}N\text{-}NH_4^+ = \delta^{15}N\text{-}NH_3 - 28$ (Eq4)

2.10. Isotopic Source Calculations

The Bayesian mixing model performed with the *R* package SIMMR (stable isotopes mixing models in R; Parnell *et al*., 2013) was applied. It calculates a high number of possible solutions of source contributions to each sample measurement by employing Bayes theorem. This model is equipped with a Monte Carlo Markov Chain algorithm that computes likely solutions for each source's influence on individual samples (Parnell *et al*., 2010, 2013; Cooper *et al*., 2014). From these *n* realizations, the best estimate (mean) and its uncertainty (standard deviation) can be calculated. SIMMR was used in the current study to determine the likelihood of the hypothesized sources (marine, seabird waste emissions) being the origin of the NH_3 emissions to the ocean in this region.

ISOERROR1_04 is a Microsoft Excel 2000™ spreadsheet that calculates estimates and confidence intervals of source proportional contributions to a mixture, using stable isotope analyses (Phillips and Gregg, 2001). This model was utilized to calculate % contributions of isotope signatures to a mixed signature (e.g., how much of clusters one and three made up cluster two)

3. Results and Discussion

3.1. Species Concentrations

Aerosol NH_4^+ concentrations did not vary seasonally ($p > 0.05$) with an average concentration of 3.7 ± 7.3 ng/m^3 across the dataset, including two samples with unusually high concentrations of 54.6 ng/m^3 and 27.9 ng/m^3 in May and November, respectively (Figure 2;

Table 1). Without these two high concentrations, the average concentration and standard deviation drops to 2.5 ± 2.1 ng/m^3

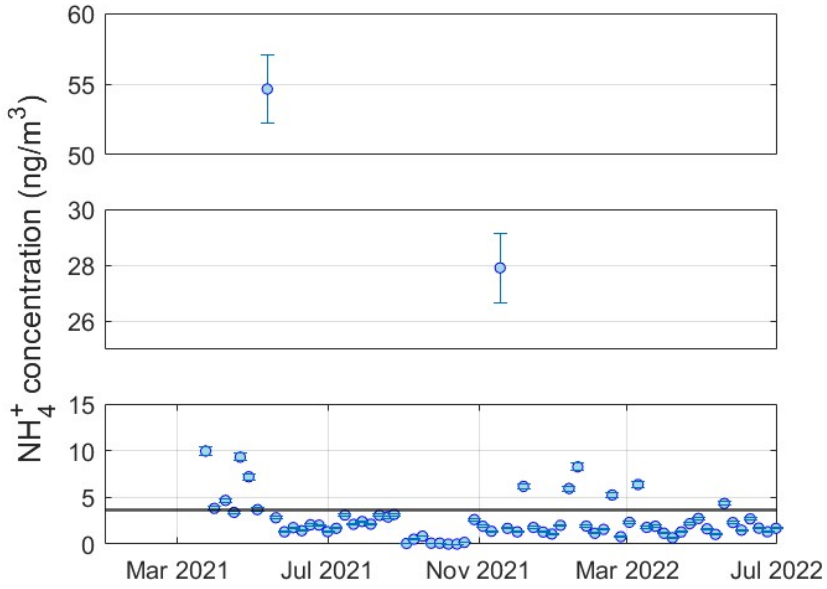

Figure 2: Time series of ammonium concentration (ng/m^3) where distinctly higher values were captured in the top and middle panels. Error bars represent the relative standard deviation for the N concentration measurement technique (4.4%). Black line depicts the average value of 3.7 ng/m^3.

This average concentration is much lower than model predictions (annual mean values from the GEOS-Chem simulation driven by COBALT-HA seawater [NH_x]), which suggested that [NH_4^+] in this region is around 60.0 ng/m^3 (Paulot *et al*., 2015).

The composition of the aerosols in this study is unsurprisingly dominated by Na^+ and Cl^- (Table 1; Figure 3). NO_3^- is the only ion that varied significantly seasonally ($p < 0.05$), though it is unclear currently what drives this.

Table 1: Average concentrations (ng/m^3 ± 1σ) of measured ions (*n*=67 for all).

Species	Average (ng/m^3)
NH_4^+	3.7 ± 7.3
NO_3^-	51 ± 22
K^+	21 ± 13
Ca^{2+}	110 ± 38
Mg^{2+}	600 ± 160
SO_4^{2-}	440 ± 260
Cl^-	7,900 ± 4,200
Na^+	6,300 ± 4,200

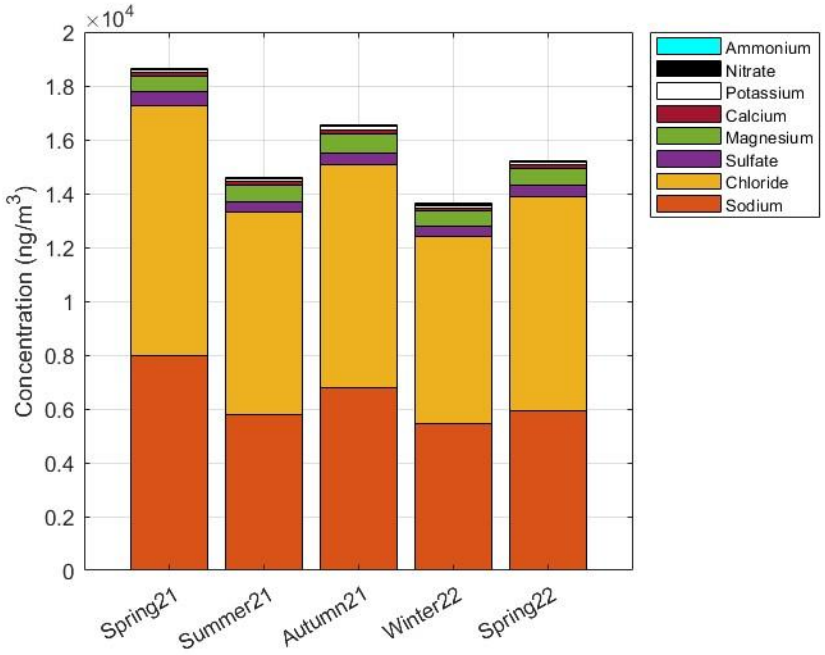

Figure 3: Stacked bar graph of species concentration changes among the collection seasons. Numbers after season are indicative of collection year (*n*=13 per season).

There are no recent studies in the literature that investigate open ocean aerosol composition near Hawaii. Carrillo *et al*. (2002) measured aerosol ion concentrations and deposition on the island of Hawaii, near the Thurston Lava Tube in Hawaii Volcanoes National Park. They concluded that from 1998-2000, NaCl was the largest % of the aerosol composition (100 out of 177.4 nmol m^{-3}, 57%), followed by SO_4^{2-} (30%), NH_4^+ (5%), Mg^{2+} (4%), NO_3^- (2%), Ca^{2+} (1%), and K^+

(1%). Carrillo *et al*. did not discuss seasonality for the aerosol compositions or calculate non-sea salt (nss) values. Phinney *et al*. (2006) analyzed the composition of aerosol samples collected near Ocean Station Papa (Gulf of Alaska) during the July 2002 Canadian SOLAS SERIES experiment. They concluded the oxidation of dimethyl sulfide, sea salt emissions, and ship emissions to be the chief contributors to their aerosol compositions. The mass fraction of NaCl ranged from 3% to 20% in the fine mode and dominated the coarse mode (>70%). Given the current study's sample collection location and onshore flow, the expected dominant composition of bulk aerosol was from NaCl (>90%).

Model estimates predict that chloride depletion in this region is anywhere from 30-60% (Paulot *et al*., 2015). In this model, sea salt and total nss-SO_4 are presumed to be entirely mixed, which preferences gas phase NH_3 and HCl because sea salt alkalinity would neutralize some of the acidity of the sulfate and HCl would volatilize in the process (Fridlind and Jacobson, 2000). Chlorine depletion can be calculated as:

$$Cl^- \text{ depletion } (\%) = (1.81 \times [Na^+] - [Cl^-])/ (1.81 \times [Na+]) \times 100\ \% \quad \text{(Eq5)}$$

The average chlorine depletion calculated across our dataset was about 30% (29 ± 6%), which is at the low end of the model prediction. However, it is important to note that the model outputs were calculated based on 2006 data and only calculated the Cl^- depletion in fine sea salt aerosol in surface air, whereas this study measured bulk TSP.

Dry deposition velocities for NO_3^- and NH_4^+ to the NPO have a large observed/modeled range of 0.07 - 2.0 cm/s and 0.07 - 0.68 cm/s, respectively (Jung *et al*., 2011; Zhao *et al*., 2015; Baker *et al*., 2016; Baker *et al*., 2017; Qi *et al*., 2020; Seok *et al*., 2021). The large uncertainties

incorporate gravitational settling, impaction, and diffusion of particles, which all can differ in complex functions associated with particle size and meteorological conditions (e.g. wind speed, relative humidity; Duce *et al*., 1991). Still, it is interesting to consider how much inorganic dry deposition is occurring over the open ocean NPO, particularly given the air-sea interactions observed here. Using the minimum and maximum velocities above, a range of 0.1 - 2.7 Tg $N \cdot y^{-1}$ was calculated for the annual total inorganic dry deposition from Oahu to the NPO, with an average of 1.3 ± 1.1 Tg $N \cdot y^{-1}$, which was obtained by using averaged dry deposition velocities from the aforementioned literature. This indicates that the marine environment plays an active role in the oceanic N cycle. As a point of comparison, our year-round work in coastal China, where significant anthropogenic influence was detected, an annual aerosol inorganic N flux of 10.0 - 228.2 Tg $N \cdot y^{-1}$ with an average of 106.6 ± 89.2 Tg $N \cdot y^{-1}$ was found (MacFarland *et al*., 2023). In the North Atlantic, with both anthropogenic and natural influences, a year-round study yielded a combined inorganic N flux of 1.37 Tg $N \cdot y^{-1}$ (Altieri *et al*., 2014). It is noted here that Altieri *et al*. used the warm season aerosol data to obtain non-anthropogenic values and used the cool season aerosol data to obtain anthropogenic values, which means 67% of this total (0.92 Tg $N \cdot y^{-1}$) is thought to be non-anthropogenic.

3.2. Ion Composition

Pearson correlation calculations were determined annually between ions and $\delta^{15}N\text{-}NH_4^+$ to further investigate various relationships in the marine environment (Table 2).

Table 2: Pearson correlation values among ions and isotopes ($p < 0.05$ are bolded).

	NO_3^-	Cl^-	SO_4^{2-}	Mg^{2+}	Ca^{2+}	K^+	Na^+	$\delta^{15}N\text{-}NH_4^+$
NH_4^+	**0.63**	**0.75**	**0.84**	–0.04	–0.03	0.00	**0.78**	**0.54**
NO_3^-	-	**0.32**	**0.44**	**–0.26**	–0.16	–0.25	**0.35**	**0.58**
Cl^-	-	-	**0.98**	**0.92**	**0.91**	**0.93**	**0.98**	**–0.39**
SO_4^{2-}	-	-	-	**0.85**	**0.87**	**0.86**	**0.98**	–0.15
Mg^{2+}	-	-	-	-	**0.91**	**0.96**	**0.97**	**–0.29**
Ca^{2+}	-	-	-	-	-	**0.92**	**0.92**	**–0.38**
K^+	-	-	-	-	-	-	**0.97**	**–0.38**
Na^+	-	-	-	-	-	-	-	**–0.41**

Na^+ is strongly correlated with Cl^-, SO_4^{2-}, Ca^{2+}, and K^+ ($r > 0.80$). This is not surprising as they are sea salt derived ions. Mg^{2+}, the only nss ion (88 ± 0.8%), also had a strong positive correlation with Cl^- and SO_4^{2-} ($r > 0.80$). For the N species, NH_4^+ was moderately correlated with NO_3^- ($r = 0.63$) and strongly correlated with Cl^-, SO_4^{2-}, and Na^+ ($r > 0.70$). $\delta^{15}N\text{-}NH_4^+$ was moderately correlated with NH_4^+ ($r = 0.54$) and NO_3^- ($r = 0.58$).

The fraction of nss values for ions can suggest terrestrial or anthropogenic origins. Nss values were calculated based on:

$$nss\text{-}X = X_{aerosol} - (X/Na)_{seawater} \times Na_{aerosol}, \quad \text{(Eq6)}$$

where the mass ratios of $(X/Na)_{seawater}$ for SO_4^{2-}, K^+, Ca^{2+}, and Mg^{2+} were 0.2515, 0.03701, 0.03821 and 0.012, respectively (Millero, 2006; Nah *et al*., 2021). In this current study, only Mg^{2+} had nss origins (88 ± 0.8%), whereas SO_4^{2-}, K^+, and Ca^{2+} all had 0.0 ± 0.0% nss origins.

Phinney *et al*. (2006) also calculated nss values, with fine nss-SO_4^{2-} having an average mass concentration of 0.74 ± 0.04 μg/m^3, a dominant component of the fine mode particles. It is noted that they calculated nss-SO_4^{2-} differently than the current study, where they initially calculated sea salt SO_4^{2-} as: [ss-SO_4^{2-}] = 0.25[Na^+], using [Na^+] measurements from a Micro-

Orifice Uniform Deposit Impactor. Since the current study observed 0% nss-SO_4^{2-}, it is likely that NH_3 reacted with NO_3^- to form the observed NH_4^+, as they are strongly correlated (r = 0.63; Table 2).

Zhang *et al*. (2010) analyzed total suspended particle aerosol samples over the open South Pacific Ocean that were collected on a research cruise from September – December 2007. They calculated that nss-SO_4^{2-} accounted for 30% of total SO_4^{2-}, nss-Mg^{2+} accounted for 8.3 ± 7.2% of total Mg^{2+}, and nss-Ca^{2+} accounted for 88.4 ± 7.2% of total Ca^{2+}. It was further suggested that dust from the Saharan desert had a large impact on these high nss values for Mg^{2+} and Ca^{2+}. However, no terrestrial influences were observed in the current study based on calculated air back mass trajectories (section 3.5).

3.3. Observed δ^{15}N-NH_4^+

δ^{15}N-NH_4^+ values were not statistically different among seasons (p > 0.05) and ranged from –8‰ to +25‰ (Figure 4).

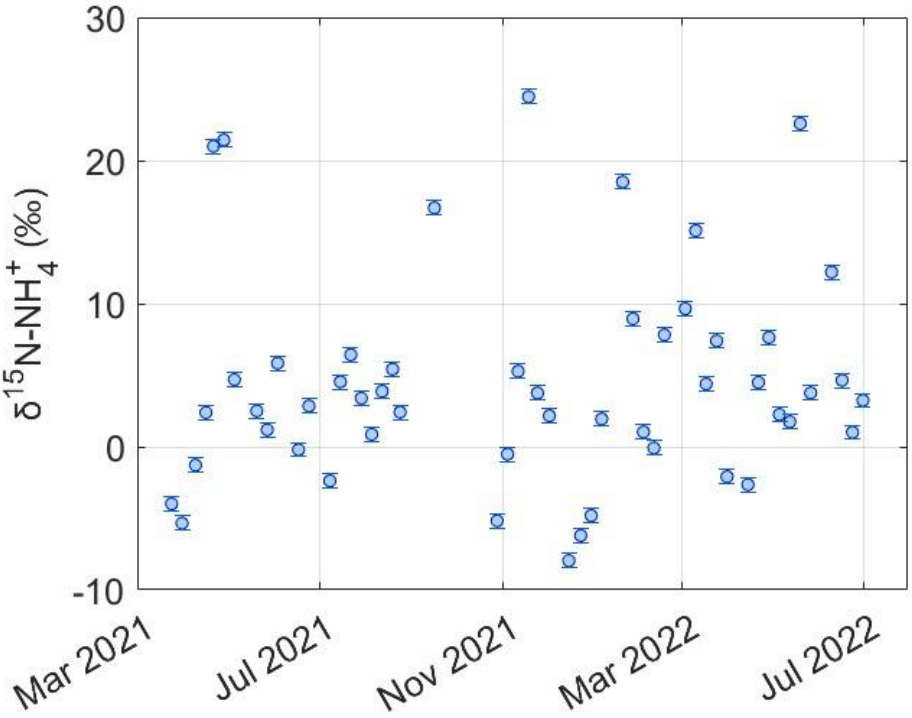

Figure 4: Time series of ammonium isotope values (‰) (*n*=52). Error bars represent the pooled standard deviation for the isotopic measurement technique (0.5‰).

Through the use of K-means clustering, the δ^{15}N-NH_4^+ data was found to divide into three distinct clusters (Figure 5).

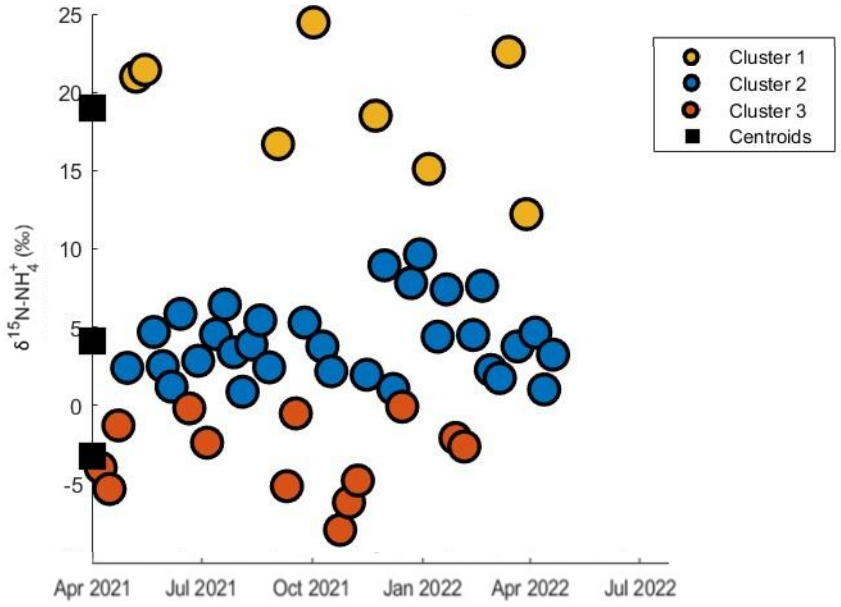

Figure 5: K means cluster plot of δ^{15}N-NH_4^+ values. Centroids (black squares) represent the central points of the clusters.

The cluster ranges are as follows: 12-25‰ for cluster one (19.0 ± 3.9‰; *n*=8), 1-10‰ for cluster two (4.1 ± 2.3‰; *n*=31), and –8 to 0‰ for cluster three (–3.3 ± 2.4‰; *n*=13). It was determined that wind direction and wind speed were not responsible for these separate clusters, as the majority of the wind came from the northeast at 0-10 m/s during the sampling period (Figure S1).

3.4. Cluster Comparisons and HOTs Data

Cluster one had significantly higher concentrations of NH_4^+ and NO_3^-, and significantly lower concentrations of Cl^- and Na^+ compared to the other two clusters ($p < 0.05$; Table 3).

Table 3: Average ion concentrations (ng/m^3 ± 1σ) of the three distinct δ^{15}N-NH_4^+ clusters.

Cluster	$[NH_4^+]$	$[NO_3^-]$	$[Cl^-]$	$[Na^+]$	$[SO_4^{2-}]$	$[Mg^{2+}]$	$[Ca^{2+}]$	$[K^+]$
1	8.4 ± 7.8	75 ± 26	6,100 ± 1,200	4,800 ± 770	380 ± 85	520 ± 100	110 ± 21	93 ± 20
2	2.2 ± 0.9	50 ± 14	7,200 ± 1,600	5,600 ± 1,300	400 ± 85	560 ± 140	130 ± 30	110 ± 28
3	2.7 ± 2.3	44 ± 19	8,300 ± 2,000	6,600 ± 1,500	440 ± 100	650 ± 140	160 ± 38	130 ± 33

The HOTs cruise samples (*n*=4) were also measured for δ^{15}N-NH_4^+, and exhibited depleted values of –9.4, –8.0, –10.6, and –30.7‰. These first three samples fall into cluster three (Figure 5). The fourth point, albeit a possible outlier, could represent predominantly $NH_{3(g)}$. The citric acid coated filters would have collected both NH_4^+ and $NH_{3(g)}$, and $NH_{3(g)}$ has a significantly lower δ^{15}N compared to NH_4^+ due to a large equilibrium isotope effect when converting from a gas to an aerosol (~ 35‰; Walters *et al*., 2019b). The oceanic phase partitioning model (section 3.6) predicts a δ^{15}N-$NH_{3(g)}$ value of ~ –33‰, such that although it is possible that the fourth point is an outlier, it is more likely that the citric acid coating resulted in the sample representing total NHx, of which the majority is NH_3.

3.5. Oceanic Phase Partitioning Model Results

For the oceanic phase partitioning model, ocean pH, ocean salinity, and ocean temperature were based on observations from the Hawaii Ocean Time-series Data Organization & Graphical System (HOT-DOGS) (data obtained via the Hawaii Ocean Time-series HOT-DOGS application; University of Hawai'i at Mānoa. National Science Foundation Award # 1756517). Only the data from 0-10 m was utilized to represent surface water measurements.

Atmospheric temperature and wind speed were recorded via the weather sampler stationed next to the aerosol sampler in this study and were averaged over each sample period.

Several scenarios were considered for the concentration and isotope compositions of surface water NH_x and the isotopic impact of partitioning between NH_3 and NH_4^+ in various phases. For scenario one, it was assumed that equilibrium is achieved between NH_3 and NH_4^+ (Eq1 and Eq2). Scenario two assumes that NH_x is in phase equilibrium with the atmosphere and ocean, and that NH_3 is absorbed into H_2O followed by the formation of $NH_4^+{}_{(aq)}$ (Eq3). Scenario three tests non-equilibrium conditions, where NH_3 observes unidirectional neutralization reactions involving $H_2SO4_{(g)}$ during nucleation, so $NH_{3(g)}$ and aerosol NH_4^+ equilibrium is not achieved and results in a kinetic isotope effect of –28‰ (Eq4). For surface water [NH_4^+] and surface water δ^{15}N- NH_4^+, combinations of a range of 0.01 - 0.1 µM (Karl and Knauer 1984; Shilova *et al*., 2017) and –1.0 – 0.0‰ were used as model inputs respectively, for each scenario (*n*=34). While the δ^{15}N of NH_4^+ cannot be measured for such low concentration samples (Zhang *et al*., 2007), we can reasonably expect it to be low given the low δ^{15}N of suspended particulate N in the North Pacific (from which the NH_4^+ derives; Casciotti *et al*., 2008) and the fact that the δ^{15}N of subtropical phytoplankton reliant on NH_4^+ has been shown to be near 0‰ (Fawcett *et al*., 2011, 2014; Treibergs *et al*. 2014).

For scenario one, where $NH_{3(g)}$ and aerosol NH_4^+ are in equilibrium, the calculated average δ^{15}N-NH_4^+ was –2.8 ± 0.4‰ (Figure 6, Table S1). For scenario two, where NH_x is in phase equilibrium, the calculated average δ^{15}N-NH_4^+ was –28.5 ± 0.4‰, and for non-equilibrium conditions the δ^{15}N-NH_4^+ average was –60.0 ± 0.5‰. The calculated average for scenario one (–2.8 ± 0.4‰; Table S1, Figure 6) showed excellent agreement with the observed cluster three range (–3.3 ± 2.4‰; Figure 5). Therefore, we conclude that cluster three represents an ocean

source. The average calculated δ^{15}N-$NH_{3(g)}$ (–32.5 ± 0.4‰) is also similar to the HOTs cruise sample that was hypothesized to be $NH_{3(g)}$ (–30.7‰). This further supports an ocean source for cluster three as well as equilibrium conditions between NH_x. Equilibrium conditions can be expected for this region as there are no known anthropogenic emissions directly influencing mixing conditions, which would alter ^{15}N:^{14}N ratios and likely cause imbalances to the system.

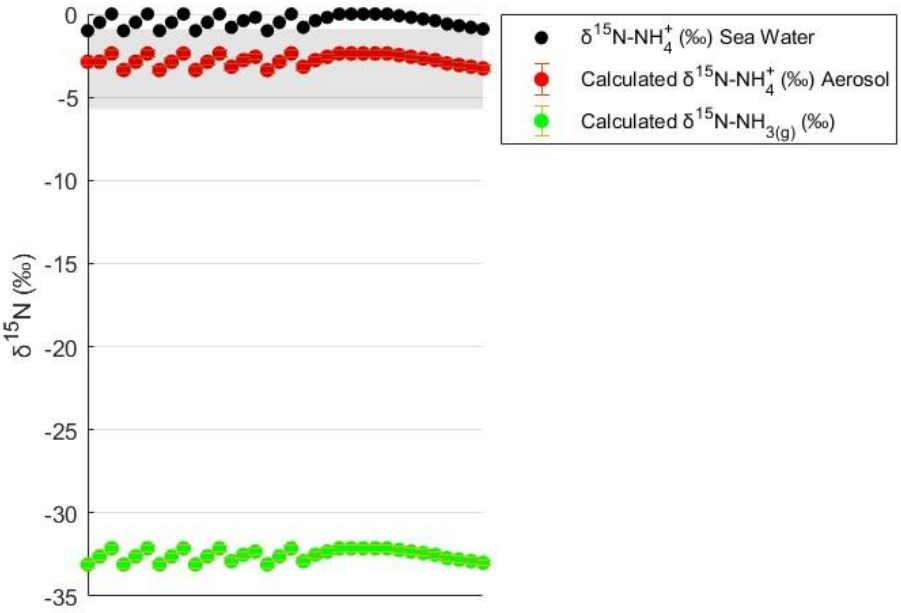

Figure 6: Plot of phase partitioning model results for scenario one (equilibrium conditions). Black points indicate the inputted NH_4^+ isotope value of surface sea water, red points indicate the average calculated aerosol NH_4^+ isotope value (σ = 0.2 for all), and green points indicated the average calculated atmospheric $NH_{3(g)}$ isotope value (σ = 0.2 for all) for each run. The x-axis represents each run (*n*=34). The grey shaded region is the average observed NH_4^+ isotope values in the current study for cluster three (–3.3 ± 2.4‰).

Given that every combination within the input range of sea water [NH_4^+] and sea water δ^{15}N-NH_4^+ resulted in an average that was within the observed range, we are confident that cluster three (Figure 5) represents an open ocean signature. We further analyzed the marine

signature hypothesis via PSCF maps, which indicate a marine system contribution for NH_3 emissions (i.e., no continental sources; Figure 7).

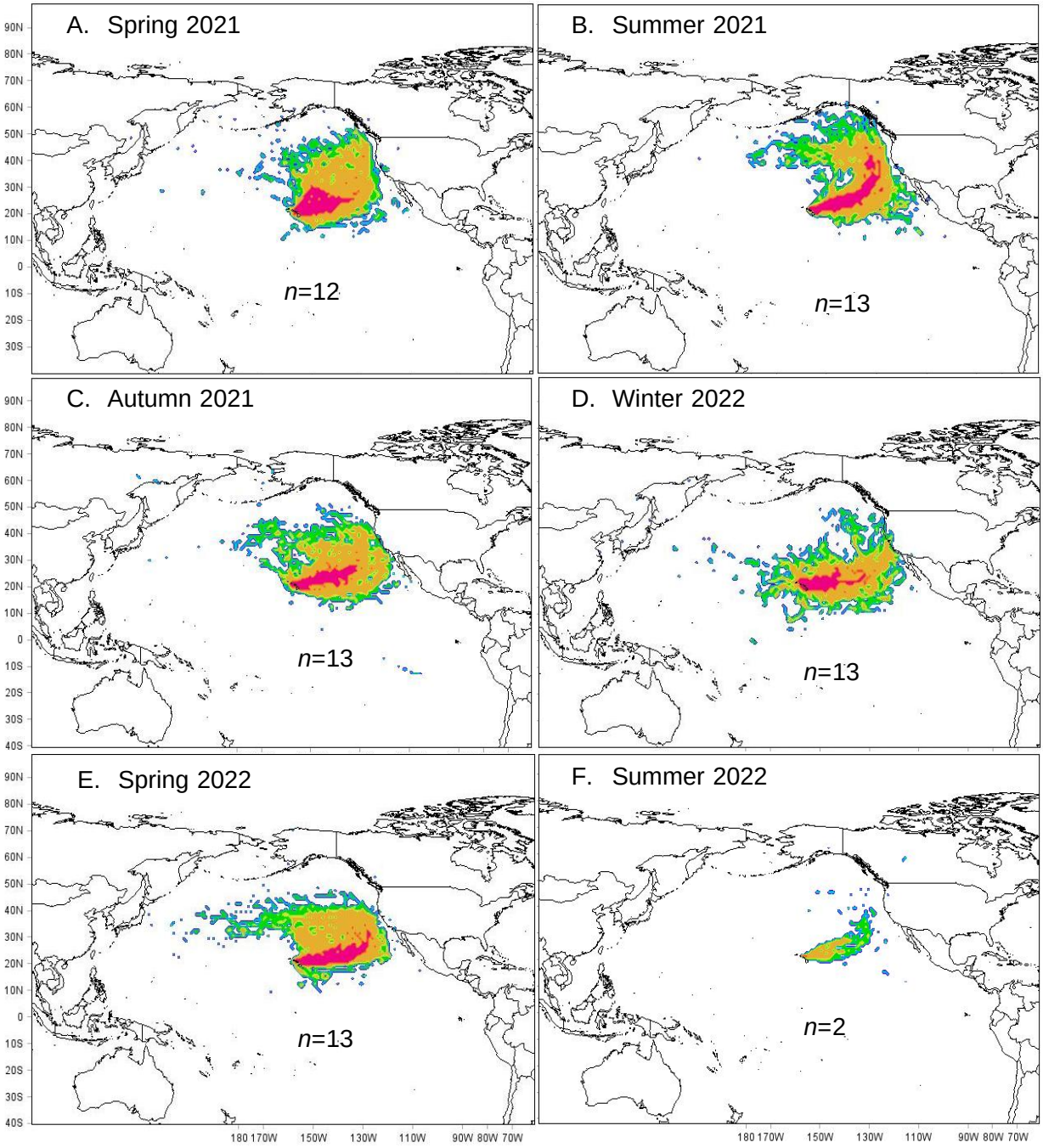

Figure 7: Potential source contribution function analysis by season (A = Spring 2021, B = Summer 2021, C = Autumn 2021, D = Winter 2022, E = Spring 2022, F = Summer 2022), with warmer colors (red, orange, yellow) representing greater relative impact of source

locations versus cooler colors (green, blue, purple) representing lower relative contributions to the measured ammonium concentrations at Oahu, Hawaii.

3.6. Evidence of a Natural External Influence

Northeast of the sampling location, in the direction of the majority of wind (Figure 7), are two seabird sanctuaries (Figure S2). Seabird guano emits NH_3 due to bacterial hydrolysis (Riddick *et al*., 2014). These emissions could be a chief source of NH_3, as observed by a study in the Arctic that was able to link seabird migration emissions to neutral atmospheric pH conditions (Wentworth *et al*., 2016). Additionally, 75% of the values for cluster one had NH_4^+ concentrations higher than the average (3.7 ng/m^3; Table 1), supporting an outside source. Due to no known $\delta^{15}N\text{-}NH_{3(g)}$ range for seabird guano, in any region, it is suggested that cluster one ($\delta^{15}N\text{-}NH_4^+ = 19.0 \pm 3.9‰$ for) most likely represents this signature. This is further supported by no other known sources in this region that it could otherwise be, besides ship emissions, which also do not have a known source range in the literature. However, ship emissions are known to emit SO_2, and there was no nss-SO_4^{2-} observed in this study. Further, it is also unlikely that ships in this region, if present, would be using reduction technologies that emit NH_3. Therefore, in terms of cluster two, it most likely represents a mixture of clusters one and three. Calculations from isoerror indicate that 67% of the isotopic composition of cluster two is from a marine source (cluster three) and 33% from seabird emissions (cluster one).

SIMMR quantified this system as having 65.0 ± 5.0% marine and 35.0 ± 5.0% seabird colony influences on the present particulate NH_4^+. SIMMR was chosen over a two-end member mixing model in order to incorporate the Monte Carlo uncertainty that is embedded in SIMMR. –32.5 ± 0.4‰ was used for the marine endmember (average calculated $\delta^{15}N\text{-}NH_3$ value for cluster three via the ocean phase partitioning model using Eq2). –16.0 ± 3.9‰ was used for the seabird

endmember (average $\delta^{15}N\text{-}NH_4^+$ for cluster one minus the 35‰ fractionation factor previously discussed (Walters *et al*., 2019b)). Every sample's calculated $\delta^{15}N\text{-}NH_{3(g)}$ value ($\delta^{15}N\text{-}NH_4^+$ – 35.0‰ for clusters one and two, $\delta^{15}N\text{-}NH_4^+$ – 29.2‰ for cluster three) were inputted into SIMMR and assessed for the likelihood that these two endmembers were the source of NH_3. The results suggest that roughly a third of NH_3 at this location is supplied from an outside source, specifically excess N from seabird emissions.

4. Conclusions

Conflicts in the literature highlight large uncertainties around the sources of N that enter the ocean in the North Pacific. This uncertainty leads to obstacles in determining whether or not the N is excess in origin, and therefore affecting the biogeochemistry of the ocean, or ocean derived, which would have minimal change on the oceanic N balance and budget. This study aimed to identify the role of the ocean in relation to NH_x dynamics by analyzing the aerosol composition of samples collected off Oahu, Hawaii (2021-2022, n=67) as well as determine source origins through $\delta^{15}N\text{-}NH_4^+$ measurements. Other tools included air mass back trajectory calculations, potential source contribution function maps, a phase partitioning model, and an isotope mixing model.

The aerosol composition was largely dominated by NaCl (> 90%), followed by Mg^{2+}, SO_4^{2-}, K^+, Ca^{2+}, NO_3^-, and NH_4^+, and did not vary seasonally ($p > 0.05$, except NO_3^- where $p < 0.05$). The $\delta^{15}N\text{-}NH_4^+$ also did not vary seasonally ($p > 0.05$) but did separate into three distinct clusters. Cluster three, the most depleted cluster (–3.3 ± 2.4‰) was identified as a marine signature which was further supported by the HOTs research cruise measurements. Cluster one, the most enriched cluster (19.0 ± 3.9‰) was hypothesized to derive from seabird emissions,

given the proximity of two seabird sanctuaries. Cluster two was proposed to be a combination of the other two clusters, specifically 67% contributed from the marine source and 33% contributed from the seabird emissions. Overall, it was calculated that a third of NH_4^+ measurements (*n*=67) resulted from an outside source (seabird emissions; 35 ± 5%). It was further calculated that the average total inorganic dry deposition at Oahu annually was 1.3 ± 1.1 Tg $N \cdot y^{-1}$. This work suggests that the ocean is playing an active role in the oceanic N cycle. However, even with minimally observed potential anthropogenic influence, excess N is still entering this remote location via animal waste, which is important when considering the total inorganic N budget, as this represents an outside source as opposed to just marine recycling.

Data Availability

The data from this study is available at https://doi.org/10.26008/1912/bco-dmo.946741.1

Funding Source

This research was funded by the National Science Foundation (NSF-OCE #1851343).

CRediT Authorship Contribution Statement

Alexandra B. MacFarland: Conceptualization, Data curation, Formal analysis, Investigation, Visualization, Writing – original draft, Writing – review and editing. **Wendell W. Walters**: Conceptualization, Data curation, Investigation, Validation, Writing – review and editing. **Katye E. Altieri**: Conceptualization, Software, Validation, Writing – review and editing. **Meredith G. Hastings**: Conceptualization, Funding acquisition, Project administration, Supervision, Validation, Writing – review and editing.

References

Altieri, K.E., Fawcett, S.E., Hastings, M.G. 2021. Reactive nitrogen cycling in the atmosphere and ocean. Ann. Rev., 49, 523−550.

Altieri, K.E., Fawcett, S.E., Peters, A.J., Sigman, D.M., Hastings, M.G. 2016. Marine biogenic source of atmospheric organic nitrogen in the subtropical North Atlantic. Proc. Natl. Acad. Sci. USA, 113(4), 925–930.

Altieri, K.E., Hastings, M.G., Gobel, A.R., Peters, A.J., Sigman, D.M. 2013. Isotopic composition of rainwater nitrate at Bermuda: The influence of air mass source and chemistry in the marine boundary layer. Journal of Geophysical Research: Atmospheres, 118(19).

Altieri, K.E., Hastings, M.G., Peters, A.J., Oleynik, S., Sigman, D.M. 2014. Isotopic evidence for a marine ammonium source in rainwater at Bermuda. Global Biogeochemical Cycles, 28(10), 1066−1080.

Baker, A.R., Kanakidou, M., Altieri, K.E., Daskalakis, N., Okin, G.S., Myriokefalitakis, S., Dentener, F., Uematsu, M., Sarin. M.M., *et al*. 2017. Observation- and model-based estimates of particulate dry nitrogen deposition to the oceans. Atmos. Chem. Phys., 17, 8189–8210.

Baker, A. R., Thomas, M., Bange, H. W., Plasencia Sánchez, E. 2016. Soluble trace metals in aerosols over the tropical south-east Pacific offshore of Peru, Biogeosciences, 13, 817–825.

Böhlke, J.K., Coplen, T.B. 1995. Interlaboratory comparison of reference materials for nitrogen-isotope-ratio measurements, reference and intercomparison materials for stable isotopes of light elements. Vienna, Austria, 1993. In: Proceedings of the IAEA-TECDOC-825 Consultants Meeting.

Böhlke, J.K., Gwinn, C.J., Coplen, T.B. 1993. New reference materials for nitrogen-isotope-ratio measurements. Geostand. Geoanal. Res., 17, 159–164.

Böttjer, D., Dore, J.E., Karl, D.M., Letelier, R.M., Mahaffey, C., Wilson, S.T., Zehr, J., Church, M.J. 2017. Temporal variability of nitrogen fixation and particulate nitrogen export at Station ALOHA. Limnology and Oceanography, 62(1), 200−216.

Carrillo, J.H., Hastings, M.G., Sigman, D.M., Huebert, B.J. 2002. Atmospheric deposition of inorganic and organic nitrogen and base cations in Hawaii. Global Biogeochemical Cycles, 16(4).

Casciotti, K.L., Buchwald, C., Santoro, A.E., Frame, C. 2011. Chapter eleven - Assessment of Nitrogen and Oxygen Isotopic Fractionation During Nitrification and Its Expression in the Marine Environment. Methods in enzymology, 486, 253−280.

Casciotti, K.L., Marshall, T.A., Fawcwtt, S.E., Knapp, A.N. 2024. Advances in Understanding the Marine Nitrogen Cycle in the GEOTRACES Era. Oceanography.

Casciotti, K.L., Trull, T.W., Glover, D.M., Davies, D. 2008. Constraints on nitrogen cycling at the subtropical North Pacific Station ALOHA from isotopic measurements of nitrate and particulate nitrogen. Deep-Sea Research II, 55, 1661–1672.

Cooper, R.J., Krueger, T., Hiscock, K.M., Rawlins, B.G. 2014. Sensitivity of fluvial sediment source apportionment to mixing model assumptions: a Bayesian model comparison. Water Resour. Res. 50, 9031–9047.

Cosper, E.M., Bricelj, V.M., Carpenter, E.J. 1989. Novelphytoplankton blooms: causes and impacts of recurrentbrown tides and other unusual blooms. Springer-Verlag,Berlin, Germany.

Duce, R.A., Liss, P.S., Merrill, J.T., Atlas, E.L., Buat-Menard, P., Hicks, B.B., Miller, J.M., Prospero, J.M., Arimoto, R., Church, T.M., Ellis, W., Galloway, J.N., Hansen, L.,

Jickells, T.D., Knap, A.H., Reinhardt, K.H., Schneider, B., Soudine, A., Tokos, J.J., Tsunogai, S., Wollast, R., Zhou, M. 1991. The atmospheric input of trace species to the world ocean. Global Biogeochem. Cycles, 5(3), 193–259.

Fawcett, S.E., Lomas, M.W., Casey, J.R., Ward, B.B., Sigman, D.M. 2011. Assimilation of upwelled nitrate by small eukaryotes in the Sargasso Sea. Nature Geoscience, 4, 717–722.

Fawcett, S.E., Lomas, M.W., Ward, B.B., Sigman, D.M. 2014. The counterintuitive effect of summer-to-fall mixed layer deepening on eukaryotic new production in the Sargasso Sea. Global Biogeochem. Cycles, 28, 86–102.

Fridlind, A. M., Jacobson, M. Z. 2000. A study of gas-aerosol equilibrium and aerosol pH in the remote marine boundary layer during the first aerosol characterization experiment (ACE 1). Geophys. Res., 105, 17,325–17,340.

Galloway, J.N., Townsend, A.R., Erisman, J.W., Bekunda, M., Cai, Z., Freney, J.R., Martinelli, L.A., Seitzinger, S.P., Sutton, M.A. 2008. Transformation of the nitrogen cycle: recent trends, questions, and potential solutions. Science, 320(5878),889–892.

Gobel, A.R., Altieri, K.E., Peters, A.J., Hastings, M.G., Sigman, D.M. 2013. Insights into anthropogenic nitrogen deposition to the North Atlantic investigated using the isotopic composition of aerosol and rainwater nitrate. Geophysical Research Letters, 40(22), 5977−5982.

Gruber, N., Sarmiento, J.L. 1997. Global patterns of marine nitrogen fixation and denitrification. Global Biogeochemical Cycles, 11(2), 235−266.

Jickells, T.D., Buitenhuis, E., Altieri, K., Baker, A.R., Capone, D., Duce, R.A., Dentener, F., *et al*. 2017. A reevaluation of the magnitude and impacts of anthropogenic atmospheric nitrogen inputs on the ocean. Global Biogeochem. Cycles 31(2), 289–305.

Jickells, T., Kelly, S., Baker, A., Biswas, K., Dennis, P., Spokes, L.J., Witt, M., Yeatman, S.G. 2003. Isotopic evidence for a marine ammonia source. Geophysical Research Letters, 30.

Johnson, K.S., Riser, S.C., Karl, D.M. 2010. Nitrate supply from deep to near-surface waters of the North Pacific subtropical gyre. Nature, 465(7301), 1062–1065.

Jung, J., Furutani, H., Uematsu, M. 2011. Atmospheric inorganic nitrogen in marine aerosol and precipitation and its deposition to the North and South Pacific Oceans. J Atmos Chem, 68, 157–181.

Karl, D.M., Church, M.J., Dore, J.E., Letelier, R.M., Mahaffey, C. 2012. Predictable and efficient carbon sequestration in the North Pacific Ocean supported by symbiotic nitrogen fixation. Proc. Natl. Acad. Sci. USA, 109(6), 1842–1849.

Karl, D.M., Knauer, G.A. 1984. Vertical distribution, transport, and exchange of carbon in the northeast Pacific Ocean: evidence for multiple zones of biological activity. Deep-Sea Research, 31(3), 221–243.

Kim, I.-N., Lee, K., Gruber, N., Karl, D.M., Bullister, J.L., Yang, S., Kim, T.-W. 2014. Increasing anthropogenic nitrogen in the North Pacific ocean. Science, 346(6213), 1102–1106.

Knapp, A.N., Hastings, M.G., Sigman, D.M., Lipschultz, F., Galloway, J.N. 2010. The flux

and isotopic composition of reduced and total nitrogen in Bermuda rain. Marine Chemistry, 120(1), 83−89.
Le Roy, E. Walters, W.W., Joyce, E.E. Hastings, M.G. 2021. Sources of ammonium in seasonal wet deposition at a coastal New England city. Atmos. Environ., 260.
Letscher, R.T., Primeau, F., Moore, J.K. 2016. Nutrient budgets in the subtropical ocean gyres dominated by lateral transport. Nature Geoscience, 9(11), 815−819.
MacFarland, A.B., Joyce, E.E., Wang, X., Walters, W. W., Altieri, K.E., Schiebel, H.N., Hastings, M.G. 2023. Investigation of coastal ammonium aerosol sources in the Northwest Pacific Ocean. Atmos. Environ., 312.
MacFarland, A.B., Walters, W.W., Hastings, M.G. 2024. Solid Phase Extraction Methodology for Robust Isotope Analysis of Atmospheric Ammonium: Concentration and Removal of Matrix Interferences. ACS Earth and Space Chemistry, 8(5).
Millero, F.J. 2006. Chemical Oceanography, third ed. CRC Press, p. 496.
Nah, T., Yang, J., Wang, J., Sullivan, A.P., Weber, R.J. 2021. Fine aerosol acidity and water during summer in the eastern North Atlantic. Atmosphere, 12(1040).
Nixon, S.W. 1995. Coastal marine eutrophication: a definition, social causes, and future consequences. Ophelia, 41, 199–219.
O'Dell, J.W. 1993a. In: Method 353.2, Revision 2.0: Determination of Nitrate-Nitrite by Automated Colorimetry. US EPA.
O'Dell, J.W., 1993b. In: Method 350.1, Revision 2.0: Determination of Ammonia Nitrogen by Semi-automated Colorimetry. US EPA.
Paerl, H.W., Dennis, R.L., Whitall, D.R. 2002. Atmospheric deposition of nitrogen: implications for nutrient over-enrichment of coastal waters. Estuaries, 25, 677–693.
Pan, Y., Tian, S., Liu, D., Fang, Y., Zhu, X., Zhang, Q., Zheng, B., Michalski, G., Wang, Y. 2016. Fossil Fuel Combustion-Related Emissions Dominate Atmospheric Ammonia Sources during Severe Haze Episodes: Evidence from 15N-Stable Isotope in Size-Resolved Aerosol Ammonium. Environ. Sci. Technol., 50(15), 8049−8056.
Parnell, A.C., Inger, R., Bearhop, S., Jackson, A.L. 2010. Source partitioning using stable isotopes: coping with too much variation. PLoS One(5), 1–6.
Parnell, A.C., Phillips, D.L., Bearhop, S., Semmens, B.X., Ward, E.J., Moore, J.W., Jackson, A.L., Grey, J., Kelly, D.J., Inger, R. 2013. Bayesian stable isotope mixing models. Environmetrics, 24(6), 387–399.
Paulot, F., Ginoux, P., Cooke, W.F., Donner, L.J., Fan, S., Lin, M.-Y., Mao, J., Naik, V., Horowitz, L.W. 2016. Sensitivity of nitrate aerosols to ammonia emissions and to nitrate chemistry: implications for present and future nitrate optical depth. Atmos. Chem. Phys., 16, 1459–1477.
Paulot, F., Jacob, D.J., Johnson, M.T., Bell, T.G., Baker, A.R., Keene, W.C., Llma, I.D., Doney, S.C., Stock, C.A. 2015. Global oceanic emission of ammonia: Constraints from seawater and atmospheric observations. Global Biogeochem. Cycles, 29, 1165–1178.
Phillips, D.L., Gregg, J.W. 2001. Uncertainty in source partitioning using stable isotopes. Oecologia, 127, 171–179.
Phinney, L., Leaitch, W.R., Lohmann, U., Boudries, H., Worsnop, D.R., Jayne, J.T., Toom-Sauntry, D., Wadleigh, M., Sharma, S., Shantz, N. 2006. Characterization of the aerosol over the sub-arctic north east Pacific Ocean. Deep-Sea Research II, 53, 2410–2433.
Qi, J., Yu, Y., Yao, X., Gang, Y., Gao, H. 2020. Dry deposition fluxes of inorganic nitrogen and phosphorus in atmospheric aerosols over the Marginal Seas and Northwest Pacific.

Atmospheric Research, 245.
Quay, P., Peacock, C., Bjorkman, K., Karl, D. 2010. Measuring primary production rates in the ocean: enigmatic results between incubation and non-incubation methods at Station ALOHA. Global Biogeochem. Cycles, 24(3).
Rabalais, N.N. 2002. Nitrogen in aquatic ecosystems. Ambio, 21, 102–112.
Riddick, S.N., Blackall, T.D., Dragosits, U., Daunt, F., Braban, C.F., Tang, Y.S., MacFarlane, W., Taylor, S., Wanless, S., Sutton, M.A. 2014. Measurement of ammonia emissions from Tropical seabird colonies. Atmospheric Environment, 89, 35−42.
Rolph, G., Stein, A., Stunder, B. 2017. Real-time environmental applications and display sYstem: READY. Environ. Model. Software, 95, 210–228.
Seok, M.-W., Kim, D., Park, G.-H., Lee, K., Kim, T.-H., Jung, J., Kim, K., Park, K.-T., Kim, Y.-H., *et al*. 2021. Atmospheric deposition of inorganic nutrients to the Western North Pacific Ocean. Science of The Total Environment, 793.
Shilova, I.N., Mills, M.M., Robidart, J.C., Turk-Kubo, K.A., Björkman, K.M., Kolber, Z., Rapp, I., *et al*. 2017. Differential effects of nitrate, ammonium, and urea as N sources for microbial communities in the North Pacific Ocean. Limnol. Oceanogr., 62, 2550–2574.
Sigman, D.M., Fripiat, F. 2019. Nitrogen Isotopes in the Ocean. Academia, Encyclopedia of Ocean Sciences (Third ed.), 263−278.
Smetacek, V., Bathmann, U., Nöthig, E.-M., Scharek, R.1991. Coastal eutrophication: causes and consequences. Pages 251–279 in R. Mantoura, C.F, Martin, J.-M., Wollast, R., editors. Ocean margin processes in global change.John Wiley and Sons, New York, New York, USA.
Song, L., Walters, W.W., Pan, Y., Li, Z., Gu, M., Duan, Y., Lü , X., Fang, Y. 2021. 15N natural abundance of vehicular exhaust ammonia, quantified by active sampling techniques. Atmos. Environ., 255.
Stein, A.F., Draxler, R.R., Rolph, G.D., Stunder, B.J.B., Cohen, M.D., Ngan, F. 2015. NOAA's HYSPLIT atmospheric transport and dispersion modeling system. Bull. Am. Meteorol. Soc., 96, 2059–2077.
Treibergs, L.A., Fawcett, S.E., Lomas, M.W., Sigman, D.M. 2014. Nitrogen isotopic response of prokaryotic and eukaryotic phytoplankton to nitrate availability in Sargasso Sea surface waters. Limnol. Oceanogr., 59(3), 972–985.
Walters, W.W., Blum, D.E., Hastings, M.G. 2019a. Selective Collection of Particulate Ammonium for Nitrogen Isotopic Characterization Using a Denuder−Filter Pack Sampling Device. Anal. Chem., 91, 7586−7594.
Walters, W.W., Chai, J., Hastings, M.G. 2019b. Theoretical Phase Resolved Ammonia−Ammonium Nitrogen Equilibrium Isotope Exchange Fractionations: Applications for Tracking Atmospheric Ammonia Gas-to-Particle Conversion. ACS Earth Space Chem., 3, 79−89.
Walters, W.W., Karod, M., Willcocks, E., Baek, B.H., Blum, D.E., Hastings, M.G. 2022. Quantifying the importance of vehicle ammonia emissions in an urban area of northeastern USA utilizing nitrogen isotopes. Atmos. Chem. Phys., 22, 13431−13448.
Walters, W.W., Song, L., Chai, J., Fang, Y., Colombi, N., Hastings, M. G. 2020. Characterizing the spatiotemporal nitrogen stable isotopic composition of ammonia in vehicle plumes. Atmos. Chem. Phys., 20, 11551−11567.
Wang, Y. Q., Zhang, X. Y., Draxler, R. 2009. TrajStat: GIS-based software that uses various trajectory statistics analysis methods to identify potential sources from long-term air

pollution measurement data. Environmental Modelling Software, 24, 938–939.
Wentworth, G.R., Murphy, J.G., Croft, B., Martin, R.V., Pierce, J.R., Côté, J-S., Courchesne, I., Tremblay, J-E., Gagnon, J., Thomas, J.L., Sharma, S., Toom-Sauntry, D., Chivulescu, A., Levasseur, M., Abbatt, J.P.D. 2016. Ammonia in the summertime Arctic marine boundary layer: sources, sinks, and implications. Atmos. Chem. Phys., 16, 1937–1953.
Xu, L., Penner, J. E. 2012. Global simulations of nitrate and ammonium aerosols and their radiative effects, Atmos. Chem. Phys., 12(20), 9479−9504.
Zhang, L., Altabet, M., Wu, T., Hadas, O. 2007. Sensitive Measurement of NH4+ 15N/14N (*d*15NH4+) at Natural Abundance Levels in Fresh and Saltwaters. Anal. Chem., 79, 5297−5303.
Zhang, M., Chen, J.M., Wang, T., Cheng, T.T., Lin, L., Bhatia, R.S., Hanvey, M. 2010. Chemical characterization of aerosols over the Atlantic Ocean and the Pacific Ocean during two cruises in 2007 and 2008. Journal of Geophysical Research, 115.
Zhao, Y., Zhang, L., Pan, Y., Wang, Y., Paulot, F., Henze, D.K. 2015. Atmospheric nitrogen deposition to the northwestern Pacific: seasonal variation and source attribution. Atmos. Chem. Phys, 15(9), 13657−13703.

Supporting Information

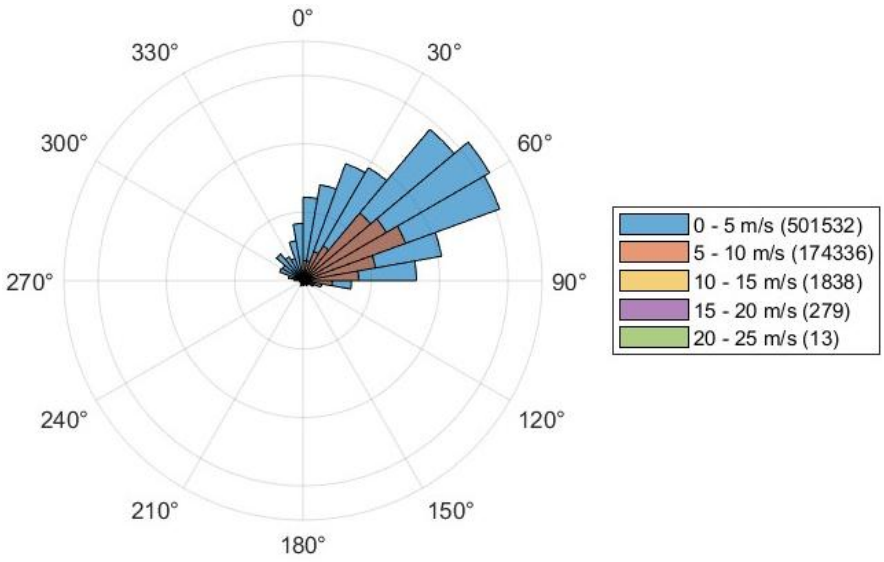

Figure S1: Wind rose plot of wind direction during sampling duration. Wind direction data was collected every minute (n= 677,999). 0° = North, 90° = East, 180° = South, 270° = West.

Table S1: Phase partitioning model results of the calculated $\delta^{15}N\text{-}NH_4^+$ (aerosol) based on specific input values of seawater $[NH_4^+]$ and seawater $\delta^{15}N\text{-}NH_4^+$. The range for 95% confidence intervals for the calculated $\delta^{15}N\text{-}NH_4^+$ (aerosols) are also included.

Run	Inputted $[NH_4^+]$ (µM) Sea Water	Inputted $\delta^{15}N\text{-}NH_4^+$ (‰) Sea Water	Calculated $\delta^{15}N\text{-}NH_4^+$ (‰) Aerosol	95% Confidence Interval Range	Calculated $\delta^{15}N\text{-}NH_{3(g)}$ (‰)
1	0.01	-1.0	-2.9 ± 0.1	-2.84 to -2.90	-33.1 ± 0.2
2	0.01	-0.5	-2.9 ± 0.1	-2.84 to -2.90	-32.6 ± 0.2
3	0.01	0.0	-2.4 ± 0.1	-2.34 to -2.40	-32.1 ± 0.2
4	0.05	-1.0	-3.4 ± 0.1	-3.34 to -3.40	-33.1 ± 0.2
5	0.05	-0.5	-2.9 ± 0.1	-2.84 to -2.90	-32.6 ± 0.2
6	0.05	0.0	-2.4 ± 0.1	-2.34 to -2.40	-32.1 ± 0.2
7	0.1	-1.0	-3.4 ± 0.1	-3.34 to -3.40	-33.1 ± 0.2
8	0.1	-0.5	-2.9 ± 0.1	-2.84 to -2.90	-32.6 ± 0.2
9	0.1	0.0	-2.4 ± 0.1	-2.34 to -2.40	-32.1 ± 0.2
10	0.03	-1.0	-3.4 ± 0.1	-3.34 to -3.40	-33.1 ± 0.2
11	0.03	-0.5	-2.9 ± 0.1	-2.84 to -2.90	-32.6 ± 0.2
12	0.03	0.0	-2.4 ± 0.1	-2.34 to -2.40	-32.1 ± 0.2

13	0.03	-0.8	-3.2 ± 0.1	-3.14 to -3.20	-32.9 ± 0.2
14	0.03	-0.4	-2.8 ± 0.1	-2.74 to -2.80	-32.5 ± 0.2
15	0.03	-0.2	-2.6 ± 0.1	-2.54 to -2.60	-32.3 ± 0.2
16	0.08	-1.0	-3.4 ± 0.1	-3.34 to -3.40	-33.1 ± 0.2
17	0.08	-0.5	-2.9 ± 0.1	-2.84 to -2.90	-32.6 ± 0.2
18	0.08	0.0	-2.4 ± 0.1	-2.34 to -2.40	-32.1 ± 0.2
19	0.08	-0.8	-3.2 ± 0.1	-3.14 to -3.20	-32.9 ± 0.2
20	0.08	-0.4	-2.8 ± 0.1	-2.74 to -2.80	-32.5 ± 0.2
21	0.08	-0.2	-2.6 ± 0.1	-2.54 to -2.60	-32.3 ± 0.2
22	0.02	0.0	-2.4 ± 0.1	-2.34 to -2.40	-32.1 ± 0.2
23	0.04	0.0	-2.4 ± 0.1	-2.34 to -2.40	-32.1 ± 0.2
24	0.06	0.0	-2.4 ± 0.1	-2.34 to -2.40	-32.1 ± 0.2
25	0.07	0.0	-2.4 ± 0.1	-2.34 to -2.40	-32.1 ± 0.2
26	0.09	0.0	-2.4 ± 0.1	-2.34 to -2.40	-32.1 ± 0.2
27	0.01	-0.1	-2.5 ± 0.1	-2.44 to -2.50	-32.2 ± 0.2
28	0.01	-0.2	-2.6 ± 0.1	-2.54 to -2.60	-32.3 ± 0.2
29	0.01	-0.3	-2.7 ± 0.1	-2.64 to 2.70	-32.4 ± 0.2
30	0.01	-0.4	-2.8 ± 0.1	-2.74 to -2.80	-32.5 ± 0.2
31	0.01	-0.6	-3.0 ± 0.1	-2.94 to -3.00	-32.7 ± 0.2
32	0.01	-0.7	-3.1 ± 0.1	-3.04 to -3.10	-32.8 ± 0.2
33	0.01	-0.8	-3.2 ± 0.1	-3.14 to -3.20	-32.9 ± 0.2
34	0.01	-0.9	-3.3 ± 0.1	-3.24 to -3.30	-33.0 ± 0.2

Figure S2: Google earth image of study site (yellow star) and surrounding area. Distance from study site to middle of Manana Island Seabird Sanctuary is ~ 1.6 km, and ~ 1.2 km to middle of Kaohikaipu Island State Seabird Sanctuary (distances measured using Google Earth tools). Manana Island Seabird Sanctuary is the largest offshore islet in Oahu (~25 hectares). Kaohikaipu Island State Seabird Sanctuary is ~ 4.5 hectares. Both sanctuaries are home to varying bird species year-round.

Supplemental text:

Model inputs include surface ocean pH, temperature, salinity, ammonium concentration and $\delta^{15}N\text{-}NH_4^+$ as well as atmospheric temperature and wind speed. The flux of ammonia from the ocean to the atmosphere was calculated following (Altieri *et al*., 2021). The $\delta^{15}N\text{-}NH_{3(g)}$ that resulted from that flux, assuming the system was at equilibrium, was calculated following (Altieri *et al*., 2014). The isotopic composition of aerosol $\delta^{15}N\text{-}NH_4^+$ was calculated in three ways assuming 1) equilibrium between $NH_{3(g)}$ and $NH_4^+{}_{(p)}$ and the temperature dependent equilibrium fractionation (equation 11 Walters *et al*., 2019), 2) NH_x phase equilibrium with atmospheric water whereby NH_3 is absorbed in H_2O followed by formation of $NH_4^+{}_{(aq)}$ aerosols (equation 8 Walters *et al*., 2019), and 3) non-equilibrium conditions with $NH_{3(g)}$ unidirectional neutralization reactions with H_2SO_4 with a kinetic isotope effect of -28‰ (Walters *et al*., 2019).

Chapter 5

Conclusion: Quantifying Coastal and Open Ocean Nitrogen Deposition to the North Pacific Ocean

Alexandra B. MacFarland

Department of Earth, Environmental, and Planetary Sciences, Institute at Brown for Environment and Society, Brown University, Providence, RI 02912, USA

Abstract

Few studies investigate dry atmospheric nitrogen deposition to the ocean. Here, two ammonium (NH_4^+) aerosol studies are compared: (1) Changdao Island, China, a coastal site heavily influenced by anthropogenic pollution, and (2) Oahu, Hawaii, an open ocean site dominated by marine sources, where these two sites serve as endmembers. $\delta^{15}N\text{-}NH_4^+$ analyses reveal that deposition to the ocean at Changdao Island is dominated by agricultural emissions, while deposition at Oahu is dominated by marine emissions and seabird guano emissions. Monte Carlo simulations based on a three-endmember isotopic mixing model equation additionally support atmospheric deposition to the surface water as a significant influence to both sites. Air mass back trajectories suggest that 50-65% of the North Pacific Ocean is coastal (e.g., not the open ocean). Further, the annual dry inorganic nitrogen (N) deposition was calculated to be between 47-61 Tg/Yr depending on the season. This research allowed for the characterization of two marine environments as well as highlighted atmospheric deposition as an important pathway for N to enter both the coastal and open ocean.

1. Introduction

Nitrogen (N) is a macronutrient that is required for photosynthesis. Inorganic fixed N refers to NO_x (nitrite (NO_2^-) and nitrate (NO_3^-)) and NH_x (ammonia (NH_3) and ammonium (NH_4^+)). It was long thought that the oceanic N budget was in balance, with N-fixation converting atmospheric N_2 gas to a usable form (e.g., NO_x or NH_x), and denitrification converting usable N back to N_2 gas. Recently, however, studies have indicated that anthropogenic emissions have altered this balance, specifically in the North Pacific Ocean (NPO) where excess N (quantified as relative to the expected ratio of N to phosphorus in the open ocean (i.e., $N^* = N - (R_{N:P}) \times P$; where $R_{N:P}$ is the ratio of N to phosphorus; Gruber and Sarmiento,

1997) has been observed (Kim *et al*., 2011; Kim *et al*., 2014a; MacFarland *et al*., 2023). There are disagreements regarding the origins of this excess N, as other studies explain this without the consideration of anthropogenic inputs (Johnson *et al*., 2010; Casciotti *et al*., 2011; Letscher *et al*., 2016). Nonetheless, since N deposition in the ocean has been increasing since preindustrial times (Galloway *et al*., 2004), the oceanic N budget, too, also has been changing.

Although exact budgets are uncertain, global marine N sources include N-fixation, riverine inputs, runoff, groundwater, and atmospheric deposition, while N sinks include organic N export, denitrification, sediment burial, and N_2O loss to the atmosphere. The estimated rate of global anthropogenic N emissions is ~160 Tg N/yr, which is currently on the same order of magnitude as N-fixation (~250 Tg N/yr) and could very well continue to rise with an expanding human population (Gruber & Galloway, 2008). This has the potential for adverse effects on oceanic biogeochemical cycles (Duce *et al*., 2008).

A global modeling study proposes that anthropogenic emissions have resulted in an increase in carbon sequestration of ~0.15 Pg C/yr (~0.4%; Jickells *et al*., 2017). External N inputs could also move nutrient limitations from N to phosphorus, which in turn could alter the composition of phytoplankton species and the structure of oceanic ecosystems (Elser *et al*., 2009). Further, a rise in primary production from this external N could lead oxygen minimum zones to expand (Jickells *et al*., 2017). Yet, the scale and influence of these potential changes to the ocean is poorly understood.

This current study focuses on aerosol inorganic N, specifically NH_x, as it is readily bioavailable with an increasing emission rate over time (Altieri *et al*., 2021). NH_3 is a precursor to NH_4^+, and has multiple natural and anthropogenic sources, including N-fixation, waste, decomposition, agriculture, industrial processes, biomass burning, and vehicle emissions (Zhao

et al., 2015). A powerful tool that can aid in discerning sources is the stable N isotopic analysis of NH_4^+ (Jickells *et al*., 2003; Altieri *et al*., 2014; Le Roy *et al*., 2021; Walters *et al*., 2022; MacFarland *et al*., 2023). The N composition is determined as: $\delta^{15}N$ (‰) = $[(^{15}N/^{14}N)_{sample}/(^{15}N/^{14}N)_{standard} - 1] \times 1000$, where $\delta^{15}N$ is the composition of stable N isotopes and air-N_2 is the N isotopic reference. Noticeable alterations in the ratio of ^{15}N:^{14}N are measurable for chemical, biological, and physical processes in addition to different source origins (Sigman & Fripiat, 2019).

Here, I compare two year-round aerosol inorganic N studies at two opposite but vital oceanic environments: Changdao Island, China where there is a dominant anthropogenic signal and Oahu, Hawaii where there is a dominant marine signal. I aim to (1) characterize the two systems based on aerosol compositions, $\delta^{15}N$-NH_4^+ values, and air mass back trajectory origins, and (2) calculate the rate of annual dry inorganic N deposition to aid in determining the average deposition to the NPO based on observations.

2. Methodology

2.1. Sample Collection and Analyses

Methodology regarding sample collection and analyses for the Changdao Island and Oahu samples can be found in Chapters 2 & 4. The methodology below was completed in addition to the results discussed in Chapters 2 & 4.

2.2. $\delta^{15}N$-NO_3^- Analyses

Measurements of $\delta^{15}N$-NO_3^- for the Changdao Island samples were previously completed in a separate study (Joyce, 2022), which was determined using the denitrifier method. Denitrifying bacteria (*Pseudomonas aureofaciens*) that lack the N_2O reductase enzyme needed to

convert N_2O to N_2, thus stopping the reaction at N_2O, were used to convert 20 nmol of NO_3^- to N_2O (i.e., $2NO_3^- \rightarrow 2NO_2 \rightarrow 2NO \rightarrow N_2O$) (Sigman *et al*., 2001; Casciotti *et al*., 2002; Kaiser *et al*., 2007). The N_2O was purified and analyzed via a Gas-Chromatograph Isotope Ratio Mass Spectrometer (Thermo-Scientific Delta V Plus). The pooled standard deviations of sample references IAEA-N3, USGS-34, USGS-35 were 0.1‰ (n=19), 0.1‰ (n=19), and 0.1‰ (n=20). The pooled standard deviation of duplicates for was 0.4‰ (n=21 pairs). The Oahu samples were analyzed using the same method, but only half of the dataset (n=25) was able to successfully be measured as the sample volume was too low for the other half of the samples. The pooled standard deviation of sample references IAEA-N3, USGS-34, USGS-35 were 0.1‰ (n=6), 0.2‰ (n=6), and 0.1‰ (n=5). The pooled standard deviation of sample duplicates and replicates was 0.1‰ (n=2 pairs) and 0.3‰ (n=2 pairs).

2.3. Nitrogen Deposition Calculations

Liquid concentrations (μmol/L; $[NH_4^+] + [NO_3^-]$) were converted to air concentrations (ng/m^3) based on extraction volume (L) and average volume of air sampled through the filter (m^3). These values were then converted to $nmol/m^3$ using the molar mass of N. To calculate the deposition rate (Tg N/yr) at each site, a series of unit conversions were used, along with a dry deposition velocity of 0.1 cm/s and 0.9 cm/s, for NH_4^+ and NO_3^-, respectively (Baker *et al*., 2017).

2.4. Monte Carlo Simulations

Monte Carlo simulations were run to determine the likelihood of three variables (N-fixation, NO_3^- upwelling, and atmospheric deposition) contributing new N to the oceanic N pool.

Simulations (n=10,000) were run per test that calculated the most likely % contribution from these three sources given their isotopic source ranges and the following equation:

$$\delta^{15}N(PN_{sink}) = x(-1‰) + y(\delta^{15}N(NU)) + (1-x-y)(\delta^{15}N(AD)) \quad \text{(Eq1)}$$

Where '$\delta^{15}N(PN_{sink})$' represents the isotopic signature of sinking particulate N, '$\delta^{15}N(NU)$' represents the isotopic signature of nitrate upwelling, '$\delta^{15}N(AD)$' represents the isotopic signature of atmospheric deposition, 'x' is the proportion of N-fixation, 'y' is the proportion of nitrate upwelling, and 'z' is the proportion of atmospheric deposition.

A range of inputs were tested for Hawaii and China when running the Monte Carlo simulations (Table 1).

Table 1: Range of inputs used for the three-endmember isotope mixing model (Monte Carlo simulation) for three separate tests.* PN = particulate nitrogen, NU = nitrate upwelling, AD = atmospheric deposition.

	PNsink (‰)	δ^{15}N-N-fixation (‰)	δ^{15}N(NU) (‰)	δ^{15}N(AD) (‰)	x (%)	n runs
Hawaii	3.5 ± 0.5-2.0	-1.0 ± 0.2-1	5.0-7.0 ± 1.0-2.0	-1.5 ± 1.5	48 ± 10-20	12
China Test 1	3.5 ± 0.5-2.0	-1.0 ± 0.2-1	5.0-7.0 ± 1.0-2.0	-5.0 ± 4.0	10 ± 10-20	12
China Test 2	3.5 ± 0.5-2.0	-1.0 ± 0.2-1	5.0-7.0 ± 1.0-2.0	-5.0 ± 4.0	20 ± 10-20	12

*****$\delta^{15}N(PN_{sink})$ value from Böttjer *et al*., 2017; δ^{15}N-N-fixation value from Hoering & Ford, 1960, Minagawa & Wada, 1986, Carpenter *et al*., 1997; δ^{15}N(NU) from Altabet, 2001, Rafter *et al*., 2019; -1.5 ± 1.5‰ for δ^{15}N(AD) from MacFarland *et al*., 2025; 48 ± 20% for 'x' from Dore *et al*., 2002; 5.0 ± 4.0‰ for δ^{15}N(AD) from MacFarland *et al*., 2022; 10-20 ± 10-20% for 'x' from Shiozaki *et al*., 2009.

The weighted δ^{15}N(AD) values per sample were calculated using the following equation:

$$W\delta^{15}N(AD) = (([NO_3^-] \times \delta^{15}N(NO_3^-)) + ([NH_4^+] \times \delta^{15}N(NH_4^+)))/([NO_3^-] + [NH_4^+]) \quad \text{(Eq2)}$$

These values were then averaged per site (Table 1). It is noted here that $\delta^{15}N(NO_3^-)$ measurements were only successful for half of the Hawaii dataset (n = 25; not enough sample volume for the remainder of the samples), so the $\delta^{15}N(NO_3^-)$ values were averaged and that singular value was used to represent $\delta^{15}N(NO_3^-)$ for all of the samples when calculating $\delta^{15}N(AD)$, so that the samples without $\delta^{15}N(NO_3^-)$ values but with $\delta^{15}N(NH_4^+)$ values could still be utilized in the calculations. It is further noted that there are no observational values in the literature for $\delta^{15}N(PN_{sink})$ or $\delta^{15}N(NU)$ along the coast of China, where atmospheric deposition is much greater.

2.5 HYSPLIT air mass back trajectory analyses

Air mass back trajectories were calculated via NOAA's Hybrid Single-Particle Lagrangian Integrated Trajectory (HYSPLIT; Rolph *et al*., 2017; Stein *et al*., 2015). The model utilizes particle dispersion simulation and meteorological data to determine the trajectory of an air mass backward in time, starting from a specified point and time. Here, back trajectories were run at a height of 500 m above ground level every 6 h for a total of 72 hours to account of the average lifetime of atmospheric NHx (Paulot *et al*., 2016). The plugin 'trajstat' (Wang *et al*., 2009) was utilized to calculate these air mass back trajectories in order to determine how far continental emissions travel across the ocean. This was done for the entire month of January 2020 and August 2020 to compare winter and summer.

2.6. Global anthropogenic NH_3 and NO_x emission data retrieval

Anthropogenic NH_3 and NO_x emissions data were retrieved from McDuffie *et al*. (2020) who updated the open-source Community Emissions Data System (CEDS; Hoesly *et al*., 2019) to develop a new global emission inventory, CEDSGBD-MAPS (https://doi.org/10.5281/zenodo.3754964). It contains global anthropogenic emission data of atmospheric pollutants from sector- and fuel specific sources from 1970 to 2017. Sector sources include agriculture, energy, industry, on road transportation, off road transportation, residential combustion, commercial combustion, other combustion, solvents, waste, and international shipping. For this analysis, I used data from 1970-2017 in five-year increments in order to compare concentrations and percentage of different anthropogenic sources contributing over time to the Changdao study region (e.g., the anthropogenic coastal site).

3. Results and Discussion

3.1 Ion Concentrations and Deposition Calculations

Changdao Island experienced more variable seasonal ion deposition, with only ~37% of the aerosol composition comprised of NaCl compared to Oahu where ~91% was NaCl (Figure 1), suggesting a lack of anthropogenic emissions at Oahu. Each measured ion was seasonally different at Changdao Island ($p < 0.05$), but only NO_3^- was seasonally different at Oahu ($p < 0.05$). Not only was ion deposition at Oahu more consistent throughout the year, but this region also experienced less input from atmospheric ions that are not sea salt (nss) derived. For example, Mg^{2+} was the only nss ion (88 ± 0.8% annual) at Oahu whereas Changdao Island experienced influences from nss Mg^{2+} (86.4 ± 4.9% annually), nss Ca^{2+} (91.9 ± 4.9% annually), nss K^+ (70.1 ± 13.4% annually), and nss SO_4^{2-} (68.5 ± 16.1% annually).

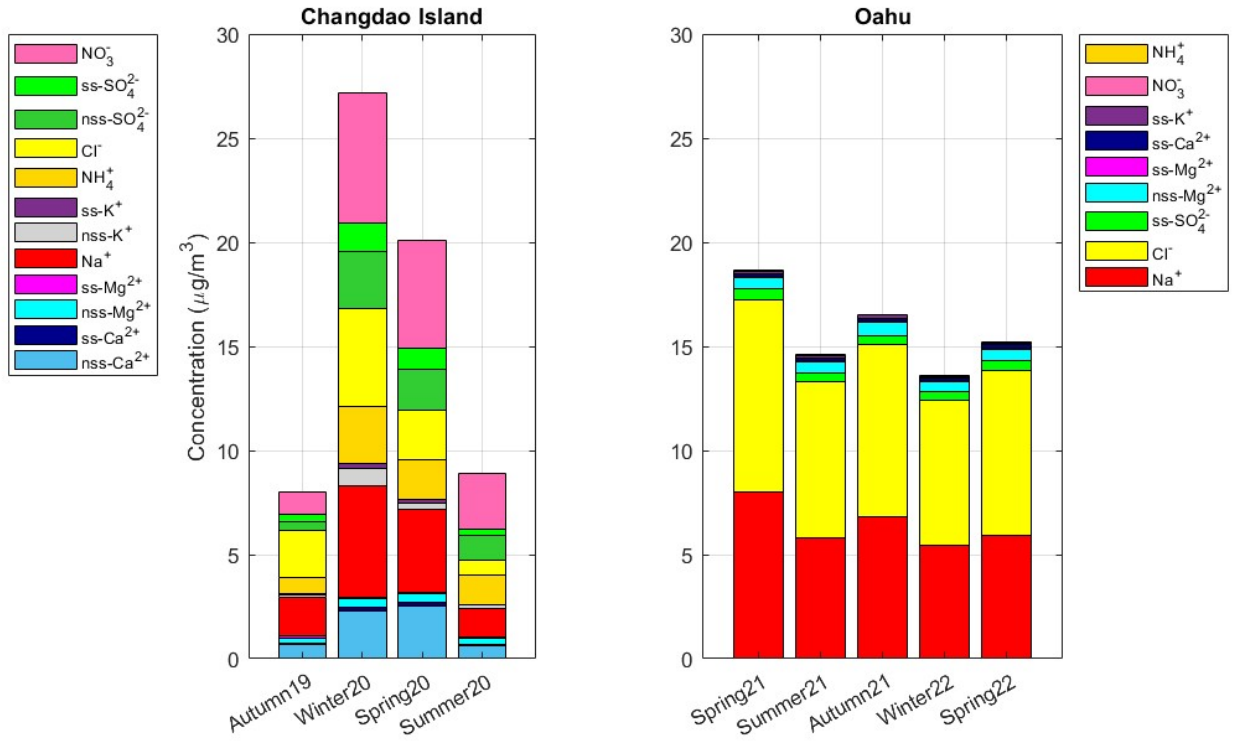

Figure 1: Left: stacked bar graph of species concentration changes among the collection seasons on Changdao Island Numbers after season are indicative of collection year (n=~30 for autumn, n=~31 for winter, n=~26 for spring, n=~16 for summer). Right: stacked bar graph of species concentration changes among the collection seasons on Oahu. Numbers after season are indicative of collection year (n=13 per season).

There are limited studies, both field and modeling, that investigate the quantity of N deposition to the NPO, but the ones that have been conducted are inconsistent and range from 7-67 Tg N/Yr (Table 2). Inorganic N (IN; NO_3^- + NH_4^+) composed less than 1% of the aerosol composition at Oahu (annual [NH_4^+] = 4 ± 7 ng/m^3, annual [NO_3^-] = 51 ± 22 ng/m^3) but about 33% of the aerosol composition at Changdao Island (annual [NH_4^+] = 1,700 ± 1,100 ng/m^3, annual [NO_3^-] = 3,800 ± 3,800 ng/m^3). Of the IN present at Oahu and Changdao Island, 93% was NO_3^- and 7% was NH_4^+, and 69% was NO_3^- and 31% was NH_4^+, respectively. When this deposition is upscaled to the NPO, there is a contribution of 1.2 Tg IN/yr from Oahu (1% NH_4^+, 99% NO_3^-) and 93.5 Tg IN/yr from Changdao Island (5% NH_4^+. 95% NO_3^-). The shift in these

percentages stems from the dry deposition velocities used, which were 0.1 cm/s and 0.9 cm/s, for NH_4^+ and NO_3^-, respectively (Baker *et al*., 2017).

Table 2: A comparison of calculated dry atmospheric N fluxes to the ocean across the literature. IN indicates inorganic nitrogen, and TN indicates total nitrogen (e.g., inorganic + organic).

Study type	Location	Dry N Flux (Tg N/yr)	Study
Field samples	Oahu, Hawaii (upscaled to the NPO)	1 (IN)	MacFarland *et al.*, (2025)
Field samples	Changdao Island, China (upscaled to the NPO)	94 (IN)	MacFarland *et al.*, *(*2022)
Field samples	Southern East China Sea (upscaled to the NPO)	32 (IN)*	Chen and Huang, (2021)
Model	Global ocean average	37 (IN)**	Kanakidou *et al.*, (2012)
Model	Global ocean average	67 (TN)	Duce *et al.*, (2008)
Model	Global ocean average	39 (IN)	Galloway *et al.*, (2004)
Model	Global ocean average	63 (TN)	Okin *et al.*, (2011)
Model	North Pacific Ocean	7 (TN)	Okin *et al.*, (2011)
Model	Global ocean average	38 (IN)	Jickells *et al.*, (2017)
Field Samples	Dongsha Atoll, South China Sea (upscaled to the NPO)	57 (TN)***	Ren *et al.*, (2017)
Field Samples	South China Sea (upscaled to the NPO)	42(IN)****	Kim *et al.*, (2014b)

*28.0 mmol IN m/yr was provided and converted here to Tg N/yr based on an NPO surface area of 8.26×10^{13} m^2, **the model yields a global IN deposition rate of 90.7 Tg N/yr of which 36.6 Tg N/yr (40%) goes to the oceans, ***Ren *et al*., (2017) calculated an average atmospheric N deposition rate of 49 mmol m/yr in 2000 which was converted here to Tg N/yr based on an NPO surface area of 8.26×10^{13} m^2, ****Supplied a TN value of 55 mmol N m/yr but included the assumption of 30% ON, so 30% was removed to obtain the 42 Tg N/yr value. A surface area of 8.26×10^{13} m^2 was used for the NPO

Through the use of air mass back trajectory calculations, it was determined that atmospheric deposition reaches farther into the ocean in the winter compared to summer (Figure 2).

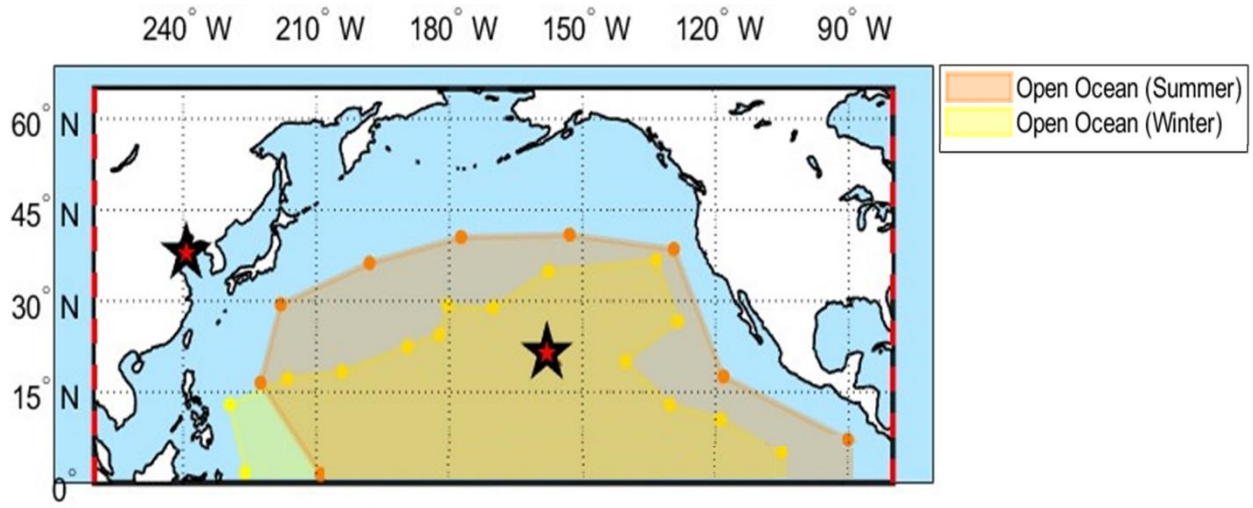

Figure 2: Yellow and orange dots represent coordinates where Trajstat was run and dominate marine origins were observed (>90%) after averaging the trajectories by day (n = 31). A perimeter was then created to outline what is here being considering the open ocean (e.g., lack of continental influence; yellow or orange shaded area). Any water that is not shaded yellow or orange is considered coastal. Yellow polygon = winter (January 2020) results vs orange polygon = summer (August 2020) results. The red stars indicate the study sites: Oahu, Hawaii (open ocean), Changdao Island, China (coastal ocean)

Roughly 35% of the NPO experienced no continental influences in the winter and about 50% of the NPO experienced no continental influences in the summer (Figure 2). This indicates that about 50-65% of the NPO experiences terrestrial input and is considered here to be coastal (e.g., not the open ocean). Higher deposition coastally is expected, as it is the main sink for a majority of anthropogenic dissolved IN for atmospheric deposition (Voss *et al*., 2013). Weighing the deposition averages from both sites based on these percentages, it would indicate an average deposition of ~47 Tg IN/Yr in the summer and ~61 Tg IN/Yr in the winter to the entire NPO. These calculations do not include organic N (ON) but it has been previously estimated that the global median ON contribution to N deposition is about 35% (Kanakidou *et al*., 2012). Using this value to consider TN instead of IN, the deposition values would increase to ~72 Tg TN/Yr in the summer and ~94 Tg TN/Yr in the winter. Although these numbers carry large uncertainties, it does highlight seasonal differences that are not typically accounted for in global modeling

studies. This summer value (~72 Tg TN/Yr) is most similar to Duce *et al*. (2008) who used a global modeling study to predict a TN deposition contribution of 67 Tg TN/Yr (Table 2), 80% of which is thought to be anthropogenic in origin.

An ocean modeling study that focuses on the NPO, north of Oahu and therefore the open ocean, estimates that 14% of the N from May to October is supplied by lateral transport and that N-fixation is the dominant process supplying 70% of the new N (Letscher *et al*., 2016). However, when considering the N budget, they combined N-fixation and atmospheric deposition to represent external sources. An observational study that focuses on the oligotrophic subtropical NPO concluded that the annual relative contribution of N-fixation to N export varied from 36 to 69% (mean = 48%) but only considered two sources of new N (NO_3^- upwelling and N-fixation; Dore *et al*., 2002). An observational study in the western NPO concluded that the contribution of N-fixation to new production ranged from 2 - 37% but this range grouped together N-fixation and NO_3^- assimilation (Shiozaki *et al*., 2009). Atmospheric dust deposition was considered in this study as a source of iron to the ocean to fuel N-fixation, but not as a source of new N. Therefore, the question becomes: how does atmospheric deposition affect these proportions when considering it as an active player in providing excess/new N to the ocean?

The Monte Carlo simulations indicate that atmospheric deposition is a pathway for N deposition both to the coastal and open ocean (Figure 3).

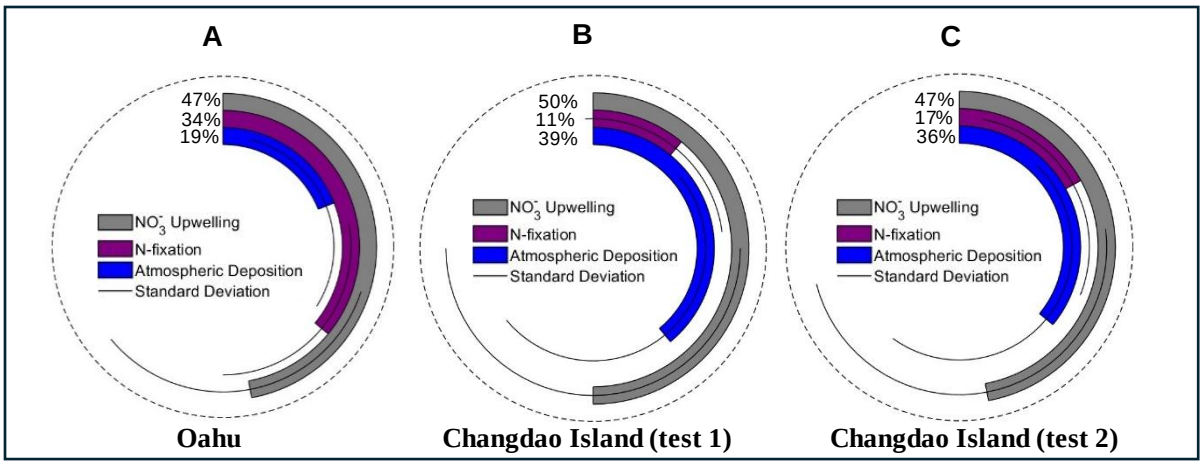

Figure 3: A radial bar chart depicting the average results from the Monte Carlo simulations. (A): Oahu, Hawaii where 12 runs took place, totaling 120,000 simulations. Averages include 47 ± 17% for NO_3^- upwelling, 34 ± 14% for N-fixation, and 19 ± 15% for atmospheric deposition. (B) and (C) both represent Changdao Island, China, where the input for 'x' (N-fixation), differed (e.g., for (B) 'x' = 10% and for (C) 'x' = 20%), as the range for 'x' in the literature was large and uncertain. (B): 12 runs took place, totaling 120,000 simulations. Averages include 50 ± 25% for NO_3^- upwelling, 11 ± 12% for N-fixation, and 39 ± 25% for atmospheric deposition. (C): 12 runs took place, totaling 120,000 simulations. Averages include 47 ± 24% for NO_3^- upwelling, 17 ± 14% for N-fixation, and 36 ± 24% for atmospheric deposition.

The 'x' input (N-fixation) differs from the 'x' output as the simulation adjusted the distribution of 'x' based on the isotopic mass-balance equation and variability in other parameters. For example, if the 'x' input frequently led to combinations of 'y' (NO_3^- upwelling) and 'z' (atmospheric deposition) that could not satisfy the observed PN_{sink}, the simulation naturally weighted values of 'x' closer to the optimal solution. The 'x' output being lower than the 'x' input makes sense given that many studies do not factor in atmospheric deposition as a significant variable, leading to the assumption that N-fixation is playing a larger role. For example, Knapp *et al*., (2018) utilizes a two-end member isotope mixing model that incorporates N-fixation and subsurface NO_3^-, assuming that atmospheric deposition is negligible. Additionally, Zhang *et al*., (2019), who conducted a modeling study, also excluded atmospheric

deposition for their study of the Northeast U.S. shelf but did discuss that atmospheric deposition in this region could have more subtle impacts on the N budget.

Assumptions for this model include: (1) the isotopic signatures of all three sources are well-defined, (2) $\delta^{15}N(PN_{sink})$ accurately reflects the contributions from the three sources, and (3) other potential sources (e.g., dissolved ON) are negligible. An added constraint of 'x+y+z = 1' was also implemented.

3.2 Isotope Values and Source Origins

Oahu experienced all natural influences, with 65 ± 5% marine origins and 35 ± 5% seabird emissions due to nearby seabird sanctuaries. $\delta^{15}N\text{-}NH_4^+$ values did not vary seasonally ($p > 0.05$) but did separate into three distinct clusters: cluster one = 19.0 ± 3.9‰ (n = 8), cluster two = 4.1 ± 2.3‰ (n = 31), and cluster three = -3.3 ± 2.4‰ (n = 13). Cluster three was best explained as an ocean emissions signature, which was determined via a phase partitioning model that incorporated N isotope fractionation associated with NH_3 conversion to NH_4^+. Cluster one had mostly higher than average $[NH_4^+]$ along with air mass origins from two seabird sanctuaries and was hypothesized to be a seabird emission signature. Cluster two was considered a mix of these two sources (67% marine, 33% seabird emissions). Although anthropogenic activities did not appear to have any significance on atmospheric N deposition at the Hawaii site (e.g., no continental air mass origins), the unexpected contribution from seabird guano remains an outside source that contributes excess N to the open ocean.

Changdao Island experienced strong anthropogenic influences, with 95% of deposition being anthropogenic in origin, 75 ± 4% of which derived from agricultural activities. Not only did air mass origins largely originate from the continent, but $\delta^{15}N\text{-}NH_4^+$ values revealed a

multitude of inputs from human activities (agriculture, industrial emissions, vehicle emissions, etc) which emit NH_3. $\delta^{15}N\text{-}NH_4^+$ values varied seasonally ($p < 0.05$), with a higher average in spring (13.3 ± 7.9‰) and summer (15.6 ± 6.2‰) compared to autumn (3.2 ± 2.5‰) and winter (3.8 ± 11.4‰), but with agriculture remaining the dominate influence year-round. This is consistent with Kim *et al*., (2017) who discusses decreasing influence of anthropogenic N as distance from the coast increases related to sediment $\delta^{15}N$. These sites highlight that sources (both natural and anthropogenic), and deposition, are more localized and can get overlooked when modeling global averages or with large upscaling.

The global emission source inventory (McDuffie *et al*., 2020) further revealed that agriculture remained the dominant NH_3 emission source off the Eastern coast of China from 1970 to 2017, annually accounting for 75 ± 6% of emissions, with a low in winter (48 ± 16%) and high in spring (85 ± 29%). This is consistent with the isotope mixing model results from the Changdao Island samples which observed a year-round dominant influence from agricultural activities, with a low also in winter. These emissions have drastically increased over time, 1.7× annually and monthly between 1970 and 2017. Annual agricultural emissions averaged 1.1×10^{-11} ± $8.9\times10^{\wedge-12}$ kg m^{-2} s^{-1} and 1.9×10^{-11} ± 1.6×10^{-11} kg m^{-2} s^{-1} for 1970 and 2017, respectively. For the month of May, which exhibited the highest concentrations consistently, the average increased from 3.6×10^{-11} kg m^{-2} s^{-1} to 6.3×10^{-11} kg m^{-2} s^{-1} from 1970 to 2017. Other notable NH_3 sources include waste (18 ± 2% annually) and resident combustion (4 ± 0.4% annually; McDuffie *et al*., 2004).

For NO_x, the main source contributors to the same area were industry (~28%), energy (~26%), and on road transportation (~23%), with these sources remaining proportionally consistent between 1970-2017. Emissions, however, increased three-fold for these sources over

the same time period. For example, the average concentration for industrial emissions increased from 3.4×10^{-12} kg m^{-2} s^{-1} to $1.2\times10^{\wedge-11}$ kg m^{-2} s^{-1} from 1970 to 2017. As more NH_3 and NO_x emissions enter the atmosphere, the greater the subsequent deposition into the ocean, and the higher the likelihood there will be increased effects on the biogeochemistry of the ocean.

4. Conclusion

Two year-round aerosol IN studies were compared at Changdao Island, China (coastal ocean) and Oahu, Hawaii (open ocean) in order to characterize these two types of environments in the NPO. The open ocean site had lower ion concentrations with a composition that was dominated by sea salt. Additionally, there were limited observations of nss ions. Presence of slightly depleted $\delta^{15}N\text{-}NH_4^+$ values were indicative of marine sources, supported by air mass back trajectories that were entirely marine in origin. Further, the enriched $\delta^{15}N\text{-}NH_4^+$ values were from a natural external NH_3 source (seabird guano emissions), not anthropogenic activities, also supported by the airmass back trajectories. The coastal ocean site, on the other hand, experienced higher ion concentrations with significantly more nss ions present due to the proximity of terrestrial/anthropogenic sources. This is reflective of both the enriched $\delta^{15}N\text{-}NH_4^+$ values and air mass back trajectories largely originating from the continent.

Monte Carlo simulations indicated that NO_3^- upwelling is the dominate source of new N to these two regions. N-fixation played a larger role than atmospheric deposition at Oahu, but atmospheric deposition played a larger role than N-fixation at Changdao Island. Still, this model highlighted that atmospheric deposition is present at both locations. Isotope values revealed a dominating anthropogenic signature at Changdao Island from agricultural activities and a dominating marine signature at Oahu, with natural external N entering the ocean from seabird guano emissions; a new external source of N to be isotopically identified and found to account

for ~35% of atmospheric NH_4^+ in that region. Therefore, atmospheric deposition should not be dismissed as a factor in future oceanic studies, both coastally and in the open ocean.

IN composed less than 1% of the aerosol composition at Oahu (55 ± 37 ng/m^3) but about 33% of the aerosol composition at Changdao Island ($5{,}500 \pm 4{,}900$ ng/m^3). When this deposition was upscaled to the NPO, there was a contribution of 1.2 Tg IN/yr from Oahu and 93.5 Tg IN/yr from Changdao Island. This work provides new inorganic N observations in the NPO where limited data was previously available. It was further calculated that about 35% of the NPO experienced no continental influence in the winter and about 50% of the NPO experienced no continental influence in the summer, characterizing it as the open ocean. Weighing the deposition averages from both sites based on these percentages suggested an average total deposition of ~47 Tg IN/Yr in the summer and ~61 Tg IN/Yr in the winter.

A separate aerosol study in the equatorial Pacific deduced via transport modeling and co-occurrence of low $\delta^{15}N$ and $\delta^{18}O$ values that marine-derived alkyl nitrates ($RONO_2$; e.g., organic nitrates) are an important influence of on aerosol NO_3^- formation (Joyce *et al*., 2022). This, in conjunction with the seabird guano emissions signature found isotopically at Oahu, suggests that additional isotopic studies are needed to aid in understanding the gradient of impact of anthropogenic vs natural emissions and whether or not there are other unknown sources to be identified. This work will further advance future research aimed at the biogeochemical impacts of atmospheric N deposition to the open ocean.

References

Altabet, M.A. (2001). Nitrogen isotopic evidence for micronutrient control of fractional NO_3^- utilization in the equatorial Pacific. *Limnology and Oceanography*, 46(2), 368–380. https://doi.org/10.4319/lo.2001.46.2.0368.

Altieri, K.E., Fawcett, S.E., & Hastings, M.G. (2021). Reactive nitrogen cycling in the atmosphere and ocean. *Annual Reviews*, 49, 523−550. https://doi.org/10.1146/annurev-earth-083120-052147.

Altieri, K.E., Hastings, M.G., Peters, A.J., Oleynik, S., & Sigman, D.M. (2014). Isotopic evidence for a marine ammonium source in rainwater at Bermuda. *Global Biogeochemical Cycles*, 28(10), 1066−1080. https://doi.org/10.1002/2014GB004809.

Baker, A.R., Kanakidou, M., Altieri, K.E., Daskalakis, N., Okin, G.S., Myriokefalitakis, S., *et al*. (2017). Observation- and model-based estimates of particulate dry nitrogen deposition to the oceans. *Atmospheric Chemistry and Physics*, 17(3), 8189–8210.https://doi.org/10.5194/acp-17-8189-2017.

Böttjer, D., Dore, J.E., Karl, D.M., Letelier, R.M., Mahaffey, C., Wilson, S.T., *et al*. (2017). Temporal variability of nitrogen fixation and particulate nitrogen export at Station ALOHA. *Limnology and Oceanography*, 62(1), 200−216. https://doi.org/10.1002/lno.10386.

Carpenter, E.J., Harvey, H.R., Fry, B., & Capone, D.G. (1997). Biogeochemical tracers of the marine cyanobacterium Trichodesmium. *Deep Sea Research Part I*, 44(1), 27–38. https://doi.org/10.1016/S0967-0637(96)00091-X.

Casciotti, K.L., Buchwald, C., Santoro, A.E., & Frame, C. (2011). Chapter eleven - Assessment of Nitrogen and Oxygen Isotopic Fractionation During Nitrification and Its Expression in the Marine Environment. *Methods in Enzymology*, 486, 253−280. https://doi.org/10.1016/B978-0-12-381294-0.00011-0.

Casciotti, K.L., Sigman, D.M., Hastings, M.G., Böhlke, J.K. & Hilkert, A. (2002). Measurement of the oxygen isotopic composition of nitrate in seawater and freshwater using the denitrifier method. *Analytical Chemistry*, 74(19), 4905–4912. https://doi.org/10.1021/ac020113w.

Chen, H.-Y., & Huang, S.-Z. (2021). Composition and supply of inorganic and organic nitrogen species in dry and wet atmospheric deposition: Use of organic nitrogen composition to calculate the Ocean's external nitrogen flux from the atmosphere. *Continental Shelf Research*, 213(15), 104316. https://doi.org/10.1016/j.csr.2020.104316.

Cooper, R.J., Krueger, T., Hiscock, K.M., & Rawlins, B.G. (2014). Sensitivity of fluvial sediment source apportionment to mixing model assumptions: a Bayesian model comparison. *Water Resources Research*, 50(11), 9031–9047. https://doi.org/10.1002/2014WR016194.

Dore, J.E., Brum, J.R., Tupas, L.M., & Karl, D.M. (2002). Seasonal and interannual variability in sources of nitrogen supporting export in the oligotrophic subtropical North Pacific Ocean. *Limnology and Oceanography*, 47(6), 1595–1607. https://doi.org/10.4319/lo.2002.47.6.1595.

Duce, R.A., LaRoche, J., Altieri, K., Arrigo, K.R., Baker, A.R., Capone, D.G., *et al*. (2008). Impacts of Atmospheric Anthropogenic Nitrogen on the Open Ocean. *Science*, 320(5878), 893-897. https://doi.org/10.1126/science.1150369.

Elser, J., Andersen, T., Baron, J., Bergstrom, A.-K., Jansson, M., Kyle, M., *et al*. (2009). Shifts in lake N:P stoichiometry and nutrient limitation driven by atmospheric nitrogen

deposition. *Science*, 326 (5954), 835–837. https://doi.org/10.1126/science.1176199.
Galloway, J.N., Dentener, F.J., Capone, D.G., Boyer, E.W., Howarth, R.W., Seitzinger, S. P., *et al*. (2004). Nitrogen cycles: past, present, and future. *Biogeochemistry*, 70(2), 153–226. https://doi.org/10.1007/s10533-004-0370-0.
Gruber, N., & Galloway, J.N. (2008). An Earth-system perspective of the global nitrogen cycle. *Nature*, 451, 293–296. https://doi.org/10.1038/nature06592.
Gruber, N., & Sarmiento, J.L. (1997). Global patterns of marine nitrogen fixation and denitrification. *Global Biogeochemical Cycles*, 11(2), 235−266. https://doi.org/10.1029/97GB00077.
Hoering, T.C., & Ford, H.T. (1960). The Isotope Effect in the Fixation of Nitrogen by Azotobacter. *Journal of the American Chemical Society*, 82(2), 376–378. https://doi.org/10.1021/ja01487a031.
Hoesly, R., O'Rourke, P., Braun, C., Feng, L., Smith, S.J., Pitkanen, T., *et al*. (2019). CEDS: Community Emissions Data System (Version Dec-23-2019), Zenodo. https://zenodo.org/records/4741285.
Jickells, T.D., Buitenhuis, E., Altieri, K., Baker, A.R., Capone, D., Duce, R.A., *et al*. (2017). A reevaluation of the magnitude and impacts of anthropogenic atmospheric nitrogen inputs on the ocean. *Global Biogeochemical Cycles*, 31(2), 289–305. https://doi.org/10.1002/2016GB005586.
Jickells, T., Kelly, S., Baker, A., Biswas, K., Dennis, P., Spokes, *et al*. (2003). Isotopic evidence for a marine ammonia source. *Geophysical Research Letters*, 30(7). https://doi.org/10.1029/2002GL016728.
Johnson, K.S., Riser, S.C., & Karl, D.M. (2010). Nitrate supply from deep to near-surface waters of the North Pacific subtropical gyre. *Nature*, 465(7301), 1062–1065. https://doi.org/10.1038/nature09170.
Joyce, E.E. 2022. From the Atmosphere to the Sea: Atmospheric Nitrogen Deposition to Aquatic Ecosystems. *Earth, Environmental and Planetary Sciences Theses and Dissertations.* Brown Digital Repository. Brown University Library. https://repository.library.brown.edu/studio/item/bdr:ytp8w8gx/.
Joyce, E.E., Balint, S.J., & Hastings, M.G. (2022). Isotopic Evidence That Alkyl Nitrates Are Important to Aerosol Nitrate Formation in the Equatorial Pacific. *Geophysical Research Letters*, 49(16). https://doi.org/10.1029/2022GL099960.
Kaiser, J., Hastings, M.G., Houlton, B.Z., Röckmann, T. & Sigman, D.M. (2007). Triple oxygen isotope analysis of nitrate using the denitrifier method and thermal decomposition of N2O. *Analytical Chemistry*, 79(2), 599–607. https://doi.org/10.1021/ac061022s
Kanakidou, M., Duce, R.A., Prospero, J.M., Baker, A.R., Benitez-Nelson, C., Dentener, F.J., et al. (2012). Atmospheric fluxes of organic N and P to the global ocean. *Global Biogeochemical Cycles*, 26(3). https://doi.org/10.1029/2011GB004277.
Kim, H., Lee, K., Lim, D.-I., Nam, S.-I., Kim, T.-W., Yang, J.-Y.T., *et al*. (2017). Widespread Anthropogenic Nitrogen in Northwestern Pacific Ocean Sediment. Environmental Science and Technology, 51(11), 6044-6052. https://doi.org/10.1021/acs.est.6b05316.
Kim, I.-N., Lee, K., Gruber, N., Karl, D.M., Bullister, J.L., Yang, S., & Kim, T.-W. (2014a). Increasing anthropogenic nitrogen in the North Pacific Ocean. *Science*, 346(6213), 1102–1106. https://doi.org/10.1126/science.1258396.
Kim, T.W., Lee, K., Duce, R., & Liss, P. (2014b). Impact of atmospheric nitrogen deposition on phytoplankton productivity in the South China Sea. *Geophysical Research Letters*, 41(9),

3156-3162. https://doi.org/10.1002/2014GL059665.
Kim, T.W., Lee, K., Najjar, R.G., Jeong, H.D., & Jeong, H.J. (2011). Increasing N abundance in the northwestern Pacific Ocean due to atmospheric nitrogen deposition. *Science*, 334(6055), 505–509. https://doi.org/10.1126/science.1206583.
Knapp, A.N., McCabe, K.M., Grosso, O., Leblond, N., Moutin, T., & Bonnet, S. 2018. Distribution and rates of nitrogen fixation in the western tropical South Pacific Ocean constrained by nitrogen isotope budgets. *Biogeosciences*, 15, 2619–2628, https://doi.org/10.5194/bg-15-2619-2018.
Le Roy, E. Walters, W.W., Joyce, E.E., & Hastings, M.G. (2021). Sources of ammonium in seasonal wet deposition at a coastal New England city. *Atmospheric Environnent*, 260, 118557. https://doi.org/10.1016/j.atmosenv.2021.118557.
Letscher, R.T., Primeau, F., & Moore, J.K. (2016). Nutrient budgets in the subtropical ocean gyres dominated by lateral transport. *Nature Geoscience*, 9(11), 815−819. https://doi.org/10.1038/ngeo2812.
MacFarland, A.B., Joyce, E.E., Wang, X., Walters, W. W., Altieri, K.E., Schiebel, H.N., & Hastings, M.G. (2023). Investigation of coastal ammonium aerosol sources in the Northwest Pacific Ocean. *Atmospheric Environment*, 312, 120034. https://doi.org/10.1016/j.atmosenv.2023.120034.
MacFarland, A.B., Walters, W.W., & Hastings, M.G. (2024). Solid Phase Extraction Methodology for Robust Isotope Analysis of Atmospheric Ammonium: Concentration and Removal of Matrix Interferences. *ACS Earth and Space Chemistry*, 8(5), 1039-1047. https://doi.org/10.1021/acsearthspacechem.3c00375.
MacFarland, A., Hastings, M., & Schiebel, H.N. (2025). Aerosol composition data of ion concentrations (ammonium, nitrate, nitrite, sodium, chloride, magnesium, calcium, potassium, sulfate); and ammonium and nitrate isotope (15N) of atmospheric particulates collected in Hawaii from March 2021 to August 2022. Biological and Chemical Oceanography Data Management Office (BCO-DMO). (Version 1) Version Date 2025-02-13. https://doi.org/10.26008/1912/bco-dmo.946741.1.
Minagawa, M., & Wada, E. (1986). Nitrogen Isotope Ratios of Red Tide Organisms in the East China Sea: a Characterization of Biological Nitrogen-Fixation. *Marine Chemistry*, 19(3), 245–259. https://doi.org/10.1016/0304-4203(86)90026-5.
O'Dell, J.W. (1993a). In: Method 353.2, Revision 2.0: Determination of Nitrate-Nitrite by Automated Colorimetry. US EPA.
O'Dell, J.W., (1993b). In: Method 350.1, Revision 2.0: Determination of Ammonia Nitrogen by Semi-automated Colorimetry. US EPA.
Okin, G.S., Baker, A.R., Tegan, I., Mahowald, N.M., Dentener, F.J., Duce, R.A., *et al*. (2011). Impacts of atmospheric nutrient deposition on marine productivity: Roles of nitrogen, phosphorus, and iron. *Global Biogeochemical Cycles*, 25(2). https://doi.org/10.1029/2010GB003858.
Parnell, A.C., Phillips, D.L., Bearhop, S., Semmens, B.X., Ward, E.J., Moore, J.W., *et al*. (2013). Bayesian stable isotope mixing models. *Environmetrics*, 24(6), 387–399. https://doi.org/10.1002/env.2221.
Rafter, P.A., Bagnell, A., Marconi, D., & DeVries, T. (2019). Global trends in marine nitrate N isotopes from observations and a neural network-based climatology. *Biogeosciences*, 16(13), 2617–2633. https://doi.org/10.5194/bg-16-2617-2019.
Rolph, G., Stein, A., & Stunder, B. (2017). Real-time environmental applications and display

sYstem: READY. *Environmental Modellimg & Software*, 95, 210–228. https://doi.org/10.1016/j.envsoft.2017.06.025.

Shiozaki, T., Furuya, K., Kodama, T., & Takeda, S. (2009). Contribution of N2 fixation to new production in the western North Pacific Ocean along 155°E. *Marine Ecology Progress Series*, 377, 19-32. https://doi.org/10.3354/meps07837.

Sigman, D.M., Casciotti, K.L., Andreani, M., Barford, C., Galanter, M.B.J.K. & Böhlke, J.K. (2001). A bacterial method for the nitrogen isotopic analysis of nitrate in seawater and freshwater. *Analytical chemistry*, 73(17), 4145–4153. https://doi.org/10.1021/ac010088e.

Sigman, D.M., & Fripiat, F. (2019). Nitrogen Isotopes in the Ocean. Academia, Encyclopedia of Ocean Sciences (Third ed.), 263−278. Editors in Chief: J. Kirk Cochran, Patricia L. Yager, Henry J. Bokuniewicz. ISBN: 978-0-12-813082-7.

Stein, A.F., Draxler, R.R., Rolph, G.D., Stunder, B.J.B., Cohen, M.D., & Ngan, F. (2015). NOAA's HYSPLIT atmospheric transport and dispersion modeling system. *Bulletin of the American Meteorological Society*, 96(12), 2059–2077. https://doi.org/10.1175/BAMS-D-14-00110.1.

Voss, M., Bange, H.W., Dippner, J.W., Middleburg, J.J., Montoya, J.P., & Ward, B. (2013). The marine nitrogen cycle: recent discoveries, uncertainties and the potential relevance of climate change. *Philosophical Transactions of the Royal Society B*, 368, 20130121. http://dx.doi.org/10.1098/rstb.2013.0121.

Walters, W.W., Karod, M., Willcocks, E., Baek, B.H., Blum, D.E., & Hastings, M.G. (2022). Quantifying the importance of vehicle ammonia emissions in an urban area of northeastern USA utilizing nitrogen isotopes. *Atmospheric Chemistry and Physics*, 22(20), 13431−13448. https://doi.org/10.5194/acp-22-13431-2022.

Wang, Y. Q., Zhang, X. Y., & Draxler, R. (2009). TrajStat: GIS-based software that uses various trajectory statistics analysis methods to identify potential sources from long-term air pollution measurement data. *Environmental Modelling & Software*, 24, 938–939. https://doi.org/10.1016/j.envsoft.2009.01.004.

Xu, L., & Penner, J. E. (2012). Global simulations of nitrate and ammonium aerosols and their radiative effects. *Atmospheric Chemistry and Physics*, 12, 9479–9504. https://doi.org/10.5194/acp-12-9479-2012.

Zhang, L., Altabet, M., Wu, T., & Hadas, O. (2007). Sensitive Measurement of NH4+ 15N/14N (*d*15NH4+) at Natural Abundance Levels in Fresh and Saltwaters. *Analytical Chemistry*, 79(14), 5297-5303. https://doi.org/10.1021/ac070106d.

Zhang, S., Stock, C.A., Curchitser, E.N., & Dussin, R. (2019). A Numerical Model Analysis of the Mean and Seasonal Nitrogen Budget on the Northeast U.S. Shelf. Journal of Geophysical Research: Oceans, 124(5), 2969-2991. https://doi.org/10.1029/2018JC014308.

Appendix

Alexandra B. MacFarland

Department of Earth, Environmental, and Planetary Sciences, Institute at Brown for Environment and Society, Brown University, Providence, RI 02912, USA

Measurement Report

Background

San Juan Bay Estuary (SJBE) is a system that covers roughly 240 km^2 of area (25 km^2 of water cover) and is composed of multiple ecological sub-systems (Bunch *et al*., 2000). This system is not well connected and as a result the flow among the different sub-estuaries is constricted. The biota in these sub-sections mix and remix after a disturbance, resulting in a dynamic system both biotically and environmentally. For example, SJBE is exposed to extreme events such as storms and hurricanes, which depending on the intensity of these occurrences, can impact the functionality of the estuary for months to years (Lugo *et al*., 2024).

The watershed itself is ~68% developed, with an additional ~7% of mangrove forest coverage and ~5% moist forest coverage (Brandeis *et al*. 2014). The nitrogen (N) dynamics in the water are complex due to the anaerobic conditions linked with sewage input – both through direct stream input as well as indirect input from leaky pipes and sewage contaminated storm drains. Improving N models requires a better understanding of these dynamics, specifically the N cycle (Potter *et al*. 2014). Currently, the highly modified Caño Martín Peña (CMP), an urbanized channel that runs through the city, is affected by dense residential development coupled with a lack of adequate infrastructure for managing this regions wastewater (Lugo *et al*., 2024). These issues pose consequences both to human and environmental health. However, tropical, urban estuarine systems are not well studied, making it difficult to assess impacts. Here, I aim to analyze the relationship between ion concentrations as well as δ^{15}N-PN (particulate N), δ^{15}N-NH_4^+ (ammonium) and δ^{15}N-NO_3^- (nitrate) from the surface waters of three specific regions: Bahía de San Juan (BSJ) stations 1, 2, and 3 (coastal ocean); CMP2 (urban channel); and Laguna

de Piñones (LP) (mangrove forest) in order to better understand how N is moving through this complex system (Figure 1).

Figure 1: Google Earth image of San Juan Bay Estuary in Puerto Rico (bottom image; 18°25'36"N 66°01'59"W). Study sites from left to right (top image, yellow stars): BSJ1, BSJ2, BSJ3 (coastal ocean), CMP2 (urban channel), LP1 (mangrove forest).

Collaboration

I collaborated with the Environmental Protection Agency's (EPA) Atlantic Coastal Environmental Sciences Division (ACESD) in Narragansett, RI to aid in their mission to better understand nutrient cycling in tropical, urban estuarine systems. Dr. Autumn Oczkowski and her team sampled water throughout the SJBE twice monthly. They measured conductivity, salinity, pH, dissolved oxygen, temperature (°C), turbidity, NH_4^+, NO_3^-, NO_2^-, orthophosphate (PO_4^{3-}), and δ^{15}N-PN. However, the instruments needed to analyze δ^{15}N-NH_4^+ and δ^{15}N-NO_3^- were not

available, yet necessary, to fully understand how N is cycling through this system. Therefore, I conducted those $\delta^{15}N$ analyses at Brown University.

Sample type/collection

From 2021 - 2023, surface water samples were collected twice a month at various stations throughout the SJBE (Figure 1). Samples were collected by placing a 1 L bottle (precleaned with 1 M HCl) just below the water surface to fill them and then placing them on ice (approximately 4 ± 2°C) until arrival at the laboratory for processing. Bottles were cleaned in between collections and nitrile gloves were worn.

Measurements performed

In-situ measurements of conductivity, salinity (parts per thousand or ppt), pH, dissolved oxygen (DO, mg l^{-1}), barometric pressure (mm Hg) and temperature (°C) of the water were taken with a calibrated YSI multi-parameter meter (YSI Inc., Yellow Springs, OH). Turbidity was measured via a turbidity meter (2020i, LaMotte).

Each surface water sample was filtered in duplicate through pre-combusted (450 °C, 4 hours) glass fiber filters (Whatman GFF, 0.7 µm pore size, 25 mm diameter) using an electric vacuum pump. After filtration, 20 mL vials were rinsed with a small portion of filtered water, swirled, emptied, and then filled to just below the rim. Filters were carefully removed using forceps, folded into foil, and placed in labeled bags. Between samples, the filter funnels were rinsed three times with deionized (DI) water and new flasks were used for each station to avoid cross-contamination. Both water and filters were stored at −20°C until shipment on dry ice to the EPA lab in Narragansett, RI for further analysis.

Analyses for NH_4^+ (run as ammonia (NH_3)), nitrate+nitrite (NO_3^-+NO_2^-), NO_2^-, and PO_4^{3-} were run simultaneously on two connected Astoria 2 segmented flow analyzers (Astoria-Pacific, Clackamas, Oregon, USA). EPA methods (350.1, 353.2, and 365.1; O'Dell, 1993a, O'Dell, 1993b).

Filters were transferred to pre-combusted metal weigh boats and dried at 60°C for at least 24 hours. Dried filters were rolled into tinfoil squares and pelletized using a pellet press. Pellets were then analyzed for N stable isotopes ($\delta^{15}N$) using an Elementar Vario Micro elemental analyzer connected via continuous flow to an Isoprime 100 isotope ratio mass spectrometer (Elementar Americas, Mt. Laurel, NJ). The filtered surface water samples, once received at Brown University, where further analyzed for $\delta^{15}N$-NO_3^- and $\delta^{15}N$-NH_4^+ values. $\delta^{15}N$-NO_3^- was determined using the denitrifier method (Casciotti *et al*., 2002; Kaiser *et al*., 2007; Sigman *et al*., 2001) and $\delta^{15}N$-NH_4^+ was determined using the azide method (Zhang *et al*., 2007) coupled with a pre-treatment cation exchange resin method to purify the NH_4^+ (MacFarland *et al*., 2024).

Statistical analyses

Multiple Factor Analysis (MFA) is a statistical tool used to analyze complex datasets where variables are structured into groups and provides information on the relationships between multiple sets of variables measured to determine how different groups of variables contribute to the overall pattern within the data. This tool was utilized for the provided variables (temp, DO, salinity, pH, turbidity, PO_4^{3-}, NH_4^+, NO_x, PN) at each site per year (2021, 2022, 2023).

Analysis of variance (ANOVA) is a statistical tool that compares the means of multiple (3+) groups. It's used to determine if the differences between groups are significant. This test was

used to determine if the various isotopic groups (δ^{15}N-PN, δ^{15}N-NH_4^+, δ^{15}N-NO_3^-) were significantly different from one another.

Violin plots are a data visualization tool that combines elements of a box plot and a kernel density plot and were made to display dissolved inorganic nitrogen (DIN) concentrations at the three regions over the three years as well as to display the three types of isotope measurements. The isotope data were grouped in two different ways, first as a combined plot of the sites and the second plot focused just on CMP2 as that site had the most available data. Pearson correlation coefficients, which measures how strongly two variables are linearly related, were further calculated among these isotopic values.

Results

Table 1: Different variable measurements ($\bar{x} \pm \sigma$ (n)) at each station (BSJ1, BSJ2, BSJ3, CMP2, LP1) among three separate years (2021, 2022, 2023).

Station	Year	Temp (C)	DO (mg/L)	Salinity (ppt)	pH	Turbidity (NTU)	PO_4^{3-} (µM/L)	NH_4^+ (µM/L)	NO_x (µM/L)	PN (mg/L)
BSJ1	2021	28.8 ± 1.4 (12)	7.3 ± 1.4 (12)	35.5 ± 0.8 (12)	7.7 ± 0.1 (10)	1.6 ± 0.7 (12)	1.2 ± 0.3 (12)	5.6 ± 0.6 (12)	1.4 ± 1.0 (12)	0.1 ± 0.0 (12)
BSJ2	2021	28.6 ± 1.0 (11)	7.2 ± 1.5 (11)	35.8 ± 1.0 (11)	7.7 ± 0.1 (10)	1.4 ± 0.8 (11)	1.2 ± 0.3 (11)	5.9 ± 1.1 (11)	1.4 ± 1.0 (11)	0.1 ± 0.0 (11)
BSJ3	2021	29.1 ± 1.1 (11)	6.5 ± 1.0 (11)	35.8 ± 0.7 (11)	7.7 ± 0.1 (10)	2.2 ± 1.0 (11)	1.2 ± 0.3 (11)	6.2 ± 0.8 (11)	1.7 ± 0.8 (11)	0.1 ± 0.0 (11)
CMP2	2021	27.6 ± 1.4 (19)	2.1 ± 1.0 (19)	23.4 ± 8.1 (19)	7.0 ± 0.2 (17)	4.5 ± 2.1 (19)	2.4 ± 0.8 (19)	36.7 ± 23.1 (19)	6.4 ± 3.7 (19)	0.2 ± 0.1 (19)
LP1	2021	29.1 ± 2.3 (18)	5.3 ± 2.9 (18)	26.9 ± 3.9 (18)	7.6 ± 0.3 (16)	27.7 ± 25.9 (18)	1.3 ± 1.3 (18)	26.2 ± 53.9 (18)	1.4 ± 1.3 (18)	2.0 ± 1.6 (18)
BSJ1	2022	28.2 ± 1.0 (12)	6.6 ± 0.6 (12)	35.9 ± 1.3 (12)	8.0 ± 0.2 (12)	1.9 ± 0.6 (11)	1.1 ± 0.3 (12)	5.9 ± 0.9 (12)	1.2 ± 0.7 (12)	0.0 ± 0.0 (12)
BSJ2	2022	28.1 ± 1.0 (13)	6.7 ± 0.9 (13)	34.1 ± 3.4 (13)	8.0 ± 0.1 (13)	2.2 ± 1.2 (12)	1.1 ± 0.3 (13)	5.8 ± 1.0 (13)	1.3 ± 1.5 (12)	0.1 ± 0.0 (13)
BSJ3	2022	28.5 ± 1.1 (13)	6.2 ± 0.6 (13)	35.9 ± 1.0 (13)	7.9 ± 0.1 (13)	3.3 ±1.4 (11)	1.1 ± 0.4 (13)	6.4 ± 2.4 (13)	1.1 ± 0.4 (13)	0.1 ± 0.0 (13)
CMP2	2022	26.8 ± 1.6 (22)	2.6 ± 1.2 (22)	23.3 ± 5.9 (22)	7.4 ± 0.3 (22)	4.7 ± 2.4 (22)	2.3 ± 0.8 (23)	27.6 ± 16.5 (23)	5.9 ± 4.1 (23)	0.3 ± 0.2 (23)
LP1	2022	27.7 ± 1.8 (27)	4.3 ± 1.5 (27)	22.5 ± 10.0 (27)	7.6 ± 0.6 (27)	14.6 ± 18.4 (27)	2.2 ± 1.9 (27)	16.6 ± 20.3 (27)	2.3 ± 1.9 (27)	0.8 ± 0.8 (24)

BSJ1	2023	28.9 ± 1.3 (14)	6.4 ± 0.4 (14)	36.2 ± 0.5 (14)	8.1 ± 0.1 (14)	0.8 ± 0.7 (12)	1.3 ± 0.2 (14)	6.9 ± 2.1 (14)	1.3 ± 0.6 (14)	0.0 ± 0.0 (14)
BSJ2	2023	28.6 ± 1.5 (13)	6.8 ± 1.0 (13)	35.7 ± 0.8 (13)	8.0 ± 0.1 (13)	1.3 ± 0.8 (12)	1.3 ± 0.2 (13)	6.8 ± 2.4 (13)	1.3 ± 1.0 (13)	0.0 ± 0.0 (13)
BSJ3	2023	28.7 ±1.4 (11)	6.2 ± 0.7 (11)	35.4 ± 1.8 (11)	7.9 ± 0.2 (11)	1.5 ± 0.4 (10)	1.4 ± 0.2 (11)	7.1 ± 2.6 (11)	1.9 ± 0.9 (11)	0.1 ± 0.0 (11)
CMP2	2023	28.7 ± 1.3 (27)	3.2 ± 1.5 (27)	24.6 ± 7.8 (27)	7.5 ± 0.2 (27)	2.6 ± 1.6 (25)	1.4 ± 0.4 (18)	16.1 ± 6.5 (18)	4.7 ± 2.7 (18)	0.4 ± 0.2 (18)
LP1	2023	30.4 ± 3.1 (19)	4.0 ± 2.0 (19)	22.8 ± 8.6 (19)	8.0 ± 0.4 (19)	18.4 ± 18.6 (14)	2.0 ± 2.7 (17)	30.8 ± 48.0 (17)	3.8 ± 4.8 (17)	1.2 ± 0.7 (15)

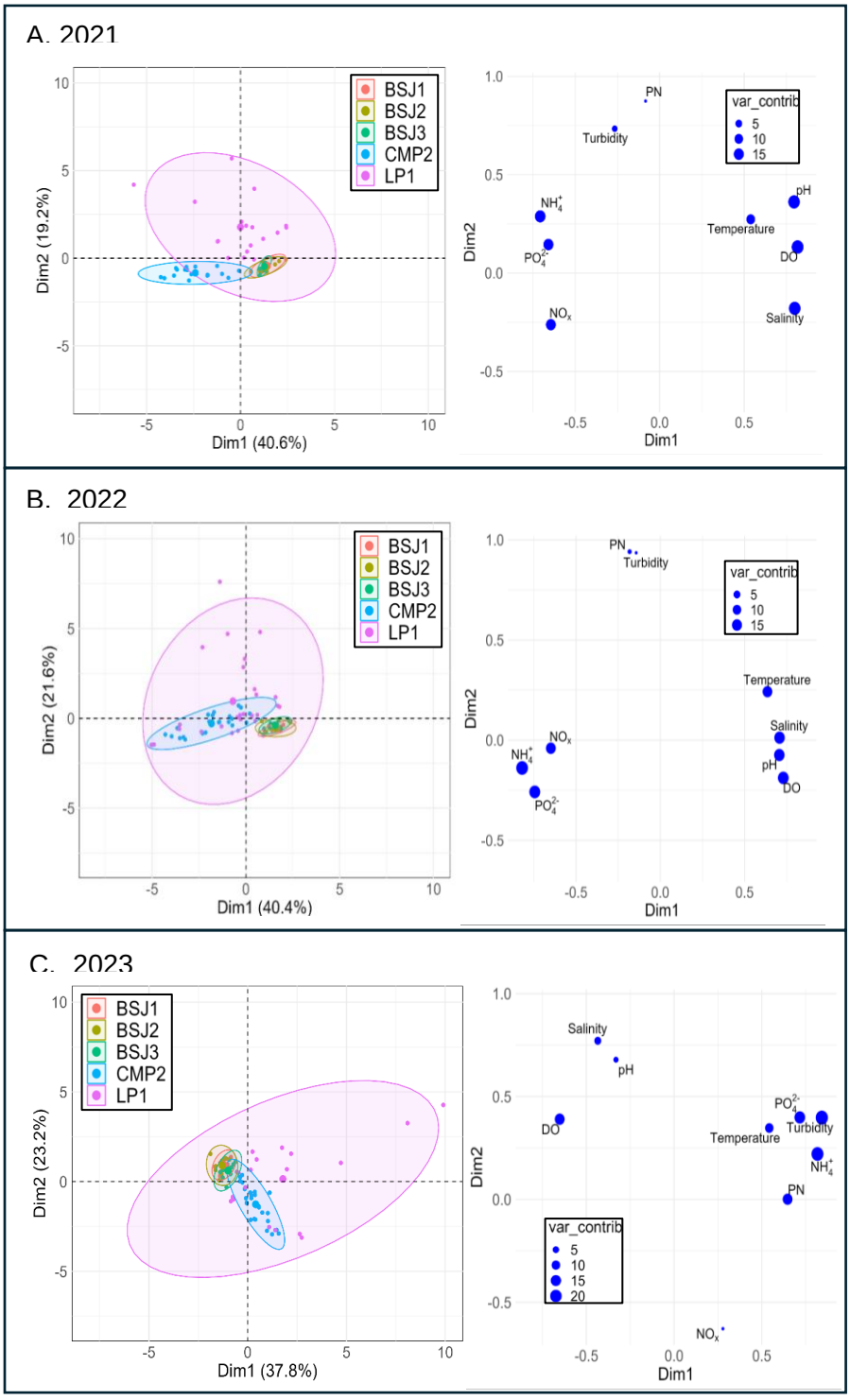

Figure 2: Multiple factor analysis plots (left) and variable contribution plots (right) per year (A = 2021, B = 2022, C = 2023). Variable contribution plot (right): larger points indicate that the variable has a higher contribution to the specific dimension (e.g., 15%) and plays a significant role in defining the structure captured by that dimension. Smaller points represent variables with lower contributions (e.g., 5%), indicating that they are less

influential in shaping the dimension. Values for these points can be found in Table 2. MFA plot (left): dimension 1 is DO, salinity, pH, NH_4^+, and PO_4^{3-}, suggesting a focus on water chemistry and a nutrient gradient. Dimension 2 is PN and turbidity, suggesting a focus on particulate matter and water clarity. Dimension 1 has a greater influence than dimension 2, but combined they explain roughly 60% of the total variability. The variables across these five sites are similar, indicated by the overlapping ellipses. LP1 is considered the generalist site as the measurements are most variable at this site but still encompass the variability of the other sites as well.

Table 2: Variable contribution values for the multiple factor analysis per year for each dimension. These values quantitively represent the variable contribution plots in Figure 1. A value below 10% indicates that variable is contributing less than 10% is here categorized as having a low contribution and therefore have relatively little influence on the dimension, suggesting they are less important in explaining the variation captured by that dimension. A value between 10-20% indicates that variable is contributing to the dimension, and a value higher than 20% indicates that variable has a high contribution to the dimension. These thresholds are a bit subjective and depend on the specific dataset, but the ranges provided are the general guidelines.

	2021		2022		2023	
Variable	**Dim 1 (%)**	**Dim 2 (%)**	**Dim 1 (%)**	**Dim 2 (%)**	**Dim 1 (%)**	**Dim 2 (%)**
Temperature	7.9	4.3	11.1	3.0	8.6	5.8
DO	18.2	1.0	14.6	1.8	12.5	7.3
Salinity	17.5	1.9	13.8	8.0E-3	5.6	28.5
pH	17.3	7.5	13.7	0.3	3.2	22.1
Turbidity	1.9	31.1	0.6	44.9	20.8	7.6
PO_4^{3-}	11.9	1.2	15.3	3.4	15.1	7.6
NH_4^+	13.7	4.8	18.5	1.0	19.6	2.3
NO_x	11.4	4.0	11.6	8.0E-2	2.3	18.9
PN	0.2	44.2	0.9	45.5	12.3	4.9E-05

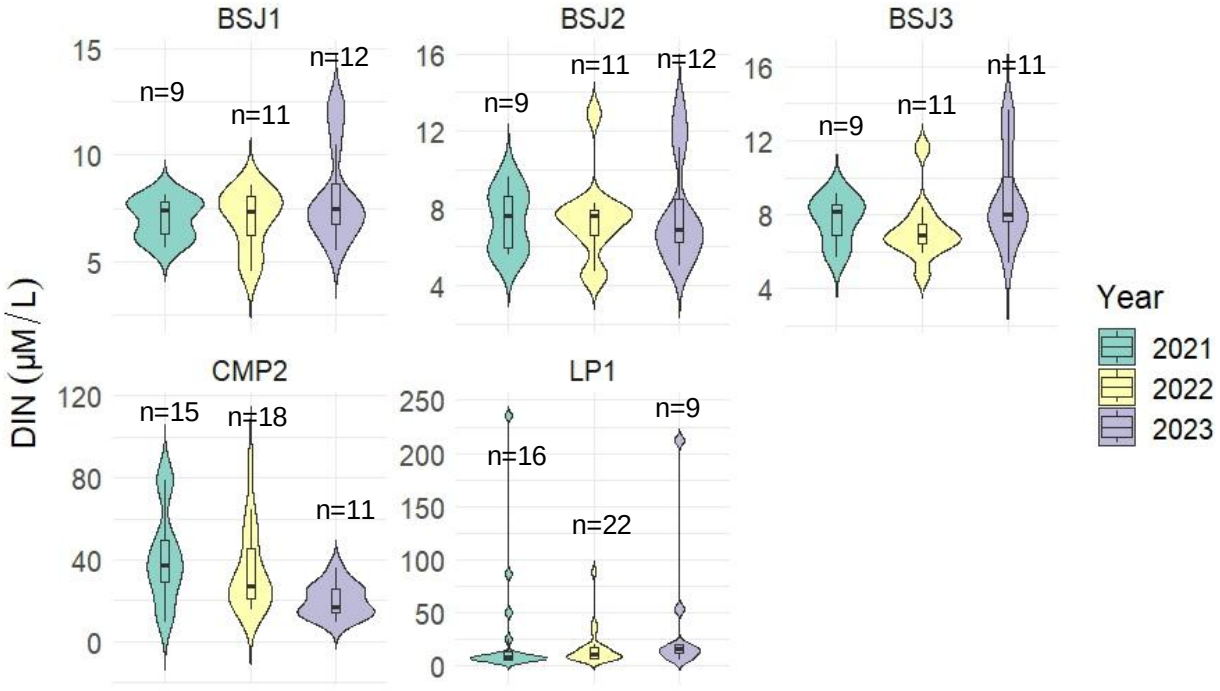

Figure 3: Violin plots of DIN (NH_4^+ + NO_3^- + NO_2^-; µM/L) by site (BSJ1, BSJ2, BSJ3, CMP2, LP1) over three separate years (blue = 2021, yellow = 2022, purple = 2023). Note the different Y-Axes. Refer to Table 1 for number of samples (n). DIN concentrations are lowest as the BSJ sites and highest at LP1. Variability is also the highest at CMP2 and LP1, with LP1 having the most outliers. The pooled standard deviation for DIN duplicates (all three years combined) at BSJ1 = 0.9 µM/L (n=6), BSJ1 = 0.8 µM/L (n=5), BSJ3 = 2.8 µM/L (n=4), CMP2 = 4.5 µM/L (n=16), and LP1 = 2.9 µM/L (n=13).

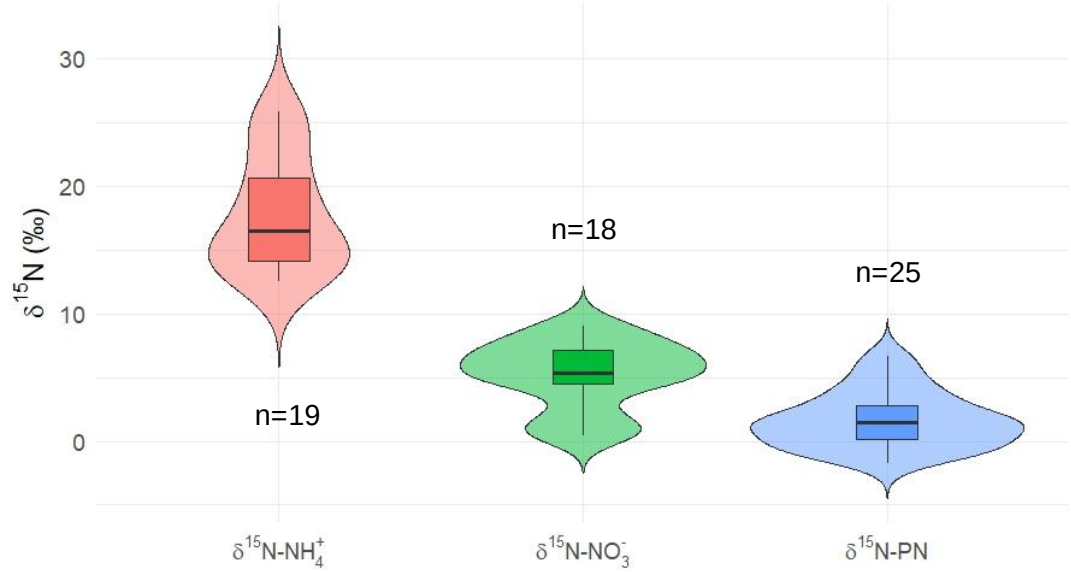

Figure 4: Violin plot of $\delta^{15}N$ values (NH_4^+ = orange, NO_3^- = green, PN = blue) where the sites (BSJ1, BSJ2, BSJ3, CMP2, LP1) and years (2021, 2022, 2023) are combined. The pooled standard deviation for $\delta^{15}N$-NO_3^- duplicates was < 0.3‰ (n=7). The pooled standard deviation for $\delta^{15}N$-NO_3^- replicates was < 0.3‰ (n=3). The pooled standard deviation for $\delta^{15}N$-NH_4^+ duplicates = 1.1‰ (n=6). The pooled standard deviation for $\delta^{15}N$-NH_4^+ replicates = 1.6‰ (n=2). These three groups are significantly different ($p < 0.05$) but $\delta^{15}N$-NH_4^+ and $\delta^{15}N$-NO_3^- are moderately correlated (r = 0.52)

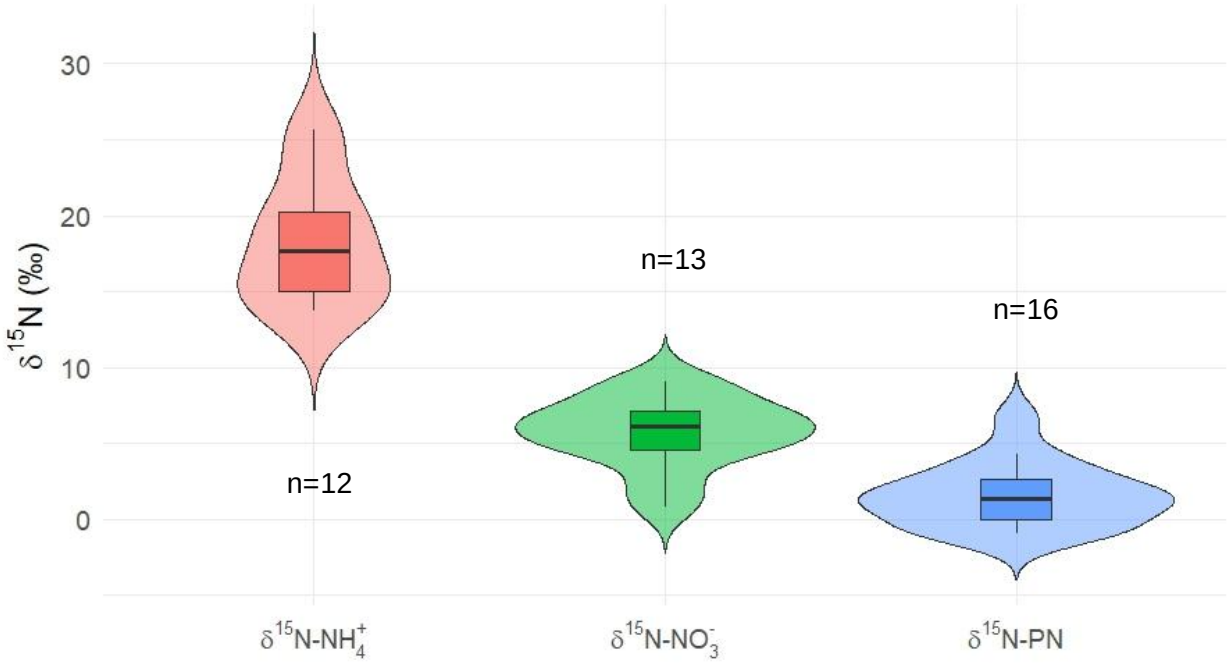

Figure 5: Violin plot of $\delta^{15}N$ values (NH_4^+ = orange, NO_3^- = green, PN = blue) at CMP2 (urban channel) over three combined years (2021, 2022, 2023). These three groups are significantly different ($p < 0.05$) but $\delta^{15}N$-NH_4^+ and $\delta^{15}N$-NO_3^- are strongly correlated (r = 0.67)

The full dataset was unable to be analyzed for $\delta^{15}N$-NH_4^+ and $\delta^{15}N$-NO_3^- as a matrix interference issue was present. The cation exchange resins removed anions and organic material, so it is still unclear exactly what the matrix interference was. Only about ~20% of the samples provided were able to be successfully analyzed, resulting in an incomplete dataset, which made it difficult to compare sites among years. Specifically, the BSJ sites displayed the most obstacles,

with only two samples from the year 2022 being successfully measured, which was unexpected. It is vital to study these matrix interference issues and to create a methodology that allows for proper analysis of $\delta^{15}N\text{-}NH_4^+$ and $\delta^{15}N\text{-}NO_3^-$, as it is possible that these issues could arise at other tropical, urban estuarine ecosystems, preventing data acquisition.

Summary

The SJBE is a complex estuary consisting of an open bay, canals, and interior lagoons. It experiences natural disturbances such as storms and hurricanes but is also highly influenced by urban development and anthropogenic sewage inputs. This can strongly impact the N cycle of the estuary, yet tropical, urban estuaries have not been a focus in the literature. The MFA analysis revealed that 60% of the variability in the data (NH_4^+, NO_3^-, PN, PO_4^{3-}, temperature, DO, salinity, pH, turbidity) was from water chemistry, nutrient gradient, PN, and turbidity. Further, the data at these sites were all similar, indicated by the overlapping ellipses (Figure 2). Isotopic values were significantly difference ($p < 0.05$) among $\delta^{15}N\text{-}NH_4^+$, $\delta^{15}N\text{-}NO_3^-$, and $\delta^{15}N$-PN (Figures 4 and 5). This incomplete dataset provides a small insight into how N cycles through tropical, urban estuaries but requires more long-term research, especially if matrix interference issues are observed at other locations.

References

Brandeis, T.J., Escobedo, F.J., Staudhammer, C.L., Nowak, D.J., & Zipperer, W.C. 2014. San Juan Bay Estuary Watershed urban forest inventory. Page 44. USDA Forest Service, Southern Forest Experiment Station General Technical Report SRS-190, Asheville, NC.

Bunch, B.W., Cerco, C.F., Dortch, M.S., Johnson, B.H., & Kim, K.W. 2000. Hydrodynamic and water quality model study of San Juan Bay estuary. ERDC TR-00-1. U.S. Army Engineering Research and Development Center. Vicksburg, MS.

Casciotti, K.L., Sigman, D.M., Hastings, M.G., Böhlke, J.K., & Hilkert, A. 2002. Measurement of the oxygen isotopic composition of nitrate in seawater and freshwater using the denitrifier method. *Analytical Chemistry*, 74(19), 4905–4912. https://doi.org/10.1021/ac020113w.

Kaiser, J., Hastings, M.G., Houlton, B.Z., Röckmann, T., & Sigman, D.M. 2007. Triple oxygen isotope analysis of nitrate using the denitrifier method and thermal decomposition of N_2O. *Analytical Chemistry*, 79(2), 599–607. https://doi.org/10.1021/ac061022s.

Lugo, A., Bauzá Ortega, J., Oczkowski, A., Meléndez Lázaro, P., Quiñones Márquez, F., Cintrón Molero, G., *et al*. 2024. San Juan Bay Estuary: Research History and Opportunities. U.S. Environmental Protection Agency, Washington, DC, EPA/600/R-23/308.

MacFarland, A.B., Walters, W.W., & Hastings, M.G. 2024. Solid Phase Extraction Methodology for Robust Isotope Analysis of Atmospheric Ammonium: Concentration and Removal of Matrix Interferences. *ACS Earth and Space Chemistry*, 8(5), 1039-1047. https://doi.org/10.1021/acsearthspacechem.3c00375.

O'Dell, J.W. 1993a. In: Method 353.2, Revision 2.0: Determination of Nitrate-Nitrite by Automated Colorimetry. US EPA.

O'Dell, J.W., 1993b. In: Method 350.1, Revision 2.0: Determination of Ammonia Nitrogen by Semi-automated Colorimetry. US EPA.

Potter, J.D., McDowell, W.H., Helton, A.M., & Daley, M.L. 2014. Incorporating urban infrastructure into biogeochemical assessment of urban tropical streams in Puerto Rico. *Biogeochemistry*, 12, 271-286. https://doi.org/10.1007/s10533-013-9914-5.

Sigman, D.M., Casciotti, K.L., Andreani, M., Barford, C., Galanter, M.B.J.K., & Böhlke, J.K. 2001. A bacterial method for the nitrogen isotopic analysis of nitrate in seawater and freshwater. *Analytical Chemistry*, 73(17), 4145–4153. https://doi.org/10.1021/ac010088e.

Zhang, L., Altabet, M., Wu, T., & Hadas, O. 2007. Sensitive measurement of NH4+ 15N/14N (d15NH4+) at natural abundance levels in fresh and saltwaters. *Analytical Chemistry*, 79, 5297–5303. https://doi.org/10.1021/ac070106d.